

NATL INST OF STAND & TECH



A11107 241932











National Bureau of Standards  
Library, E-01 Admin. Bldg.

OCT 6 1981

191137

QC

100

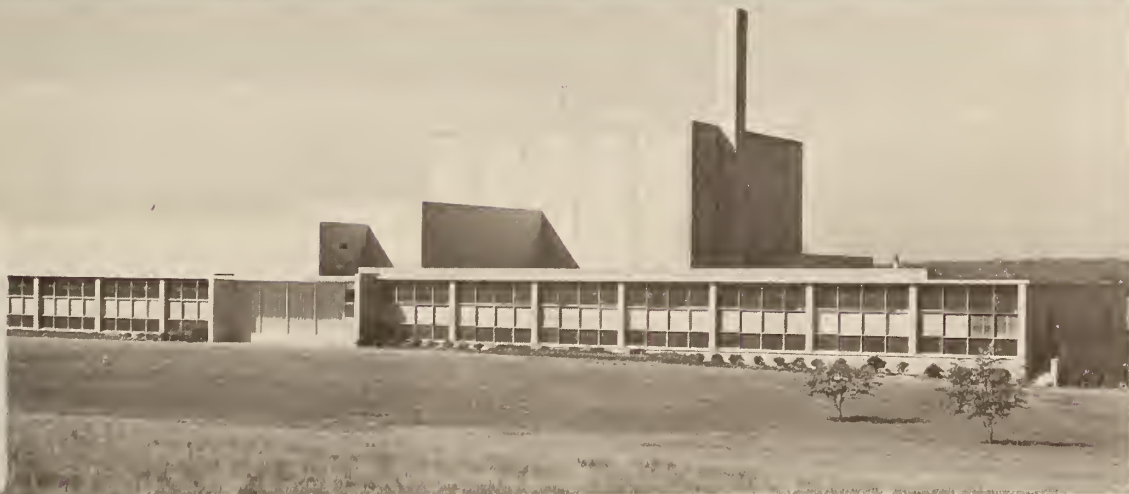
.U5753



# NBS TECHNICAL NOTE 995

U.S. DEPARTMENT OF COMMERCE / National Bureau of Standards

## NBS Reactor: Summary of Activities July 1977 to June 1978



QC

100

.U5753

NO. 995

1979

C. 2

## NATIONAL BUREAU OF STANDARDS

The National Bureau of Standards<sup>1</sup> was established by an act of Congress March 3, 1901. The Bureau's overall goal is to strengthen and advance the Nation's science and technology and facilitate their effective application for public benefit. To this end, the Bureau conducts research and provides: (1) a basis for the Nation's physical measurement system, (2) scientific and technological services for industry and government, (3) a technical basis for equity in trade, and (4) technical services to promote public safety. The Bureau's technical work is performed by the National Measurement Laboratory, the National Engineering Laboratory, and the Institute for Computer Sciences and Technology.

**THE NATIONAL MEASUREMENT LABORATORY** provides the national system of physical and chemical and materials measurement; coordinates the system with measurement systems of other nations and furnishes essential services leading to accurate and uniform physical and chemical measurement throughout the Nation's scientific community, industry, and commerce; conducts materials research leading to improved methods of measurement, standards, and data on the properties of materials needed by industry, commerce, educational institutions, and Government; provides advisory and research services to other Government Agencies; develops, produces, and distributes Standard Reference Materials; and provides calibration services. The Laboratory consists of the following centers:

Absolute Physical Quantities<sup>2</sup> — Radiation Research — Thermodynamics and Molecular Science — Analytical Chemistry — Materials Science.

**THE NATIONAL ENGINEERING LABORATORY** provides technology and technical services to users in the public and private sectors to address national needs and to solve national problems in the public interest; conducts research in engineering and applied science in support of objectives in these efforts; builds and maintains competence in the necessary disciplines required to carry out this research and technical service; develops engineering data and measurement capabilities; provides engineering measurement traceability services; develops test methods and proposes engineering standards and code changes; develops and proposes new engineering practices; and develops and improves mechanisms to transfer results of its research to the ultimate user. The Laboratory consists of the following centers:

Applied Mathematics — Electronics and Electrical Engineering<sup>2</sup> — Mechanical Engineering and Process Technology<sup>2</sup> — Building Technology — Fire Research — Consumer Product Technology — Field Methods.

**THE INSTITUTE FOR COMPUTER SCIENCES AND TECHNOLOGY** conducts research and provides scientific and technical services to aid Federal Agencies in the selection, acquisition, application, and use of computer technology to improve effectiveness and economy in Government operations in accordance with Public Law 89-306 (40 U.S.C. 759), relevant Executive Orders, and other directives; carries out this mission by managing the Federal Information Processing Standards Program, developing Federal ADP standards guidelines, and managing Federal participation in ADP voluntary standardization activities; provides scientific and technological advisory services and assistance to Federal Agencies; and provides the technical foundation for computer-related policies of the Federal Government. The Institute consists of the following divisions:

Systems and Software — Computer Systems Engineering — Information Technology.

<sup>1</sup>Headquarters and Laboratories at Gaithersburg, Maryland, unless otherwise noted; mailing address Washington, D.C. 20234.

<sup>2</sup>Some divisions within the center are located at Boulder, Colorado, 80303.

**The National Bureau of Standards was reorganized, effective April 9, 1978.**

National Bureau of Standards  
JUN 8 1979  
not available  
2001  
10.775  
1979

# NBS Reactor: Summary of Activities July 1977 to June 1978

---

Frederick J. Shorten, Editor

Reactor Radiation Division  
National Measurement Laboratory  
National Bureau of Standards  
Washington, D.C. 20234



*Technical note 312*

---

U.S. DEPARTMENT OF COMMERCE, Juanita M. Kreps, Secretary

Jordan J. Baruch, Assistant Secretary for Science and Technology

NATIONAL BUREAU OF STANDARDS, Ernest Ambler, Director

Issued May 1979

National Bureau of Standards Technical Note 995

Nat. Bur. Stand. (U.S.), Tech. Note 995, 147 pages (May. 1979)

CODEN: NBTNAE

U.S. GOVERNMENT PRINTING OFFICE

WASHINGTON: 1979

---

For sale by the Superintendent of Documents, U.S. Government Printing Office, Washington, D.C. 20402

Stock No. 003-003-02070-2 Price \$4.50

(Add 25 percent additional for other than U.S. mailing)

## FOREWORD

The National Bureau of Standards Reactor was built not only to serve the needs of the NBS but also those of other government agencies and the greater Washington Scientific Community. The Reactor Radiation Division was established to operate the reactor and to foster its scientific and technological use. Toward this end, the Division has a small nucleus of scientists experienced in the use of reactors for a wide range of scientific and technical problems. In addition to pursuing their own research and developing sophisticated experimental facilities, they actively seek out and encourage collaboration with other scientists, engaged in challenging programs, whose work can benefit from use of the reactor, but who as yet do not have the reactor experience necessary to take full advantage of the facilities available. The Division also provides irradiation services to a wide variety of users as well as engineering and other technical services.

The reactor operates at 10 MW and is designed to provide more than 25 experimental facilities ranging from intense neutron beams to extensive irradiation facilities, making it one of the most versatile high flux research reactors in the country. Thus it is able to serve a large number of scientists and engineers in a broad range of activities both within and outside the NBS.

This report attempts to summarize all the work done which is dependent on the reactor including a large number of programs outside the Division. The first section summarizes those programs based primarily on Reactor Radiation Division (RRD) initiatives whereas the second and third sections summarize collaborative programs between RRD scientists and other NBS or non-NBS scientists respectively. The fourth section summarizes NBS work originating entirely outside the RRD which requires no collaboration with RRD scientists. The section entitled, "Service Programs" covers those programs originating outside NBS but for which RRD provides irradiation services. The remaining sections are self-explanatory.

## FOREWORD

Appreciation is extended to F. J. Shorten of the Reactor Radiation Division for his extensive contributions to the editing, organization and preparation of this report, and L. Sprecher, C. O'Connor, and C. Freedman for efforts in typing manuscripts.



R. S. Carter  
Chief, Reactor Radiation Division  
National Bureau of Standards

## ABSTRACT

This report summarizes all those programs which depend on the NBS reactor. It covers the period from July 1977 through June 1978. The programs range from the use of neutron beams to study the structure and dynamics of materials through nuclear physics and neutron standards to sample irradiations for activation analysis, isotope production, radiation effects studies, neutron radiography and nondestructive evaluations.

Key words: Activation analysis; crystal structure; diffraction; isotopes; molecular dynamics; neutron; neutron radiography; nondestructive evaluation; nuclear reactor; radiation.

## TABLE OF CONTENTS

FOREWORD . . . . .	iii
ABSTRACT . . . . .	v
A. REACTOR RADIATION DIVISION PROGRAMS. . . . .	1
The Lattice Dynamics of PdD <sub>0.88</sub> . . . . .	1
Influence of Hydrogen on the Magnetic Properties of Rare Earth Compounds . . . . .	3
Studies of Robust/Resistant Refinement Techniques . . . . .	7
Observation of a Ferroelectric Transition in Zinc Cyanide . . . . .	9
Construction of a Powder Diffractometer with 5 Detectors . . . . .	10
Neutron Diffraction Powder Profile Analysis of Manganese Fluoroapatite . . . . .	10
Powder Diffraction Study of Ta <sub>2</sub> WO <sub>8</sub> . . . . .	12
Crystallography of Ribonuclease-A . . . . .	20
Rotational Dynamics and Phase Transitions in (KCN) <sub>x</sub> (KBr) <sub>1-x</sub> . . . . .	22
CN <sup>-</sup> IONS in KCl, KBr . . . . .	24
Neutrino Scattering and Weak-Interaction Gauge Theories . . . . .	26
Isotopic Shifts of Phonons . . . . .	28
Neutron Radiography . . . . .	29
B. RRD COLLABORATIVE PROGRAMS . . . . .	34
Application of Neutron Diffraction to Non-Destructive Testing Problems . . . . .	34
High Temperature Structure of NH <sub>4</sub> NO <sub>3</sub> (Phase II). . . . .	39
Refinement of Dipara-Anthracene Structure . . . . .	41
The Pressure-Induced Phase Transition in Sodium Nitrate . . . . .	43
The Structure of Sodium Zinc Chloride Trihydrate . . . . .	46
Spin Excitations in Amorphous Transition- Metal Glasses . . . . .	48
Magnetic Excitations in HoFe <sub>2</sub> . . . . .	49
Magnetic Neutron Scattering From Amorphous TmFe <sub>2</sub> . . . . .	55

## TABLE OF CONTENTS

Measurements of the Crystal-Field Splittings in Superconducting $(\text{Ce}_{1-x}\text{Ho}_x)\text{Ru}_2$ Alloys . . . . .	58
Low Temperature Phase Transition in $\text{Cs}_2\text{NaPrCl}_6$ . . . . .	61
Crystal-Field Excitations in $(\text{RE})\text{Mo}_6\text{Se}_8$ . . . . .	62
A Triple Axis Polarized Beam Spectrometer . . . . .	66
Studies of the Effects of Deuterium in Titanium . . . . .	68
Structure and Dynamics of $\beta \text{V}_2\text{D}$ . . . . .	68
Chain Deformation in Rubber . . . . .	69
<b>C. NON-RRD NBS PROGRAMS . . . . .</b>	<b>74</b>
Activation Analysis: Summary of 1978 Activities . . . . .	74
Fissionable Deposit Mass Assay . . . . .	114
Precision Gamma-Ray Wavelengths . . . . .	116
Cavity Fission Neutron Source Irradiation Facility . . . . .	120
<b>D. SUMMARY OF REACTOR OPERATIONS . . . . .</b>	<b>123</b>
<b>E. SERVICE PROGRAMS . . . . .</b>	<b>124</b>
Activation Analysis Program of the Food and Drug Administration at the NBSR . . . . .	124
ATF'S Forensic Activation Analysis Program . . . . .	126
<b>F. STAFF ROSTER . . . . .</b>	<b>128</b>
<b>G. PUBLICATIONS . . . . .</b>	<b>133</b>



## A. REACTOR RADIATION DIVISION PROGRAMS

### THE LATTICE DYNAMICS OF PdD<sub>0.88</sub>

C. J. Glinka, J. M. Rowe and J. J. Rush

There has been considerable experimental and theoretical interest in recent years in the role of the lattice vibrations, particularly the optic modes, in the inducement of high  $T_c$  superconductivity in the PdH<sub>x</sub>(D<sub>x</sub>) system when x approaches unity. Thus far, information on the phonon spectra in these materials has derived from coherent neutron scattering measurements of the phonon dispersion curves in PdD<sub>0.63</sub> and incoherent scattering measurements of the phonon density of states in PdH<sub>0.63</sub><sup>3</sup>. However, at this concentration, which is the equilibrium concentration at atmospheric pressure, palladium hydride does not become superconducting.

In order to obtain phonon data on a sample which is a superconductor, we have prepared, in collaboration with H. Flotow of Argonne National Laboratory, a single crystal of palladium deuteride with the composition PdD<sub>0.88</sub>. To reach this concentration, the crystal was loaded with D<sub>2</sub> gas in a specially designed high pressure scattering cell under a pressure of 2 kbars. The final composition was determined by a careful measurement of the lattice constant at 80K. At the concentration PdD<sub>0.88</sub>, the crystal is expected to have a superconducting transition between 4 to 5K.

We have carried out coherent inelastic neutron scattering measurements of both the optic and acoustic phonon dispersion curves along the [100], [110] and [111] symmetry directions in the PdD<sub>0.88</sub> crystal at 80K. The results of these measurements are summarized in figure 1 where the squares and circles refer to transverse and longitudinal modes, respectively. For comparison, the dispersion curves for PdD<sub>0.63</sub> are shown as solid lines in figure 1. From the figure it is apparent that there is rather little difference between the phonon spectra at these two concentrations. In particular, we observe no change in the position

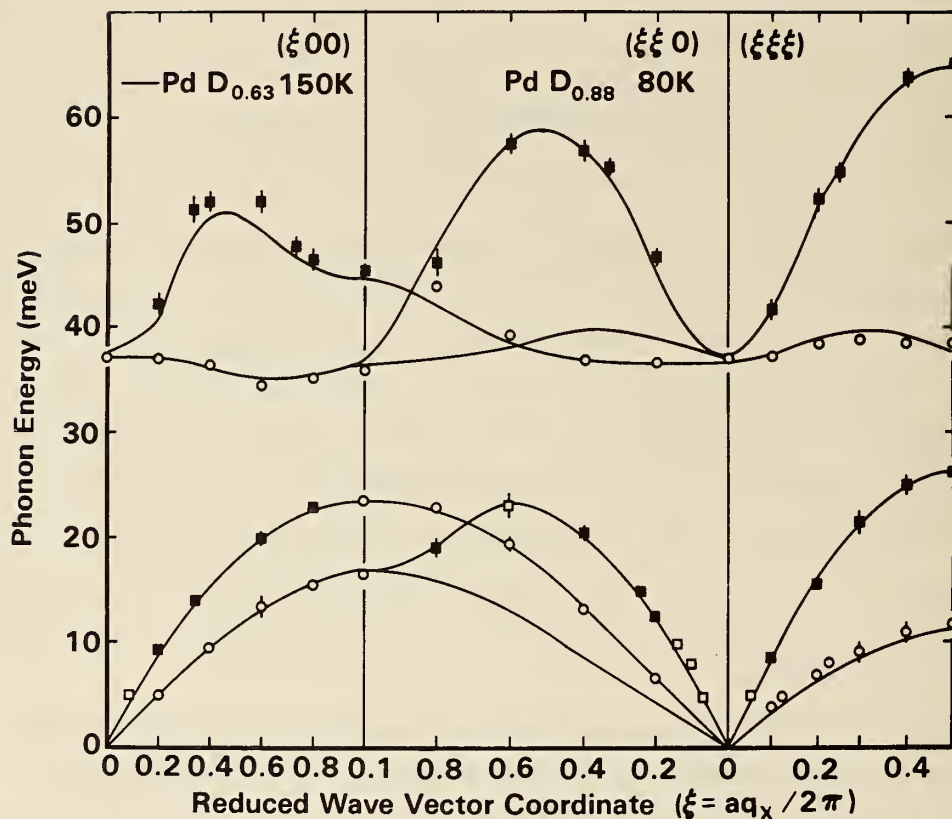


Figure 1. Data points are phonon frequencies measured in  $\text{PdD}_{0.88}$  at 80K. Squares and circles refer to longitudinal and transverse modes, respectively. The solid curves are the corresponding dispersion curves for  $\text{PdD}_{0.63}$ .

of the peak in the optic phonon density of states which occurs at 37 meV due to the several nearly flat transverse phonon branches near this energy. Neither is there any shift in the critical points of the acoustic phonon density of states. The only significant shift in phonon frequencies occurs along the [100] longitudinal optic branch where the frequencies are 5 to 10% higher in  $\text{PdD}_{0.88}$  than in  $\text{PdD}_{0.63}$ . These results suggest that whatever features of the phonon spectrum of palladium hydride that are related to superconductivity are already present in the spectrum for  $\text{PdD}_{0.63}$ . Beyond this concentration, changes in the electronic properties due to the added hydrogen, rather than changes in the phonons, are responsible for the onset of superconductivity.

## REACTOR RADIATION DIVISION PROGRAMS

1. J. M. Rowe, J. J. Rush, H. G. Smith, M. Mostoller and H. E. Flotow, *Physical Review Letters* 33, 1297 (1974).
2. C. J. Glinka, J. M. Rowe, J. J. Rush, A. Rahman, S. K. Sinha and H. E. Flotow, *Physical Review* B17, 488 (1978).
3. A. Rahman, K. Skold, C. Pelizzari, S. K. Sinha and H. E. Flotow, *Physical Review* B14, 3630 (1976).

## INFLUENCE OF HYDROGEN ON THE MAGNETIC PROPERTIES OF RARE EARTH COMPOUNDS

J. J. Rhyne and G. E. Fish

and

S. G. Sankar and W. E. Wallace  
(University of Pittsburgh, Pittsburgh, PA)

In the last few years it has been found that a large variety of rare earth-intermetallic compounds absorb large amounts of hydrogen, generally at only moderately increased temperature and/or pressure; forming hydride phases. The density of hydrogen atoms in these compounds often exceeds that of liquid hydrogen, approaching  $6 \times 10^{+22}$  atoms/cm<sup>3</sup>.

Due to the influence of hydrogen on the electronic density of states, lattice parameter, crystal field screening, etc., profound changes in the magnetic interactions in rare earth compounds can occur on hydriding. We have studied the effect of H on the sublattice magnetization in several RFe<sub>2</sub> (R = heavy rare earth) Laves phase compounds.

These compounds readily absorb hydrogen up to a concentration of approximately 4 hydrogen atoms per formula unit. The hydride can be made stable against desorption of hydrogen at room temperature and ambient pressure by poisoning the surface with SO<sub>2</sub>. X-ray diffraction has shown that the materials remain in the Laves phase structure, but exhibit a significant increase in lattice parameter  $a_0$ . For example,  $a_0 = 7.28$  Å for ErFe<sub>2</sub> and is increased to  $a_0 = 7.83$  for ErFe<sub>2</sub>H<sub>3.9</sub>.

REACTOR RADIATION DIVISION PROGRAMS

The heavy rare earth ( $RFe_2$ ) compounds (non-hydride) are ferrimagnetic with the R moment equal to the free ion moment (at 0 K) aligned anti-parallel to the two Fe moments each equal to approximately  $1.6 \mu_B$ . The Curie temperatures of the  $RFe_2$  compounds range from 535 K for  $YFe_2$  to 793 K for  $GdFe_2$ .<sup>1</sup>

After hydriding, bulk magnetization data<sup>1</sup> show the Curie temperatures to be significantly reduced from that of the pure compounds and to be fairly sensitive to small change in hydrogen occupation and/or preferential occupation of sites. Because of the large crystal field anisotropy (except for Gd) magnetic moment data on the compounds do not saturate in normally available laboratory fields ( $\approx 100$  kOe) and thus a definitive determination of the full moment is not possible by conven-

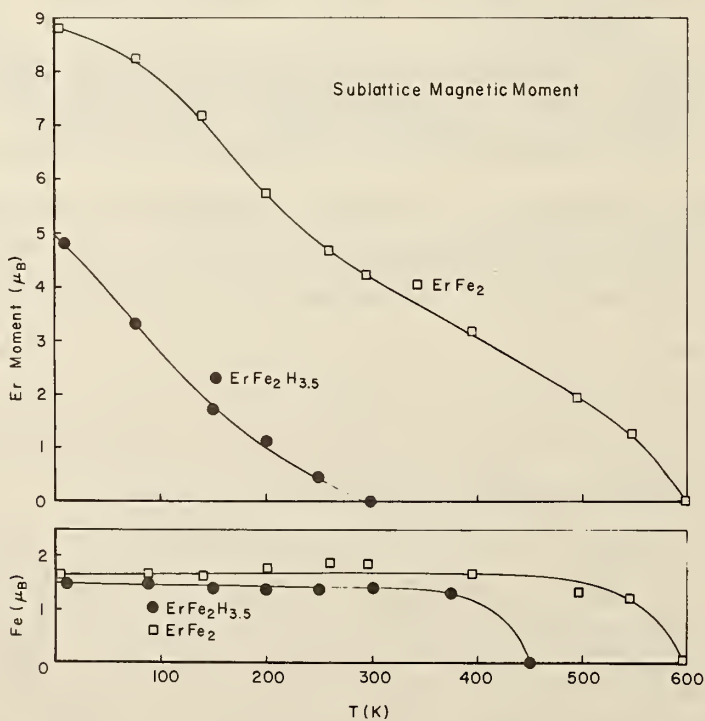


Figure 1. Sublattice magnetic moments as a function of temperature for Er and Fe in  $ErFe_2$  and  $ErFe_2H_{3.5}$ . The uncertainty in the moment shown is approximately  $\pm 0.3\mu_B$  largely due to the effect of the incoherent scattering of H.

REACTOR RADIATION DIVISION PROGRAMS

tional methods. Therefore, we have used neutron scattering to study the effect of hydrogen on the sublattice magnetization and Curie temperature of  $\text{HoFe}_2$ ,  $\text{ErFe}_2$  and  $\text{TmFe}_2$ .

In the hydride compounds, due to the unknown site occupancy of the hydrogen, an absolute determination of the scattering intensity was made by normalization to a copper powder. In the case of  $\text{ErFe}_2\text{H}_{3.5}$  data were taken on a deuterated sample which further reduced the incoherent contribution. Results for the sublattice moment on the R site are shown in figures 1 and 2 for  $\text{HoFe}_2\text{D}_{3.5}$ ,  $\text{HoFe}_2$ ,  $\text{TmFe}_2\text{H}_{3.5}$ ,  $\text{TmFe}_2$ , and on both R and Fe sites for  $\text{ErFe}_2\text{H}_{3.5}$  and  $\text{ErFe}_2$ .

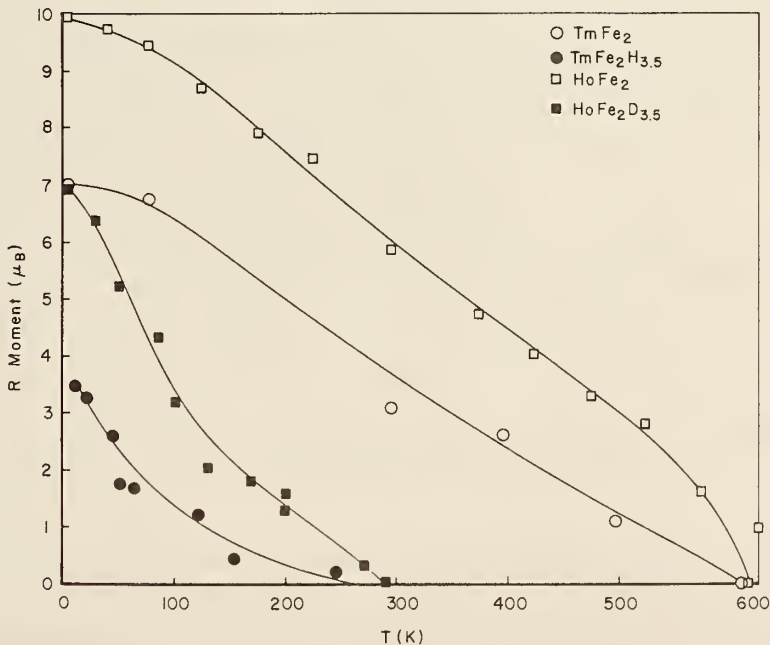


Figure 2. Tm and Ho sublattice moment versus temperature for  $\text{TmFe}_2$ ,  $\text{HoFe}_2$ , and for  $\text{TmFe}_2\text{H}_{3.5}$  and  $\text{HoFe}_2\text{D}_{3.5}$ . The overall Curie temperature of the Tm hydride is approximately 300 K and of the Ho deuteride 320 K.

## REACTOR RADIATION DIVISION PROGRAMS

As is evident from the figures, the overall Curie temperature is reduced by more than 20% on hydriding. This reflects a reduction in Fe-Fe exchange due to the increased lattice parameter and Fe-Fe exchange due to the increased lattice parameter and Fe-Fe interatomic spacing. The magnitude of the iron sublattice moment and its relatively flat temperature dependence remain essentially unchanged. The effect on the rare earth is much more dramatic. First, the 0 K moment in the hydride is sharply reduced from its free ion value. In addition the moment rapidly decreases with elevated temperature, reaching essentially zero in  $\text{ErFe}_2\text{-H}_{3.5}$  below the overall Curie temperature. These features suggest a severe weakening of the R-Fe (and R-R) exchange coupling. The Fe-Fe coupling may proceed by nearest-neighbor direct overlap exchange which would not be strongly influenced.

The weaker rare-earth exchange in the hydride compound suggests also that the crystal field interactions may perturb the energy levels away from pure  $J_Z$  states, effectively reducing the observed sublattice moment. Inelastic neutron scattering studies are in progress to examine the magnetic excitations. Alternately the loosely-coupled rare earth moments may be "fanning" about the direction of the net iron exchange field. The random occupation of the hydrogen sites can significantly distort the local anisotropy field in a manner similar to that found in amorphous rare earth alloys<sup>2</sup> leading to a reduction in spatially averaged moment as measured by the neutrons.

- 
1. Gualtieri, D. M., Narasimhan, K.S.V.L., and Wallace, W. E., *A.I.P. Conference Proceedings Series* 34, 219(1976).
  2. Rhyne, J. J., Schelleng, J. H., and Koon, N. C., *Phys. Rev.* B10, 4672(1974).

## REACTOR RADIATION DIVISION PROGRAMS

### STUDIES OF ROBUST/RESISTANT REFINEMENT TECHNIQUES

E. Prince

and

W. L. Nicholson

(Battelle Pacific Northwest Laboratories, Richland, WA)

Studies<sup>1</sup> of the behavior of a robust/resistant modification of the conventional least-squares algorithm used for crystal structure refinement have continued. Previous work has shown the modified algorithm to be "resistant", ie, that it is insensitive to small numbers of "out-lier" points in the data, but a demonstration that the procedure is also "robust", that it works for a broad range of error distributions, requires that the error distributions in particular data sets be known. Since the true error distribution in a real experimental data set is never accurately known, we have studied the behavior of the algorithm for several synthetic data sets derived from the calculated structure factors for a known crystal structure by adding random errors generated according to several error distributions.

Altogether, four data sets were refined:

- 1) The error distribution was Gaussian, with weights assigned equal to the reciprocals of the variances of the individual points;
- 2) An error distribution the same as in 1, but unit weights used throughout;
- 3) A Gaussian error distribution contaminated by 10% of another Gaussian distribution with a variance 9 times greater; and
- 4) a long-tailed distribution derived by dividing a Gaussian random variable.

Distribution 1 is the condition for which least-squares theoretically gives the best possible result.

For the other distributions, least-squares gives the best linear estimates of the parameters of the model, but in general non-linear estimates exist which are better. A robust procedure should nearly as well as least-squares for distribution 1, and as well or better for the

REACTOR RADIATION DIVISION PROGRAMS

other distributions.

Each data set was refined twice, once using the modified algorithm, in which the weights are adjusted in each cycle according to the relation

$$\begin{aligned} w' &= w(1 - 2X^2 + X^4) & \left| \frac{X}{\sigma} \right| < 1, \\ w' &= 0 & \left| \frac{X}{\sigma} \right| > 1, \end{aligned}$$

where  $X = \Delta F / (k\sigma)$ , and  $k$  is set equal to 9 times the median value of  $\Delta F / \sigma$  in the previous cycle. The starting model in each case was the model from which the error free structure factors were calculated. The standard deviations of the parameter estimates for the conventional refinement of distribution 1 were taken as a scale for comparison with all of the others. The results are summarized in table 1. For each of the 8 refinements we give the unweighted R index ( $R = \sum ||F_o| - |F_c|| / \sum |F_o|$ ), the weighted R index ( $R_w = [\sum w (|F_o| - |F_c|)^2 / \sum w |F_o|^2]^{1/2}$ ), and the slope of a half-normal quantile-quantile plot<sup>2</sup> of the differences between the estimated parameters and their corrected values, divided by the standard deviations from distribution 1. For a properly weighted least-squares fit to a linear model this slope should be 1.0. The fact that it is not 1.0 for the least-squares refinement of distribution 1 is due to the fact that the structure factor model is non-linear, so that several iterations are required to find the minimum. It appears that

Table 1. Summary of results of refinement of synthetic data sets.

Distribution	Conventional algorithm			Robust/resistant algorithm		
	R	R <sub>w</sub>	S	R	R <sub>w</sub>	S
1	0.018	0.023	1.2	0.018	0.021	1.2
2	0.018	0.020	1.4	0.017	0.017	1.2
3	0.022	0.028	1.8	0.022	0.024	1.6
4	0.082	0.137	9.9	0.028	0.032	1.6

the modified algorithm gives results almost identical to the conventional algorithm for distribution 1, slightly better results in cases 2 and 3, and very much better results in case 4. This suggests that the

## REACTOR RADIATION DIVISION PROGRAMS

modified algorithm is seldom, if ever, inferior to the conventional one, and is sometimes very markedly superior.

- 
1. E. Prince and W. L. Nicholson, *NBS Tech. Note 969*, 13 (1978).
  2. S. C. Abrahams and E. T. Keve, *Acta. Cryst.* A27, 157 (1971).

### OBSERVATION OF A FERROELECTRIC TRANSITION IN ZINC CYANIDE.

E. Prince and J. M. Rowe

and

C. S. Choi

(Energetic Materials Division, LCWSL, ARRD COM, Dover, NJ)

In previous annual reports we have described crystallographic studies on sodium and postassium cyanides.<sup>1</sup> Each of these alkali cyanides is cubic at room temperature, with a disordered arrangement of cyanide ions. In each there is a lower temperature phase with orthorhombic symmetry in which the cyanide ions are all parallel to one direction, but the sense of the C-N vector is random, and a still lower temperature phase in which the C-N dipoles show antiferroelectric ordering. Zinc cyanide,  $Zn(CN)_2$  has a structure which is also cubic<sup>2</sup> at room temperature, but with a different space group from the alkali cyanides. Each CN ion is parallel to a particular [111] direction, but, again, the sense of the CN vector is random. Dipole energy considerations would lead one to expect a transition at some temperature to a tetragonal (pseudo-cubic) ferroelectric phase at some low temperature. Mellor<sup>2</sup> looked for this transition, but did not find any evidence for it down to 77K. In preliminary measurements on a crystal kindly supplied by Prof. D. P. Shoemaker there are indications that a transition occurs between 40K and 50K. Additional measurements will be taken in an attempt to confirm this transition.

- 
1. J. M. Rowe, J. J. Rush, E. Prince, N. J. Chesser, S. Susman, and D. G. Hinks, *NBS Tech. Note 969* (1977).
  2. J. Mellor, Thesis, M. I. T. (1962).

## REACTOR RADIATION DIVISION PROGRAMS

### CONSTRUCTION OF A POWDER DIFFRACTOMETER WITH 5 DETECTORS

E. Prince and A. Santoro

The full potential of neutron powder diffractometry and profile analysis can only be realized if the resolution of the powder pattern is the best practically obtainable, which implies a penalty in the form of low intensity and correspondingly long counting times. On the other hand, intensity is present in all parts of the powder diffraction pattern all of the time, so great improvements in efficiency can be obtained by measuring different parts of the diffraction pattern simultaneously. A detector shield has been designed for the diffractometer at BT-1 which has five independent collimators with a  $20^\circ$  angle between each pair. It will be possible, for any given resolution, to collect data 4 or 5 times faster than before. Installation and check-out of this instrument will occur in the late summer and early fall of 1978.

### NEUTRON DIFFRACTION POWDER PROFILE ANALYSIS OF MANGANESE FLUOROAPATITE

A. Santoro

and

L. W. Schroeder

(Food and Drug Administration, Washington DC)

Manganese fluoroapatite provides a good example of the challenges presented during the determination of cation distributions in substituted apatite. The present sample has manganese ions substituted for two of the ten cations which allows both ordered and disordered arrangements. The apatite structure is such that ordered cation distributions are also possible in space groups  $P6_3$ ,  $P\bar{6}$ ,  $P\bar{3}$  and  $P3$ . Disordered distributions are also possible in  $P6_3/m$ , the nominal apatite space group in addition to the space groups mentioned above. Neutron Diffraction Powder Profile Analysis is well suited to problems of this type because a bulk sample which is more reflective of the actual

## REACTOR RADIATION DIVISION PROGRAMS

situation is studied rather than one crystal which may provide biased results.

Powder diffraction data was collected on a well-crystallized sample. The experimental conditions were as follows:

monochromatic beam; reflection 220 of a Cu crystal,  
wavelength  $1.5416(3)\text{\AA}$

mosaic spread of Cu monochromator 15 minutes of arc

Horizontal divergences

(a) in-pile collimator -  $10'$

(b) monochromatic beam collimator -  $20'$

(c) diffracted beam collimator -  $10'$

Sample container: Vanadium can  $\sim 1$  cm in diameter

The region from  $2\theta = 5^\circ$  to  $110^\circ$  was scanned in  $0.05^\circ$  steps.

We decided to first try and determine if the cation distribution in manganese fluoroapatite is ordered. Modes in space groups  $P6_3$  and  $P\bar{6}$  gave refinements in which the manganese ion shifted spuriously even though the initial positions were chemically reasonable. Refinements in space group  $P\bar{3}$  were stable and converged to agreement factors about twice those expected from counting statistics. However, the resulting bond distances and angles especially for the  $PO_4$  group and about the manganese ions deviated greatly from literature values. We concluded that the extra degrees of freedom possible in  $P\bar{3}$  are not utilized in a manner reflective of the actual structure. Results obtained so far indicate that:

(a) the cation distribution in our sample of manganese fluoroapatite is not ordered.

(b) Refinements must be carefully evaluated because for these structures there is a tendency for false minima.

Future efforts will be directed towards the development of disordered models for the cation distribution.

REACTOR RADIATION DIVISION PROGRAMS

POWDER DIFFRACTION STUDY OF Ta<sub>2</sub>WO<sub>8</sub>

A. Santoro

and

R. S. Roth

(Ceramics, Glass, and Solid State Science Division)

and

D. Minor

(Information Technology Division)

The compound Ta<sub>2</sub>WO<sub>8</sub> has been first considered structurally related to Nb<sub>2</sub>WO<sub>8</sub> [Stephenson, N.C. (1968). Acta Cryst., B24, 637-653.] which is orthorhombic with space group Pbcm. [Lundberg, M. (1972). Acta Chem. Scan., 26, 2932-2940]. In a subsequent investigation [Holcombe, C. E. (1976). Oak Ridge Report Y-2061] it was noted that the x-ray powder pattern of Ta<sub>2</sub>WO<sub>8</sub> can be fully indexed on a unit cell similar to that of LiNb<sub>6</sub>O<sub>15</sub>F, which is orthorhombic with space group Pmma [Lundberg, M. (1965). Acta Chem. Scan., 19, 2274-2284], and it was concluded that the two compounds must be isostructural.

The relationship between the two proposed structural models is illustrated in figure 1. The mirror m, perpendicular to [010] in space group Pmma, is replaced by the glide b in space group Pbcm. The metal and oxygen atoms, constrained to lie on the mirror in the first case, are free to move perpendicularly to the plane of projection in the second case. The change of point symmetry of the atomic positions, in turn, causes the doubling of the unit cell in space group Pbcm. When structures are as closely related as those shown in figure 1, the indexing of powder patterns may not be the best way for choosing one model rather than the other. In fact, angular positions of non-extinct reflections are identical in most cases and the superlattice reflections are in general very weak and difficult to detect even in those regions of the pattern free from interferences.

An accurate knowledge of the structure of Ta<sub>2</sub>WO<sub>8</sub> is important in understanding the thermal expansion properties of the compound [Holcombe,

REACTOR RADIATION DIVISION PROGRAMS

C.E. and Smith, D.D. (1978). *J. Am. Ceramic Soc.*, 61, 163-169]. For this reason an attempt was made to solve the structural uncertainty with the method of profile analysis [Rietveld, H.M. (1969). *J. Appl. Cryst.*, 2, 65-71].

The single phase composition was prepared by heating the appropriate mixture of  $Ta_2O_5$  and  $WO_3$  at  $1350^\circ C$  for 31.5h and was found to occur at 52.4  $Ta_2O_5$ :47.6 $WO_3$ . Assuming the existence of a single phase, this composition may be interpreted as oxygen deficient ( $M_3O_{7.968}$ ,  $M=Ta, W$ ) or as containing metal excess ( $M_{3.012}O_8$ ). Neutron diffraction measurements were made with the conditions indicated in table 1. Refinements were carried out using 262 reflections over the angular range  $7.0^\circ < 2\theta < 84.5^\circ$  for  $Pmma$  and 298 reflections for  $Pbcm$ . In both cases intensities were measured at  $2\theta$  intervals of  $0.05^\circ$ . The results for both space groups are given in table 2, and they clearly show that  $Ta_2WO_8$  is isostructural with  $Nb_2WO_8$ .

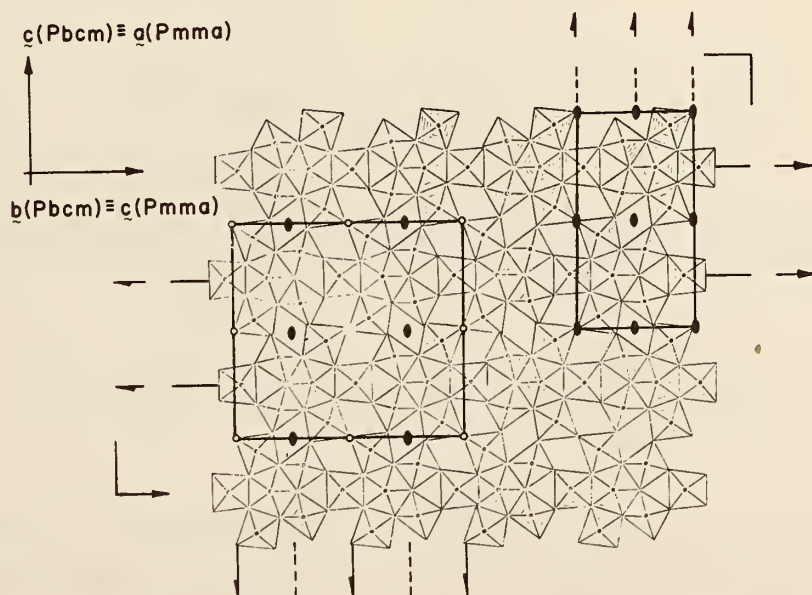


Figure 1. Projections of the structures of  $Nb_2WO_8$  and  $LiNb_6O_{15}F$ . The unit all in space group  $Pbcm$  is outlined on the left side of figure, and the unit cell in  $Pmma$  on the right side. The symbols of the symmetry elements are those used in *Int. Tables for X-Ray Crystallography*, Vol. 1.

## REACTOR RADIATION DIVISION PROGRAMS

The possibility of variable occupancies at the metal sites for this and for related compounds has been reported (Holcombe, *Loc. cit.*) and, in fact, Nb/W ratios different from those corresponding to random distribution have been found in  $\text{Nb}_2\text{WO}_8$  (Lundberg, *Loc.cit.*). In this study no attempt has been made to refine the Ta/W ratios because tests on the validity of the Gaussian approximation, made on a sample of  $\text{Al}_2\text{O}_3$ , gave a "goodness of fit"  $X$  ranging between 1.0 and 1.3, ie. close to the value of 1.36 obtained for  $R_w/R_e$  for Pbcm. This indicates that our refinements are essentially complete and that it would not be meaningful to refine more detailed models. For the same reason all calculations were carried out assuming perfect stoichiometry.

The final atomic parameters for space group Pbcm are given in table 3 and a comparison of observed and calculated profiles is shown in figure 2.

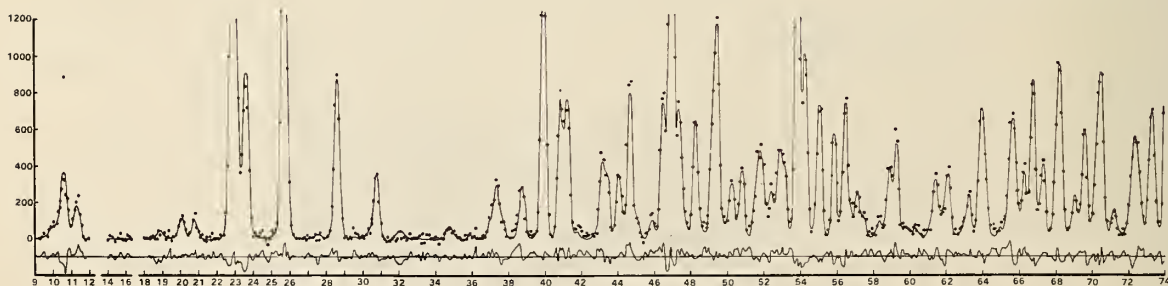


Figure 2. Observed (dots) and calculated (continuous line) profiles. On the lower part of the diagram the curve  $y(\text{obs})$ ,  $y(\text{cal})$  is shown.

In  $\text{Ta}_2\text{WO}_8$ , 5/6 of the metal cations are octahedrally coordinated and they are located in three crystallographically independent positions, two general and one special. The remaining cations are surrounded by seven oxygen atoms in a pentagonal bipyramidal configuration. Octahedra and pentagonal bipyramid are connected by edge sharing, as indicated in figure 3, to form the same structural unit found in the structures of  $\text{Nb}_2\text{WO}_8$ ,  $\text{LiNb}_8\text{O}_{15}\text{F}$ , and numerous other compounds (e.g. Stephenson, 1968).

REACTOR RADIATION DIVISION PROGRAMS

Table 1. Experimental conditions used to collect the powder intensity data for  $Ta_2WO_8$ .

Monochromatic beam: reflection 220 of a Cu monochromator  
(transmission geometry)

Mean neutron wavelength:  $1.5416(3) \text{ \AA}$

Horizontal divergences -

- (i) In-pile collimator: 10 min. arc;
- (ii) Monochromatic beam collimator: 20 min. arc;
- (iii) Diffracted beam collimator: 10 min. arc.

Monochromator mosaic spread:  $\sim 15$  min. arc

Sample container: Vanadium can of  $\sim 1$  cm diameter

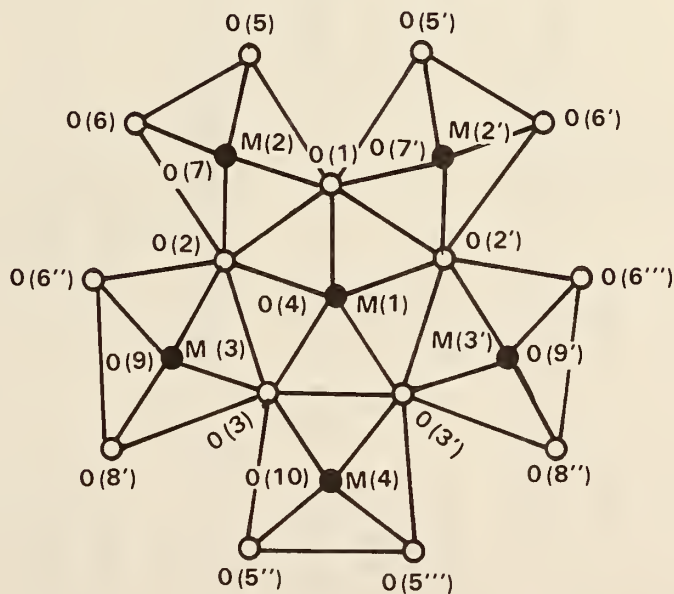


Figure 3. Basic unit in the structure of  $Ta_2WO_8$ . A mirror perpendicular to the plane of figure passes through the atoms O(1), M(1)-O(4), M(4) and O(10).

Table 2. Results of the structural refinements of Ta<sub>2</sub>WO<sub>8</sub> in the space groups Pmma and Pbcm. (\*)

	R - factors(**)							
	R	R <sub>p</sub>	R <sub>w</sub>	N-P+C	wy <sup>2</sup> (obs)x10 <sup>-2</sup>	P	R <sub>E</sub>	R <sub>w</sub> /R <sub>E</sub>
Pmma	8.29	11.32	12.95	1319	2454	30	7.33	1.77
Pbcm	4.67	8.45	10.08	1134	2062	44	7.42	1.36

Lattice and thermal parameters(\*\*\*)

	a	b	c Å	Q <sub>overall</sub> Å <sup>2</sup>
Pmma	16.685 (1)	3.8762(2)	9.9571(4)	0.63(4)
Pbcm	3.8762(2)	17.716 (1)	16.684 (1)	0.46(4)
X-rays	16.70 (1)	3.877 (1)	8.864 (2)	

Profile parameters

	U	V	W deg. <sup>2</sup>
Pmma	0.55(3)	-0.56(3)	0.228(6)
Pbcm	0.59(3)	-0.60(2)	0.236(5)
Calculated	0.21	-0.23	0.11

(\*) These results differ from those reported previously (Santoro, Roth and Minor, 1978) for a powder pattern measured with different experimental conditions. The conclusions in the two cases are

identical, however.

$$\begin{aligned}
 (**) \quad R &= 100 \times \{ \Sigma | I(\text{obs}) - I(\text{cal}) | / \Sigma I(\text{obs}) \} \\
 R_p &= 100 \times \{ \Sigma | y(\text{obs}) - y(\text{cal}) | / \Sigma y(\text{obs}) \} \\
 R_w &= 100 \times \{ \Sigma w [ y(\text{obs}) - y(\text{cal}) ]^2 / \Sigma w [ y(\text{obs}) ]^2 \}^{1/2} \\
 RE &= 100 \times \{ (N - P + C) / \Sigma w [ (\text{obs}) ]^2 \}^{1/2}
 \end{aligned}$$

In the above formulas I are integrated intensities, y the profile intensities of weight  $W=1/[y(\text{obs}) + y(\text{background})]$ , N the number of observations above background, P the number of refined parameters and C the number of constraints.

(\*\*\*) The cell dimension errors obtained in the neutron refinements do not include the error in the neutron wavelength.

REACTOR RADIATION DIVISION PROGRAMS

Table 3. Atomic parameters for Ta<sub>2</sub>WO<sub>8</sub> in space group Pbcm

Atom	X	Y	Z
M(1) (*)	0.016(5) (**)	0.3426(5)	1/4
M(2)	0.019(4)	0.1982(3)	0.1296(4)
M(3)	0.980(3)	0.4061(4)	0.0612(4)
M(4)	0.083(3)	0.0277(5)	1/4
O(1)	0.006(7)	0.2288(4)	1/4
O(2)	0.997(3)	0.3108(3)	0.1307(4)
O(3)	0.995(4)	0.4402(3)	0.1767(4)
O(4)	0.491(6)	0.3456(5)	1/4
O(5)	0.971(3)	0.0972(4)	0.1668(3)
O(6)	0.988(5)	0.1668(3)	0.0224(4)
O(7)	0.484(3)	0.2008(3)	0.1317(4)
O(8)	0	0	0
O(9)	0.519(4)	0.4077(4)	0.0629(5)
O(10)	0.530(5)	0.0229(5)	1/4

(\*) Figures in parentheses are standard deviations in the last decimal figure.

(\*\*) M indicates 0.687 Ta + 0.313W.

REACTOR RADIATION DIVISION PROGRAMS

Table 4. Interatomic distances in the structure of Ta<sub>2</sub>W<sub>10</sub>O<sub>8</sub>. Numbers in parentheses are standard deviations in the last decimal figure. The labeling of the atoms is the one shown in figure 4.

M(1) - M(2)	3.254(9)	O(1) - O(2)	2.467(8)
M(1) - M(3)	3.351(8)	O(2) - O(3)	2.420(8)
M(1) - M(4)	3.30 (1)	O(3) - O(3')	2.45 (1)
M(2) - O(7)	1.81 (2)	M(3) - O(9)	1.79 (2)
M(2) - O(7)*	2.07 (2)	M(3) - O(9) (*)	2.09 (2)
M(2) - O(1)	2.083(7)	M(3) - O(2)	2.050(9)
M(2) - O(2)	1.998(8)	M(3) - O(3)	2.024(9)
M(2) - O(5)	1.905(9)	M(3) - O(6'')	1.902(9)
M(2) - O(6)	1.878(9)	M(3) - O(8')	1.955(7)
M(1) - O(4)	1.84 (3)		
M(1) - O(4) (*)	2.04 (3)		
M(1) - O(1) <sub>1</sub>	2.02 (1)		
M(1) - O(2)	2.072(7)		
M(1) - O(3)	2.122(9)		
M(4) - O(10)	1.74 (2)		
M(4) - O(10) (*)	2.14 (2)		
M(4) - O(3)	1.998(9)		
M(4) - O(5'')	1.908(9)		

(\*)Oxygen atom belonging to the structural unit below the plane of fig. 4.

## REACTOR RADIATION DIVISION PROGRAMS

Some relevant interatomic distances are shown in table 4. The pentagonal bipyramid is quite regular, the O-O distances corresponding to the edges shared with the octahedra vary from 2.420(8) to 2.46(8) Å and the remaining distances from 2.80(3) to 2.88(3). On the other hand, the M<sub>6</sub> octahedra are highly distorted with O-O distances between 2.420(8) and 3.129(8) Å. The average M-O distances of the three octahedrally coordinated cations are 1.957(5), 1.969(6) and 1.950(5) Å, while that for the seven-coordinated cation is 2.041(7) Å. These values agree closely with those found for Nb<sub>2</sub>WO<sub>8</sub> (Lundberg, 1972).

The symmetry of the structural units and the mechanism by which they are connected to form the structure are in general different from compound to compound. In Ta<sub>2</sub>WO<sub>8</sub> and Nb<sub>2</sub>WO<sub>8</sub> they are linked by corner sharing and form layers as the one shown in figure 1. In the third direction the layers are stacked on top of one another, and each polyhedron shares a vertex with the corresponding one of the next layer. The array of corner sharing octahedra creates large tunnels extending in the direction of the  $\alpha$ (Pbcm) axis and surrounded by three or four octahedra rings. Probably these are the locations in which the lithium ions are located in the structures of LiNb<sub>6</sub>O<sub>15</sub>F and of the high-temperature form of LiTa<sub>3</sub>O<sub>8</sub>.

## CRYSTALLOGRAPHY OF RIBONUCLEASE-A

A. Wlodawer

Several sets of neutron diffraction data have been collected on a large deuterated crystal of ribonuclease-A (space group P2<sub>1</sub>,  $a = 30.18$  Å,  $b = 38.4$ ,  $c = 53.32$ ,  $\beta = 105.85^\circ$ , crystal volume 30 mm<sup>3</sup>). Data were collected using the flat-cone diffractometer in equatorial geometry and counting each reflection for 10 min. The agreement between these data sets was good ( $R = 4.8\%$ , defined as  $R = \Sigma |F_1 - F_2| / \Sigma F$ ). Incomplete data to 2.1 Å resolution were collected in the flat-cone mode. An example of the output for several frames is shown in figure 1. The quality of the data

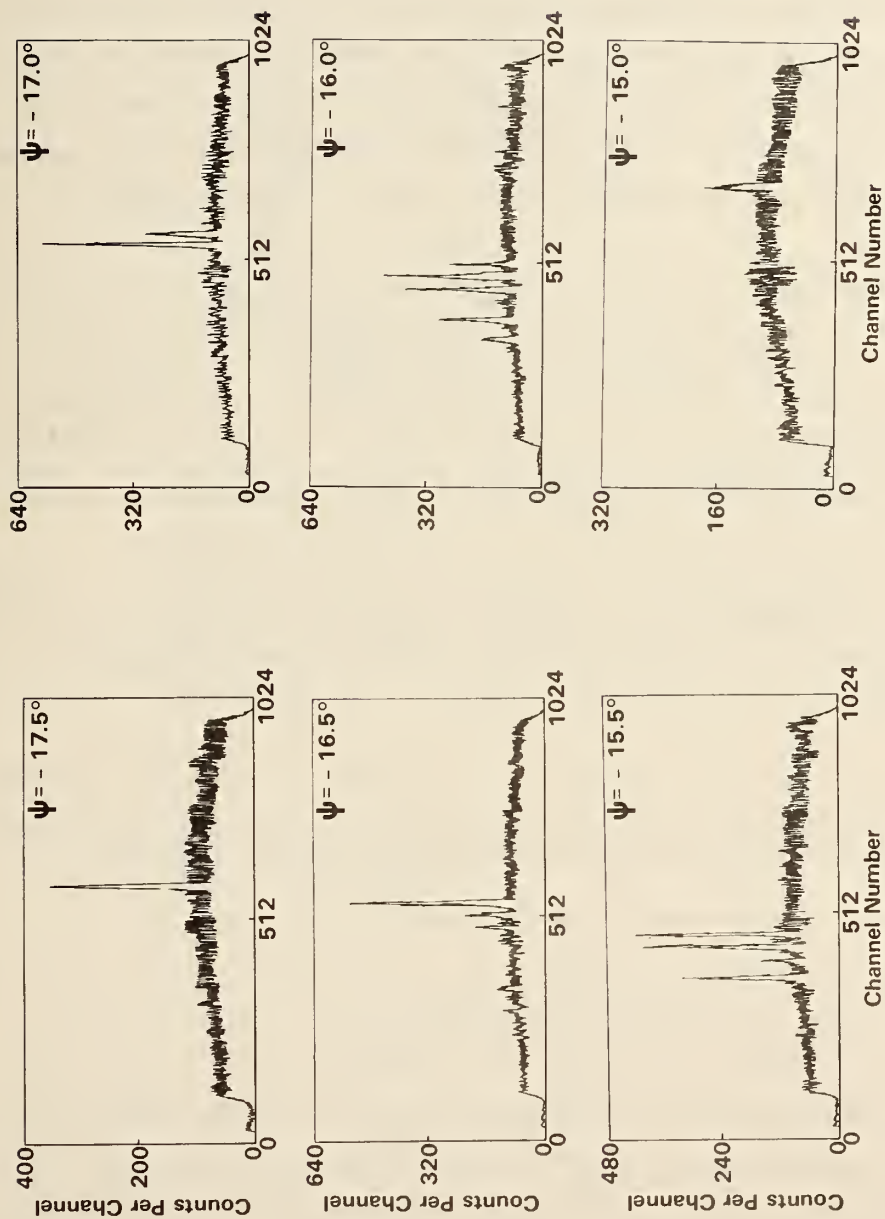


Figure 1. An example of the diffraction patterns of a ribonuclease-A crystal. The data were collected on the flat-cone diffractometer. Each frame was counted for 1 min. and the rotation between frames was  $0.5^\circ$  (during actual data collection  $\psi$  was stepped in the increments of  $0.05^\circ$ ).

## REACTOR RADIATION DIVISION PROGRAMS

was adversely affected by a faulty ADC circuit (since replaced) and the agreement with the lower resolution data was fair ( $R = 9.0\%$ ).

X-ray diffraction data on identically treated ribonuclease crystals were also collected to  $2.5 \text{ \AA}$  resolution. The comparison with the data collected on similar crystals by Carlisle et al.<sup>2</sup> suggested that there are some small differences in the conformation of protein molecules, due to different solvent and deuteration (manifested by high R factor of  $11.2\%$ ).

We are planning to run several cycles of refinement of x-ray structure of Carlisle et al. using structure amplitudes collected by us to obtain the best starting model for neutron refinement. This will be followed by refinement of the  $2.8 \text{ \AA}$  neutron data and later  $2.1 \text{ \AA}$  data, when the latter set has been recollected.

- 
1. E. Prince, A. Wlodawer and A. Santoro, *J. Appl. Cryst.* 11, 167 (1978).
  2. C. H. Carlisle, R. A. Palmer, S. K. Mazumdar, B. A. Gorinsky and D. G. R. Yeates *J. Mol. Biol.* 1 (1974).

### ROTATIONAL DYNAMICS AND PHASE TRANSITIONS IN $(\text{KCN})_x (\text{KBr})_{1-x}$

J. M. Rowe and J. J. Rush

and

S. Susman and D. Hinks

(Argonne National Laboratory, Argonne, IL)

Work is continuing on this interesting set of mixed crystals. Since last year, further measurements on the  $(\text{KCN})_{0.25} (\text{KBr})_{0.75}$  crystals have led us to the explanation of the results reported last year - namely that the energy of the [100] TA modes initially decrease with decreasing temperatures, then increase for even lower temperatures. The new results are shown in figure 1. As can be seen in the figure, the energy of the modes decreases, then increases as T is reduced from

## REACTOR RADIATION DIVISION PROGRAMS

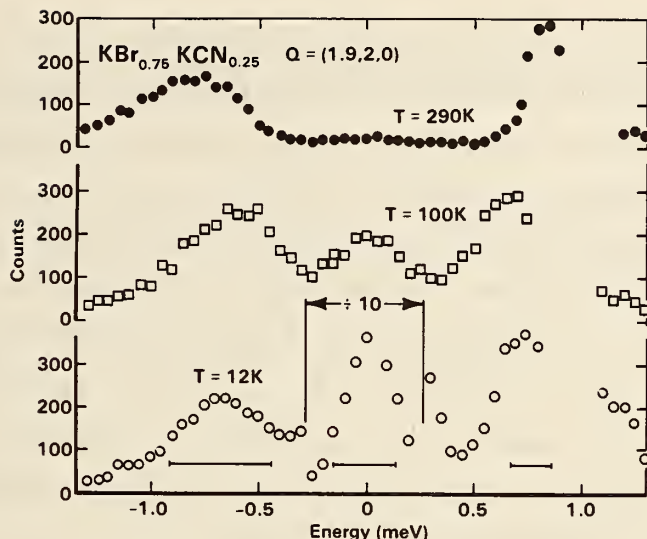


Figure 1. Neutron scattering line shapes in  $(\text{KCN})_{0.25}(\text{KBr})_{0.75}$  for transverse acoustic phonons propagating along a  $[100]$  axis. Note the existence of an experimental contaminant near energy transfers of  $+0.8$  meV (contaminated points are omitted). There is no contamination for negative energy transfers (neutron energy gain). The data are uncorrected for resolution effects. The size of the resolution is shown by the horizontal bars.

300K to 100K to 12K. At the same time, the scattering at  $\hbar\omega=0$  (elastic scattering) increases anomalously over the same temperature range as the phonon energy increases again.

It is this behavior which provides the clue to the origin of the effect. As has been pointed out previously, there is a strong coupling in alkali cyanide crystals between the acoustic phonons (particularly  $[100]$  TA) and the reorientation of the cyanide ions. A central parameter in the theory of these systems (as derived by Michel and Naudts in collaboration with the present authors) is the ratio of the reorientation rate ( $1/\lambda$ ) to the bare (unperturbed) phonon frequency  $\omega_0$ . For  $\omega_0 \gg 1/\lambda$ , one expects the central peak critical scattering behavior shown by  $\text{ND}_4\text{Dr}$  while for  $\omega_0 \ll 1/\lambda$ , one expects the soft mode behavior shown by KCN. However,  $1/\lambda$  is related both to collective behavior and to single particle behavior. If the temperature is reduced,  $1/\lambda$  decreases

## REACTOR RADIATION DIVISION PROGRAMS

(in one approximation, exponentially as  $1/\lambda\alpha e^{-\lambda K}$ ). Thus, if the temperature can be lowered far enough,  $1/\lambda$  will always be much less than  $\omega_0$ . In KCN, one cannot reach this regime because of the phase transition at 168K. However, in (KCN)<sub>.25</sub> (KBr)<sub>.75</sub> there is no phase transition and we can observe both regimes in the same system. Thus, these mixed crystals offer an almost perfect model system for studying the temperature behavior of coupled phonon - reorientation systems.

The experimental configuration used for these experiments is of some interest since high energy resolution and moderately high momentum transfer are required. We met these requirements by using 20-20-20-20 collimation and [004] pyrographite for both monochromator and analyses, at a  $2\theta$  of  $90^\circ$  for a total resolution of 0.2 meV for elastic scattering, with better intensity than could be obtained for 10-10-10-10 collimation which would have had worse resolution.

We are continuing this work and have a 50% crystal on which measurements are just beginning. We have also studied a sample of 0.4% KCN in KBr and are presently analysing the data. In general, the data are similar to the results of Nicklow at Oak Ridge on KCN in KCl.

### CN<sup>-</sup> IONS IN KCl, KBr

R. C. Casella

Motivated by neutron scattering experiments currently being carried out at the NBS Reactor by J. J. Rush and J. M. Rowe, I have begun a theoretical analysis of the dilute CN<sup>-</sup> substitutional impurities in KCl and KBr. One aspect of the analysis has to do with infrared experiments done elsewhere<sup>1</sup> with a view towards helping to sort out the possible CN<sup>-</sup> low temperature equilibrium orientations, e.g.  $\langle 111 \rangle$  vs.  $\langle 100 \rangle$ . I assume that the internal stretch modes are excited by the infrared and that under

## REACTOR RADIATION DIVISION PROGRAMS

Table 1. Values for the intensity ratio R under various experimental conditions (see text).

Strain s	Polarization $\epsilon$	Model CN <sup>-</sup> dipole alignments			Experiment <sup>a</sup>
		<100>	<110>	<111>	
[100]	$\epsilon    s$	0	0	1	1 <sup>b</sup>
	$\epsilon \perp s$	3/2	3/2	1	1 <sup>b</sup>
[111]	$\epsilon    s$	1	0	1/3	0.33
	$\epsilon \perp s$	1	3/2	4/3	1.15 <sup>c</sup>
[110]	$\epsilon    s$	0	0	0	0.1
	$\epsilon \perp s, \epsilon    [1\bar{1}0]$	0	3	2	—
	$\epsilon \perp s, \epsilon    [001]$	3	0	1	1

<sup>a</sup>Data from Reference 1. Maximum applied stress equals 600 dynes/cm<sup>2</sup> unless otherwise noted.

<sup>b</sup>maximum stress = 200 dynes/cm<sup>2</sup>.

<sup>c</sup>maximum stress = 100 dynes/cm<sup>2</sup>.

compressive applied stress the CN<sup>-</sup> dipoles tend to occupy those positions in the original equilibrium set which lie most nearly perpendicular to the applied-stress axis. Under various conditions of applied stress and for various polarizations  $\epsilon$  of the infrared excitation, values of the saturation ratio R of absorbed intensities are calculated for models in which the equilibrium CN<sup>-</sup> orientations are assumed to lie along the <100>, <110>, and <111> axes, respectively:

## REACTOR RADIATION DIVISION PROGRAMS

$$R = \frac{\text{(intensity of infrared absorption under saturation stress)}}{\text{(intensity of infrared absorption under no applied stress)}}$$

The calculated values of R are presented in Table 1 along with data.<sup>1</sup> These values are obtained ignoring the small ( $\sim 1 \text{ cm}^{-1}$ ) tunnel splittings, in effect summing over the intensities of the submultiplets. Whereas the results in table 1 indicate that the  $\langle 111 \rangle$  orientations are favored, there is controversy among the infrared experiments as indicated in reference 1, whence the issue is not settled. It is hoped that the neutron scattering experiments, which presumably give a measure of the interaction of the phonon modes with the local librionic and/or tunneling motions of the  $\text{CN}^-$  ions, will shed further light on this matter. In this connection, we expect that detailed tight-binding symmetry-projected tunneling states for the most probable  $\langle 111 \rangle$  and  $\langle 100 \rangle$  orientations will be of use, both for the librational ground states of the  $\text{CN}^-$  ions and also for states in which, in addition to the tunneling motion, the ions undergo rapid librational-like oscillations in each potential well with a frequency much greater than the tunneling frequency.

---

1. F. Luty, *Phys. Rev. B* 10, 3677 (1974).

## NEUTRINO SCATTERING AND WEAK-INTERACTION GAUGE THEORIES

R. C. Casella

The idea that scaling violations not accounted for in the original parton model of Feynman would allow an interpretation of diverse data on neutrino scattering without the necessity of introducing right-handed  $(V + A)$  charged-current Fermi couplings,<sup>1</sup> appears to be experimentally correct, although the amount of scale breaking required is not yet settled.

## REACTOR RADIATION DIVISION PROGRAMS

This understanding includes the neutrino and antineutrino induced (oppositely signed) dileptons, the latter in association with charm production off the strange component of the parton sea.<sup>1</sup> Moreover, the  $SU(2)_L \times U(1)$  gauge theory of Weinberg and Salam (WS) is in accord with the neutral-current neutrino scattering data, again without the necessity of introducing appreciable coupling to the heavy quark associated with the up-silon resonance.<sup>1</sup> There remains the (experimentally controversial) absence of parity violation by the neutral currents in atomic bismuth,<sup>2</sup> which runs counter to the predictions of WS. I have examined a popular version of the generalized  $SU(2)_L \times SU(2)_R \times U(1)$  gauge theories which have been proposed to explain this possible discrepancy. It is concluded that in the Higgs sector the relation  $\text{Trace} \langle \rho^\dagger \rangle \langle \rho \rangle = \text{Trace} \langle \phi^\dagger \rangle \langle \phi \rangle$ , which is required (in the model examined) to reproduce the successful WS predictions for neutral-current neutrino scattering, does not have a natural basis. This conclusion seems to hold even when (ignoring possible renormalization difficulties) the Higgs scalars  $\rho$  and  $\phi$  are treated as different composites of common fermion fields. Very recent polarized electron-deuteron scattering experiments at Stanford<sup>3</sup> tend to confirm the original WS theory, which was employed in the analysis of the neutrino scattering data in reference 1.

- 
1. R. C. Casella *Il Nuovo Cimento* 42A, 377 (1977).
  2. For nearly two years, two independent atomic physics groups, one at Oxford University and the other at the University of Washington at Seattle, have reported no parity violation at a level well below that predicted by the WS theory. Recently L. M. Barkov and M. S. Zolotarev [*Zh. Esep. Teor. Fig. Pis'ma Red* 26, 379 (1978)] report otherwise.
  3. Sinclair (private communication).

## ISOTOPIC SHIFTS OF PHONONS

R. C. Casella

To our prior work in which the molecular product rule for isotopically substituted systems was shown to hold at arbitrary wave vector  $\vec{q}$  in a periodic crystal,<sup>1</sup> we have added new inequalities relating the sums of squares of the eigenfrequencies  $\omega$  and  $\tilde{\omega}$  associated with isotopic masses  $M$  and  $\tilde{M}$ , respectively. We find for a crystal of point ions

$$x^2 \sum_{\gamma} \omega^2(\vec{q}r\gamma) < \sum_{\gamma} \tilde{\omega}^2(\vec{q}r\gamma) < \sum_{\gamma} \omega^2(\vec{q}r\gamma), \quad (1)$$

where  $r$  denotes the irreducible representation of the little group at  $\vec{q}$ ,  $\gamma$  enumerates different modes belonging to the same  $(r, \vec{q})$ , and  $x^2$  is the mass ratio of the substituted isotopes. That is,

$$x = (M/\tilde{M})^{1/2}, \quad (2)$$

where  $\tilde{M}$  signifies the heavier mass ( $x < 1$ ). For a crystal of extended molecules, treated as rigid, we find

$$\min \left\{ \begin{array}{l} x^2 \sum_{\gamma} \omega^2(\vec{q}r\gamma) \\ y^2 \sum_{\gamma} \omega^2(\vec{q}r\gamma) \end{array} \right. < \sum_{\gamma} \tilde{\omega}^2(\vec{q}r\gamma) < \sum_{\gamma} \omega^2(\vec{q}r\gamma), \quad (3)$$

where  $y^2$  is the ratio of the moments of inertia of the substituted species (assumed isotropic).

$$y = (I/\tilde{I})^{1/2} \leq 1. \quad (4)$$

The analysis was applied to the Raman spectrum of ammonium perchlorate

## REACTOR RADIATION DIVISION PROGRAMS

where the shifts under deuteration have been studied (at  $\vec{q} = 0$ ) by H. Prask and G. Rosasco at NBS. The analysis containing the product rule, the inequalities, and their application to the perchlorates was submitted for publication.<sup>2</sup> Application to  $\text{NH}_4\text{Cl} - \text{ND}_4\text{Cl}$  at general  $\vec{q}$  is anticipated.

- 
1. R. C. Casella, *NBS Technical Note No. 969*, (ed., F. J. Shorten, 1978).
  2. R. C. Casella, *Phys. Rev. B* 17, 3381 (1978).

## NEUTRON RADIOGRAPHY

D. A. Garrett

### 1. Internal NBS Activities

#### a. Facilities Development

A large effort has been devoted to the construction of the thermal column neutron radiography facility. The system has been completed with the exception of the He-filled drift tube. The significant factors this system has contributed to the NBSNR are (a) neutron radiography may be conducted without affecting the background which could affect neighboring experiments, (b) the focal-plane shutter makes it possible to make exposures ranging in time from infinity to 0.1 sec., and (c) the entire system is mounted on tracks, facilitating removal to provide space for other thermal column experiments.

#### b. Fracture and Deformation Division

Hydrided and unhydrided standard steel samples and specimens from ruptured petrochemical pressure vessels have been submitted to this group for neutron radiography in an attempt to visualize the hydride areas of the pressure vessels. Conventional neutron radiographic techniques have yielded negative results due to the high scattering cross section of Fe. This will possibly result in an ongoing program in the FY-79. Plans

## REACTOR RADIATION DIVISION PROGRAMS

are presently being made to collaborate with G. Tuckey at the Atomic Weapons Research Establishment at Aldermustern, England to employ cold neutrons from that radiographic facility to attempt to visualize the hydride layers.

### c. Building Technology

A collaborative effort is in progress with personnel of Building Technology to design experiments to assess the performance of neutron backscatter gages for the determination of water buildup in flat-topped building roofs. The role played by our staff is strictly advisory and will probably be terminated once that Building Technology personnel have been trained in the use of the instrumentation and correct assessment of the data.

### d. Composite Materials

This group has been asked to participate in the NBS composite materials program both in graphite resin and metal composite technology. Although no work has been conducted internally in these areas, evidence exists that neutron interrogation could play an important role in the destructive and nondestructive evaluation of these materials. Such problems exist as the breaking of reinforcing graphite or boron fibers in the materials under investigation, water migration through composite materials and lack of bond. Should positive results be obtained, it appears that this will be an ongoing problem. On a recent tour of the NBS Research Reactor, members of the Aerospace Industries Association indicated that the problems were many and felt that neutron NDE would be a useful methodology.

## 2. Outside Agency Activities

### a. NASA Goddard Space Flight Center - Graphite-Boron Composite Materials.

Samples of graphite-boron reinforced composite materials were submitted to this group for neutron radiographic interrogation. The graphite thickness was approximately .062 in. The filaments were not discernable to the human eye, however the spacing could be detected with microdensitometer scans of the thermal neutron radiographs. This was a

## REACTOR RADIATION DIVISION PROGRAMS

one-shot experiment and will not be an ongoing program.

- b. NASA Goddard Space Flight Center - Graphite-Resin Composite Materials.

Samples of graphite-resin composite materials were submitted to this group for neutron radiographic interrogation, to determine if resin richness or poorness could be detected. The samples were approximately 0.25 inches thick. The differences in the two samples could be discerned both radiographically and instrumentally with microdensitometry scanning of the radiograph. The possibility exists that this will be an on-going program on a OA contract basis.

- c. NRC - Measurements for Nuclear Safeguards.

The design and purchase of the electronics and scanning system for the resonance neutron radiography system has been completed. Design of the collimator and experimental cavity is in progress. Dr. Yu Tavang Cheng has been selected to fill the Nuclear Safeguards slot in the Reactor Radiation Division. Dr. Cheng obtained his Ph.D. in nuclear physics from the University of Oregon and possesses extensive experience in Fortran computer programming. He presently holds a Postdoctoral Fellowship at Johns Hopkins University and is working with Madam Dr. Wu's group at Columbia. His obligation to Johns Hopkins ended at the middle of September. We expect to hire Dr. Cheng as soon as possible contingent on his being granted U.S. Citizenship.

The Los Alamos simulation contract has been issued. The Albuquerque DOE fiscal officer has required that some changes be made. For instance, the DOE would prefer to bill our program on a monthly manpower usage basis. This should present no problem to the NBS. A detailed communication outlining the procedure to be followed has been received.

Personnel from the Neutron Field Standards Group are cooperating in this project by supplying fission detectors for the final system.

All indications are that this activity will be an on-going program at approximately \$70,000 per year plus inflation. The group received 10 percent of the general equipment budget for FY-1979.

## REACTOR RADIATION DIVISION PROGRAMS

### d. FDA Cardiac Pacemaker Battery Studies.

This group has received a \$15,000 contract to study the physical behavior of lithium iodine pacemaker battery dielectric behavior as a function of battery depletion over a 1.5 year period. The pacemaker batteries will be neutron radiographed at 3 month intervals over the projected lifetime of the batteries.

Three dimensional laminagraphy of one set of batteries at various stages of depletion has confirmed that void formation does occur in the electrolyte. Whether this is caused by pressurized gas at this point is purely conjecture until destructive analysis can be made. It is well established that Li-SO<sub>2</sub> power systems violently explode once void formation in the electrolyte begins. Chemists, however, at the manufacturer of the cells presently under examination state that there is no known mechanism by which void formation can take place in the solid dielectric used in pacemaker batteries.

### e. NAVAIR Screen Development

Work on the NAVAIR screen development project has lagged primarily due to the fact that much of the information is proprietary and that delivery of components is slow. Preliminary experiments with uv curing adhesives as a binder indicate that this procedure may be promising - however insufficient data is available at this time to make a definite statement. This could be an ongoing project.

### f. National Art Gallery - Smithsonian Institution

A proposal has been submitted by the Conservation Analytical Laboratory of the Smithsonian Institution to the National Art Gallery for the NBS to participate in neutron-induced autoradiography program for authentication and attribution of Old Masters and Early American Primitive paintings. The initial contract to the NBS would be \$22,000 for a two-month feasibility study. At the same time, a proposal is being submitted to other funding agencies for an on-going program.

g. Royal Military College of Canada

A transportable field neutron radiography system designed by the author is presently operational in Canada. The design of the system was unique in the Cf-251 source is exposed to the object under inspection, resulting in gamma fogging of the film in the direct exposure mode. The rationale for this design was that the gamma fogging can be subtracted from the composite radiograph, resulting in the production of a pure thermal neutron radiograph. Cooperative experiments are in progress to determine whether or not this can be attained in the darkroom.

3. Addendum: Symposium on Real-Time Radiologic Imaging: Medical and Industrial Applications

The author co-chaired this symposium May 8-10, 1978 with Mr. Donald Bracher of the Old Delft Corporation. In our activities in radiologic imaging, it was obvious that scientists in the medical and industrial sectors were making real strides in the development of this technology, however they were not sharing information. It was the purpose of this symposium to bring these two communities together on a common ground in which an exchange of ideas would result.

There were a total of thirty-one papers, twenty-five of which were by invited authors who were world experts in some facet of the technology.

There were a total of 230 attendees at the symposium. Eighty-three percent of the authors submitted manuscripts which will be published as a special ASTM publication in approximately nine months.

## B. RRD COLLABORATIVE PROGRAMS

### APPLICATION OF NEUTRON DIFFRACTION TO NON-DESTRUCTIVE TESTING PROBLEMS

C. S. Choi, H. J. Prask and S. F. Trevino  
(Energetic Materials Division, LCWSL, ARRADCOM, Dover, NJ)

and

(National Bureau of Standards, Washington, DC)

and

H. A. Alperin  
(Naval Surface Weapons Center, White Oak, MD)

and

(National Bureau of Standards, Washington, DC)

and

C. Bechtold  
(Metal Science and Standards Division)

The Army group at the NBSR has been engaged in a continuing program to determine "texture" (i.e., grain orientation) as a function of depth, nondestructively, in the copper liner component in shaped-charge munitions. Because the liner of interest is only 0.28 cm thick, a "difference" technique has been developed which utilizes the fact that for a given crystallographic plane, and appropriate masking, different volumes (depths) are sampled when different neutron wavelengths are employed. Alternatively, the same effect is achieved at a fixed wavelength by examining different order reflections for a given plane.<sup>1,2</sup>

Initial results have now been obtained for a shaped-charge liner, divided into "top" (0.5mm thick) and "bottom" (below 0.5mm depth) layers. Pole density distributions are shown in figures 1(a) and 1(b) for (100) and (111) planes, respectively. Although preliminary in nature, the results are in qualitative agreement with (destructive) x-ray texture studies for similarly fabricated liners.

The difference technique has also been applied to the determination



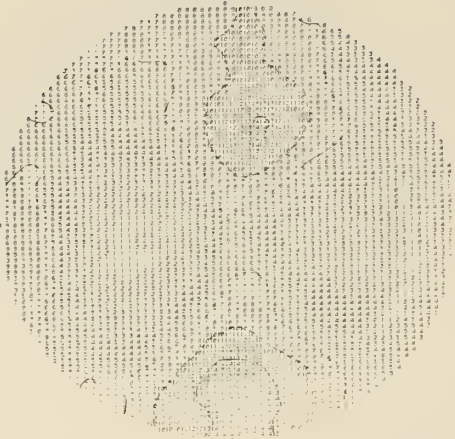
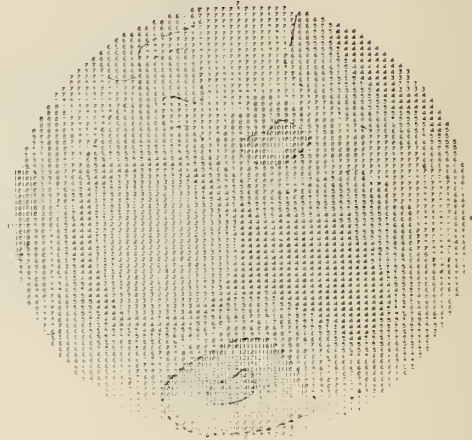
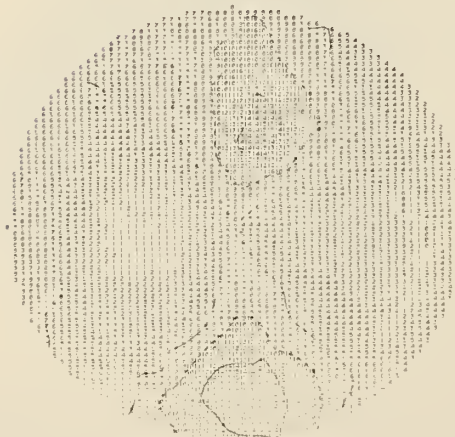
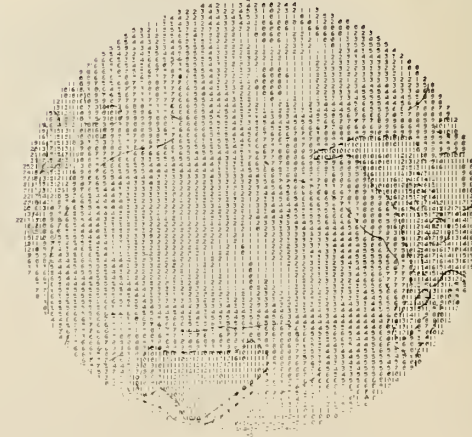
**(b) (111) Bulk****(222) Bulk****(111) Top Layer****(111) Bottom Layer**

Figure 1. "Continued".

of texture as a function of depth in an aluminum cylinder fabricated for use as an ultrasonic standard reference block. In this case, the "top" layer corresponds to a 0.1 cm thick surface layer, and the "bottom" layer extends from 0.1 cm to a maximum depth of 0.5 cm. Pole figures, shown in figure 2, indicate little change in texture as a function of depth. However, considerable anisotropy is observed in the ring of the secondary maximum ( $\alpha \approx 65^\circ$ ). The fact that the block was rejected as an

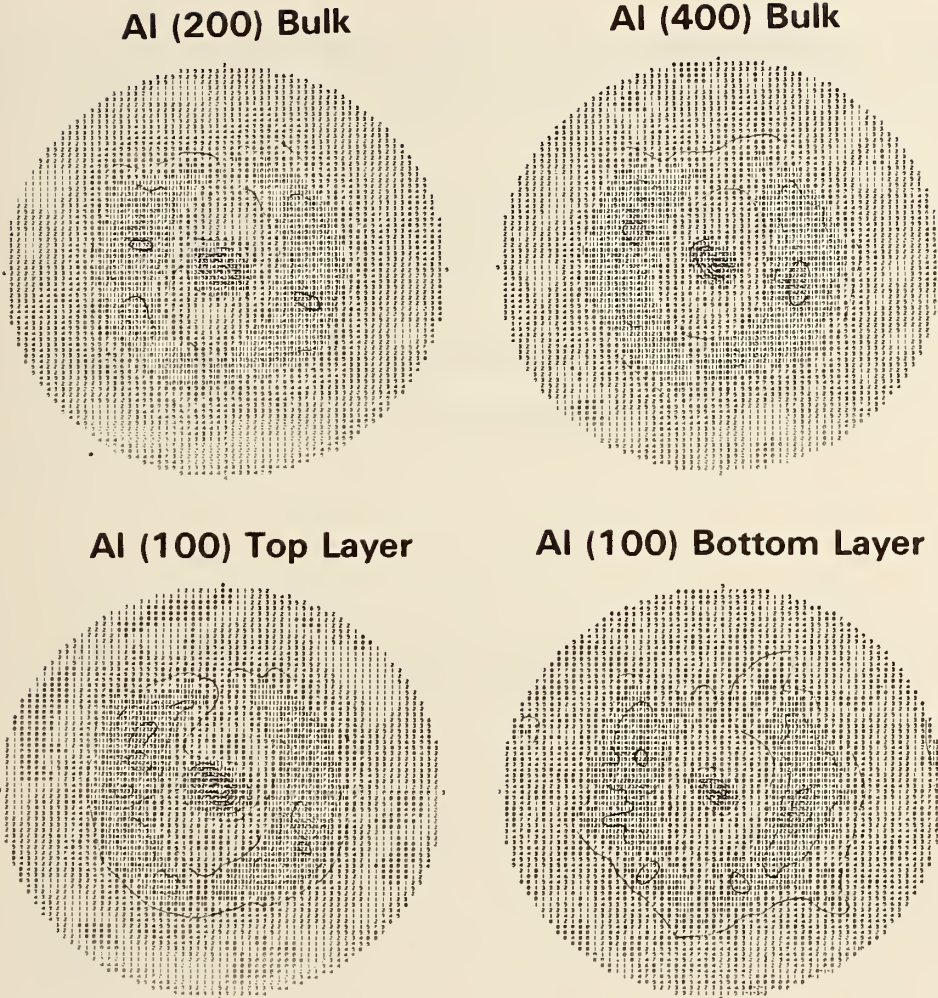


Figure 2. Pole density distribution for the flat surface of a cylindrical aluminum standard reference block. "Top" layer corresponds to a depth of  $\leq 0.1$  cm; "bottom" layer to the region  $\sim 0.1$  cm to  $\sim 0.5$  cm for  $35^\circ < \alpha < 90^\circ$ .

ultrasonic standard may be correlated with this texture anisotropy.

In the area of residual stress determination, our program is aimed toward the nondestructive determination of residual stress gradients within the bulk of metallurgical samples. However, work to date has focused on demonstrating that precision and reproducibility of the neutron diffraction technique is sufficient for residual stress characterization.

RRD COLLABORATIVE PROGRAMS

In figure 3 are shown strain vs. stress results for a 1.59 cm diameter steel rod (AISI 1017) stressed in tension. Data for (310) and (211)

Table 1. Comparison of  $\nu/E$  vs. stress for a carbon steel.

Crystal Plane	Bulk	Neutron Diffraction	Theoretical <sup>A)</sup>
(310)		$1.56 \pm 0.02$	1.69
	1.35		
(211)		$1.19 \pm 0.02$	1.25

A) E. Kroner, Z. Physik 151, 504 (1958); F. Bollenrath et al., Z. Metallkde. 58, 76 (1967).

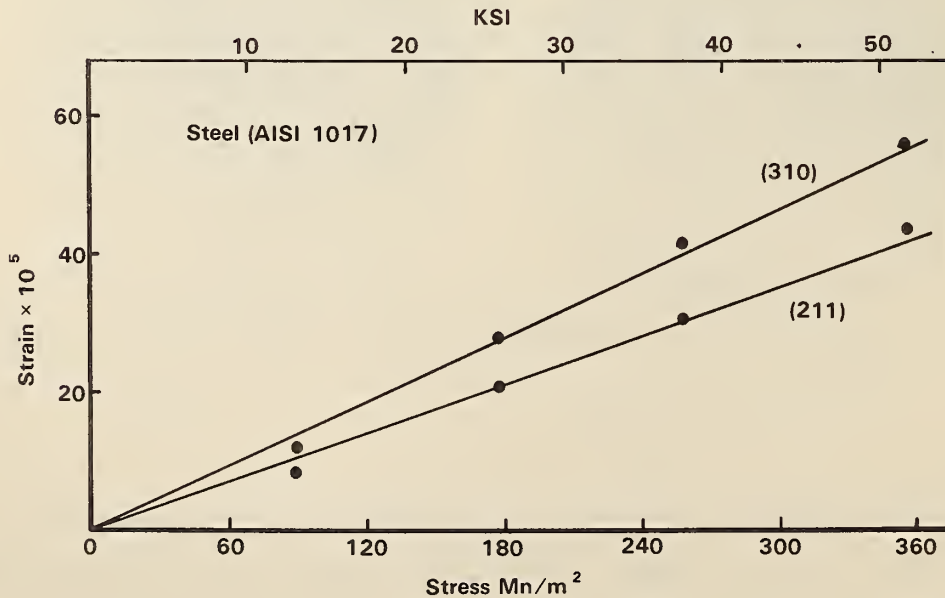


Figure 3. Strain vs. stress for a 1.59 cm diameter steel rod in tension.

## RRD COLLABORATIVE PROGRAMS

planes are shown. In table 1, a comparison of  $\nu/E$ , obtained from the slope of the strain vs. stress data, is made with theoretical predictions for a "plain carbon steel." These results confirm that the precision and reproducibility of the neutron diffraction technique is sufficient for residual stress characterization.

- 
1. Prask et al., *NBS Tech. Note 969*, p. 73 (1978).
  2. C. S. Choi, H. J. Prask and S. F. Trevino, *J. Appl. Cryst.*, to be published.

### HIGH TEMPERATURE STRUCTURE OF $\text{NH}_4\text{NO}_3$ (PHASE II)

C. S. Choi

(Energetic Materials Division, LCWSL, ARRADCOM, Dover, NJ)

and

(National Bureau of Standards, Washington, DC)

It is well known that solid ammonium nitrate exists in five different phases. The phase II form is stable at the temperature between  $84^\circ\text{C}$  and  $125^\circ\text{C}$  and crystallizes in tetragonal cell with  $P4_2m$  space group. A few years ago we had proposed a probable structure for phase II in conjunction with the structure of phase IV. This study was undertaken to confirm the proposed structure by means of profile refinement of neutron powder diffraction data. Triple axis spectrometer, equipped with  $\text{Cu}(111)$  monochromator and graphite (400) analyzer, was used for the measurement to reduce the incoherent background from hydrogen atoms. Using  $1.5357 \text{ \AA}$  neutrons, diffraction intensities were measured from  $10^\circ$  to  $120^\circ$  with  $0.1^\circ$  step. The position of the data contaminated by aluminum peaks from the sample container was removed from the refinement. The structure was refined by using a modified version of Riethveld's profile refinement program, with anisotropic thermal parameters for oxygen atoms and ammonium nitrogen. The final R-indices were rather high,  $R_1=9.89$   $R_2=19.54$   $R_3=17.35$

for expected  $R=9.47$ , which may be attributable to the poor counting statistics of the data due to the intense background and also to the anharmonic thermal motions of both ions. The refined cell parameters are  $a=5.695(1)$  and  $c=4.912(1)\text{\AA}$ . The structure is made of two dimensional hydrogen bond chain network running between  $O(1)$  atom and four hydrogens of an ammonium group, which is the same network observed in phase IV structure except slight increase in the bond length ( $2.05$  and  $2.16\text{\AA}$  in phase IV to  $2.33\text{\AA}$  in phase II). The final structure parameters are given in table 1. Figure 1 shows the thermal ellipsoids of nitrate group atoms, which indicate clearly an intense librational motion about the central nitrogen within the molecular plane. If this libration is a hindered rotation-type motion, the molecule must possess three equivalent  $O-N$  bonds (or trigonal symmetry). The observed  $N-O$  bond lengths were  $1.12(2)\text{\AA}$  for the two  $N-O(2)$  bonds with resonating double bond character, and  $1.47(2)\text{\AA}$  for the  $N-O(1)$  bond (single bond) which is also consistent with the hydrogen

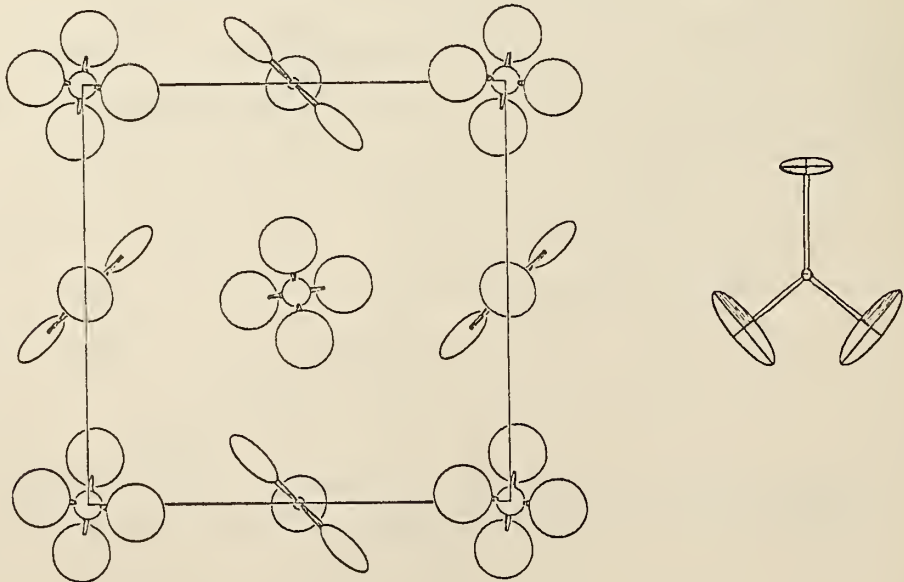


Figure 1. Structure of ammonium nitrate viewed along the  $c$ -axis direction and a nitrate anion viewed along the plane normal direction. The thermal ellipsoids are scaled to include 20% probability.

## RRD COLLABORATIVE PROGRAMS

bonds formation of the O(1)<sup>-</sup> atom. Hence this study is inconsistent with the hindered rotor model of NO<sub>3</sub> ion in phase II structure.

Table 1. Positional and thermal parameters in NH<sub>4</sub>NO<sub>3</sub>, phase II at 100°C.  
(\* indicates isotropic temperature factor B)

Atom	<u>X</u>	<u>Y</u>	<u>Z</u>	<u>B<sub>11</sub></u> (=B <sub>22</sub> )	<u>B<sub>33</sub></u>	<u>B<sub>12</sub></u>	<u>B<sub>13</sub></u> (=B <sub>23</sub> )
NH	0.	0.	0.	2.9(3)	11.4(8)	0.	0.
H	-.018(8)	-.112(3)	.139(3)	12.(1)*			
NO	0.	.5	.497(2)	.5(1)*			
O(1)	0.	.5	.198(3)	11.(1)	1.(1)	-1.(1)	
O(2)	.106(2)	.606(2)	.644(4)	8.(1)	20.(2)	6.(1)	-10.(1)

## REFINEMENT OF DIPARA-ANTHRACENE STRUCTURE

C. S. Choi

(Energetic Materials Division, LCWSL, ARRADCOM, Dover, NJ)

and

(National Bureau of Standards, Washington, DC)

This study was intended to supplement the earlier work by Ehrenburg (1969) which is based on two sets of Weissenburg data and hence is less accurate. A total of 1609 independent reflection data were collected within the sphere of  $\sin\theta/\lambda$  less than  $0.65\text{\AA}^{-1}$ , using  $M\sigma\text{-K}\alpha$  radiation. Using combination of direct method and Fourier synthesis, a complete structure including hydrogen atoms was solved. Subsequent least squares refinement reduced the R-indices to  $R=0.045$  and  $R_w=0.05$  for 1019 observable intensity reflections. The unit cell obtained were  $a=12.085(4)$ ,  $b=18.853(7)$  and  $c=8.139(3)$  in Pbc<sub>a</sub> space group. The final least squares parameters are given in table 1. The bond lengths are given in figure 1. The benzene ring in either end of anthracene molecule is very close to regular hexagon with the bond length of  $1.39\pm 1\text{\AA}$  and bond angle of  $120\pm 1^\circ$ .

RRD COLLABORATIVE PROGRAMS

Table 1. Final least squares parameters for dipara-anthracene. The thermal parameters for the heavy atoms

have the form:

$$\exp[2\lambda^2 \{U_{11}(a^*h)^2 + U_{22}(b^*k)^2 + U_{33}(c^*l)^2 + 2(U_{12}a^*b^*hk + U_{13}a^*c^*hl + U_{23}b^*c^*kl)\}]$$

Atom	X	Y	Z	U <sub>11</sub>	U <sub>22</sub>	U <sub>33</sub>	U <sub>12</sub>	U <sub>13</sub>	U <sub>23</sub>
C1	.4066(3)	.1289(2)	.2321(4)	.054(2)	.056(2)	.047(2)	-.008(2)	.006(2)	-.007(2)
C2	.3106(3)	.1672(2)	.1946(5)	.063(2)	.056(2)	.064(2)	.003(2)	.010(2)	-.001(2)
C3	.2362(3)	.1407(2)	.0813(5)	.052(2)	.069(3)	.062(2)	.006(2)	.007(2)	-.001(2)
C4	.2549(3)	.0755(2)	.0062(4)	.039(2)	.075(3)	.044(2)	-.004(2)	-.001(2)	.001(2)
C5	.3900(3)	-.1543(2)	.1037(4)	.058(2)	.054(2)	.051(2)	-.010(2)	.004(2)	-.006(2)
C6	.4373(3)	-.1977(2)	.2229(5)	.079(2)	.048(2)	.059(2)	-.008(2)	.011(2)	-.002(2)
C7	.5152(3)	-.1714(2)	.3305(5)	.073(3)	.056(2)	.054(2)	.004(2)	.006(2)	.004(2)
C8	.5458(3)	-.0999(2)	.3219(4)	.052(2)	.063(2)	.045(2)	.001(2)	.004(2)	.001(2)
C9	.5310(3)	.0217(2)	.1851(4)	.041(2)	.053(2)	.039(2)	-.006(2)	-.006(2)	-.004(2)
C10	.3787(3)	-.0333(2)	-.0391(4)	.041(2)	.056(2)	.044(2)	-.011(2)	-.004(2)	-.004(2)
C11	.4221(3)	-.0334(2)	.0921(4)	.046(2)	.051(2)	.040(2)	-.008(2)	.003(2)	-.004(2)
C12	.5000(3)	-.0563(2)	.2035(4)	.043(2)	.052(2)	.040(2)	-.003(2)	.003(2)	-.002(2)
C13	.4262(3)	.0641(2)	.1556(4)	.045(2)	.052(2)	.039(2)	-.009(2)	.003(2)	-.001(2)
C14	.3496(3)	.0367(2)	.0429(4)	.041(2)	.054(2)	.041(2)	-.009(2)	.003(2)	.001(2)
H1	.4748(32)	.1522(20)	.3138(47)	7.0					
H2	.2950(33)	.2193(20)	.2523(57)	7.6					
H3	.1568(34)	.1723(23)	.0521(50)	7.6					
H4	.1990(33)	.0569(21)	-.0841(50)	7.6					
H5	.3199(32)	-.1773(22)	.0179(51)	7.0					
H6	.4151(31)	-.2537(22)	.2285(53)	7.6					
H7	.5548(33)	-.2065(21)	.4201(51)	7.6					
H8	.6140(33)	-.0793(20)	.4043(50)	7.0					
H9	.5725(32)	.0407(20)	.2983(51)	7.0					
H10	.3040(33)	-.0581(21)	-.0935(51)	7.0					

RRD COLLABORATIVE PROGRAMS

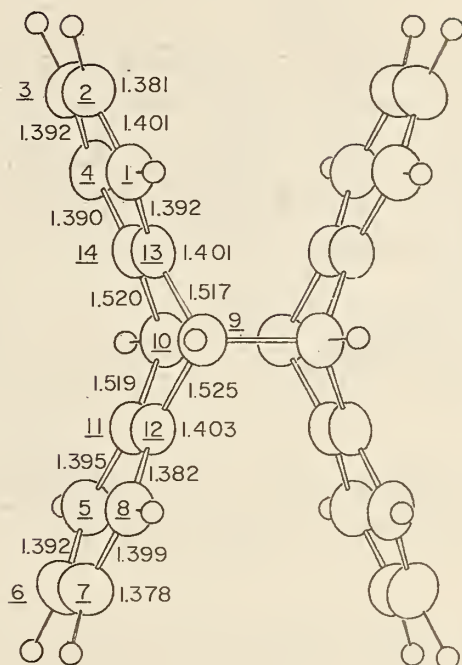


Figure 1. ORTEP drawing of dipara-anthracene molecule. Carbon atoms are labeled with underlined number, and hydrogen atoms are drawn with small circle.

Each anthracene molecule is bent at the middle by  $44^\circ$ , and coupled to other anthracene molecule through the long c-c bonds ( $1.628\text{\AA}$ ) extended from the apex atoms. There are no evidence of hydrogen bonding in this crystal.

THE PRESSURE-INDUCED PHASE TRANSITION IN SODIUM NITRATE

S. F. Trevino  
(Energetic Materials Division, LCWSL, ARRADCOM, Dover, NJ)

and

(National Bureau of Standards, Washington, DC)

and

E. M. Brody  
(University of Rochester, Rochester, NY)

RRD COLLABORATIVE PROGRAMS

Sodium nitrate undergoes a paraelectric to ferroelectric phase transition at 45 kilobars.<sup>1</sup> A soft mode has been observed by Ramon scattering in the ferroelectric phase. The mode is of  $A_1$  symmetry.<sup>2</sup> The behavior of the mode, as a function of pressure is well described using a mean field expression of the form

$$\frac{\omega_0}{2\pi} = A(P-P_c)^{1/2} \quad P > P_c$$

where  $A = 13 \pm 1 \text{ cm}^{-1} / \text{kb}^{1/2}$  and  $P_c = 45 \pm .5 \text{ Kb}$

The paraelectric form should satisfy the eq.

$$\frac{\omega_0}{2\pi} = \frac{A}{\sqrt{12}} (P_c - P)^{1/2}$$

In addition, from the known structural changes caused by the phase transition, the eigenvectors of the mode can be constructed and must have both translational motion of the Na and  $\text{NO}_3$  groups parallel to the unique axis and rotation of the  $\text{NO}_3$  group about the unique axis. In the paraelectric phase, the soft mode must have  $A_{2u}$  symmetry. Such a mode has been observed at ambient condition by neutron scattering.

Table 1. The structure in portion of the  $A_{2u}$  mode in  $\text{NaNO}_3$ ,  $\xi_R$  in the rotational part of the eigenvector and  $\xi_T$  the translational.

RLP	F
006	$1.708 \xi_T$
$02\bar{2}$	$-.16 \xi_T + .554 \xi_R$

In the present work, the polarization vector and pressure dependence of this mode are investigated to corroborate the validity of the soft mode model.

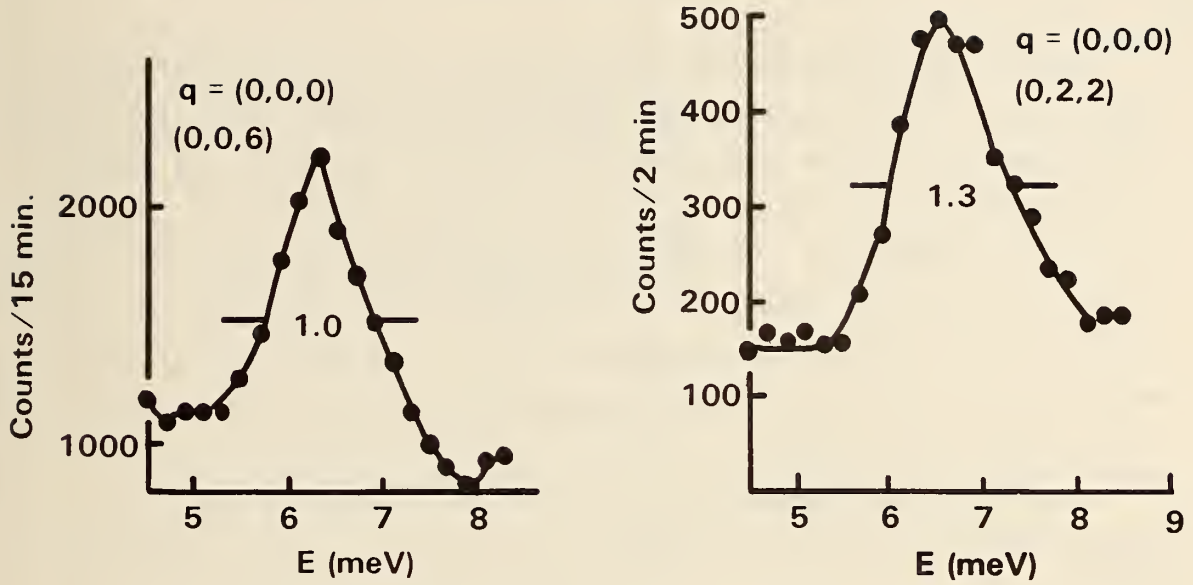


Figure 1. The  $A_{2u}$  phonon measured at two different RLP as discussed in the text.

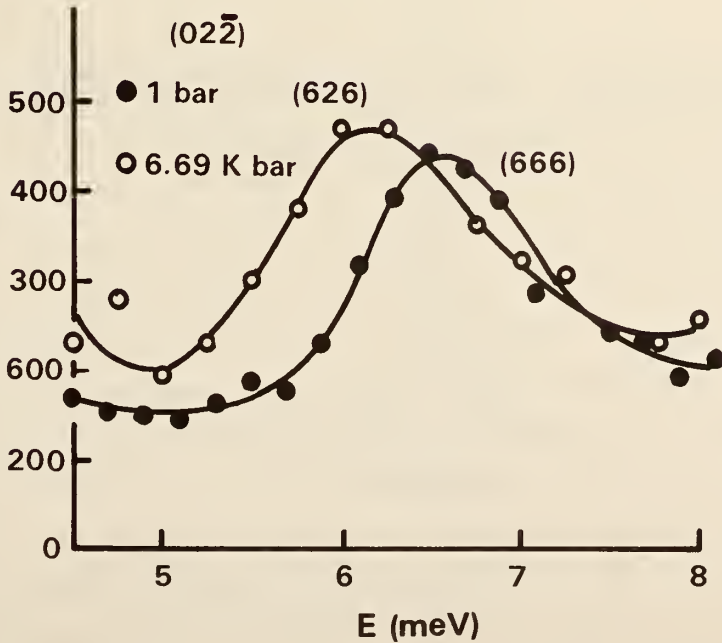


Figure 2. The pressure dependence of the  $A_{2u}$  phonon.

## RRD COLLABORATIVE PROGRAMS

Table 1 shows the structure factor for the two reciprocal lattice points (RLP) used to measure the eigenvector ( $\xi_R$  and  $\xi_T$  are respectively the eigenvectors for relation and translation of the mode) and figure 1 the measured phonon at these RLP. From the measurement  $\xi_R = .202$  and  $\xi_T = .979$  confirming the translation-rotation nature of the mode. Figure 2 shows the pressure dependence of the mode for two pressures of 1 bar and 6.69 K bar. The shift is downward by 6%. The model predict a downward shift of 7.7%. The present evidence is taken as confirming the correctness of the model.

It will be very interesting to study the behavior of the soft mode to higher pressure but we do not at present have that capability.

- 
1. Barrett, J. D., Pack, J. and Hall, H. T. *Tans. American Cryst. Dissoc.* 5 113 (1969).
  2. Letturi, T. R., Brody, E. M., *Bull. American, Phys.* 5 or 22 323 (1978).

## THE STRUCTURE OF SODIUM ZINC CHLORIDE TRIHYDRATE

H. Ammon and R. J. Khanna  
(University of Maryland, College Park, MD)

and

E. Prince

The positions of the non-hydrogen atoms in the unit cell of sodium zinc Chloride trihydrate  $\text{Na}_2\text{ZnCl}_4 \cdot 3\text{H}_2\text{O}$  eve determined by x-ray diffraction by Brehler<sup>1</sup>. The compound crystallized in space group P31m with all dimensions  $a=6.876(5)\text{\AA}$ ,  $c=5.955(5)\text{\AA}$ , with one formula unit per unit cell. A set of three dimensional neutron diffraction data was collected from a crystal of this compound several years ago<sup>2</sup>. These data have now been refined to an  $R=0.028$ , and the hydrogen positions have been determined. The water molecules lie in minor planes with  $\text{O}-\text{H}$  distances (uncorrected for thermal motion) of  $0.954\text{\AA}$  and  $0.962\text{\AA}$  and an  $\text{H}-\text{O}-\text{H}$  bond angle of  $104.23^\circ$ . Both hydrogen atoms participate in  $\text{O}-\text{H}\cdots\text{O}$  hydrogen

Table 1. Refined parameters for  $\text{Na}_2\text{Zn Cl}_4 \cdot 3\text{H}_2\text{O}$ 

Atom	X	Y	Z	$U_{11}$	$U_{22}$	$U_{33}$	$U_{12}$	$U_{13}$	$U_{23}$
Zn	.0000	.0000	.0000	2.753	2.753	2.840	1.376	0.000	0.000
Na	.3333	.6667	.1832	4.496	4.496	2.816	2.248	0.000	0.000
Cl1	.0000	.0000	.3863	4.277	4.277	2.020	2.139	0.000	0.000
Cl2	.3176	.0000	.8987	3.069	4.846	3.067	2.423	0.219	0.000
O	.5458	.0000	.4151	4.265	4.712	3.266	2.356	0.303	0.000
H1	.6783	.0000	.4623	5.984	6.832	7.482	3.416	-1.396	0.000
H2	.4729	.0000	.5531	9.148	7.268	3.753	3.634	2.384	0.000

Table 2. Selected interatomic positions and angles in  $\text{Na}_2\text{Zn Cl}_4 \cdot 3\text{H}_2\text{O}$ . Distances and angles marked by an asterisk are involved in hydrogen bonds.

Zn-Cl1	2.301Å	Cl1-Zn-Cl2	105.46°
Zn-Cl2	2.266	Cl2-Zn-Cl2 <sup>1</sup>	113.19
Na-O	2.439	O-Na-O <sup>1</sup>	91.07
Na-Cl2	2.895	O-Na-Cl2	80.17
*O-H1	0.954	O-Na-Cl2 <sup>1</sup>	164.67
*O-H2	0.962	Cl2-Na-Cl2 <sup>1</sup>	89.23
*H1-Cl1	2.259	H1-O-H2	104.23
*H2-Cl2	2.319	*O-H1-Cl1	151.31
*O-Cl1	3.128	*O-H2-Cl2	176.06

## RRD COLLABORATIVE PROGRAMS

bonds. Table 1 gives refined atomic parameters and table 2 gives selected interatomic distances and angles.

1. B. Brehler, *Z. für Krist.*, 114, 66 (1960).
2. R. J. Khanna & E. Prince, *NBS Tech. Note 873*, 54 (1974).

## SPIN EXCITATIONS IN AMORPHOUS TRANSITION-METAL GLASSES

J. J. Rhyne

and

J. W. Lynn

(University of Maryland, College Park, MD)

and

(National Bureau of Standards, Washington, DC)

and

F. E. Luborsky and J. L. Walter

(G. E. Research and Development Center, Schenectady, NY)

There has been a very strong interest in the magnetic properties of amorphous transition-metal ribbon materials principally for their very high permeability and their applicability in transformer design and magnetic shielding. In the interest of examining some of the alloys magnetic inelastic neutron scattering studies have been performed at the NBS reactor on ribbon specimens of amorphous  $\text{Fe}_{83}\text{B}_{16.5}\text{Si}_{0.5}$  and  $\text{Fe}_{20}\text{Ni}_{60}\text{B}_{19}\text{P}_1$ . The samples were prepared from boron enriched to 96%  $\text{B}^{11}$  to reduce the neutron absorption. The Curie temperatures for the two materials are 613 K and 410 K respectively, and the saturation magnetizations  $4\pi M$  are 16.0 kG and 5.1 kG at room temperature. In the  $\text{Fe}_{20}\text{Ni}_{60}\text{B}_{19}\text{P}_1$  specimen, well-defined spin waves were observed at room temperature for neutron wave vector transfers in the range  $q = 0.06\text{\AA}^{-1}$  up to  $q = 0.4\text{\AA}^{-1}$ . After correcting for instrumental resolution, the data obeyed a quadratic dispersion law with spin stiffness  $D = 80\text{ meV}\text{-\AA}^2$ . This is to be compared with a  $D$  of  $100\text{ meV}\text{-\AA}^2$  measured on a specimen of a similar commercial

## RRD COLLABORATIVE PROGRAMS

amorphous ribbon material of composition  $\text{Fe}_{40}\text{Ni}_{40}\text{P}_{14}\text{B}_6$  which has a Curie temperature of 537 K. A representative energy scan showing both energy gain and energy loss spin wave peaks is shown in the figure. Spin waves in the  $\text{Fe}_{83}\text{B}_{16.5}\text{Si}_{0.5}$  amorphous alloy were observed at somewhat higher energies than in the  $\text{Fe}_{20}\text{Ni}_{60}\text{B}_{19}\text{P}_1$ , as expected due to the difference in Curie temperatures. The spin wave stiffness parameter for this material is  $125 \text{ meV}\text{-\AA}^2$ .

### MAGNETIC EXCITATIONS IN $\text{HoFe}_2$

J. J. Rhyne

and

N. C. Koon

(Naval Research Laboratory, Washington, DC)

$\text{HoFe}_2$  is one of the series of  $\text{RFe}_2$  (R = a trivalent rare earth heavier than Nd) compounds which crystallize in the close-packed Laves-phase crystal structure. All have Curie temperatures well above room temperature ( $T_c$  for  $\text{HoFe}_2$  is  $597 \text{ K}^1$  and for the heavy rare earths exhibit a ferrimagnetic spin structure in which the rare earth spin having the free-ion moment is antiparallel to the iron moments of approximately  $1.5 \mu_B^2$ . The low iron moment is presumed to result from band structure effects.

We have made inelastic neutron measurements of the spin excitations in single crystal  $\text{HoFe}_2$ . The lattice parameter of  $\text{HoFe}_2$  is 7.30 Å at room temperature and the primitive cell contains 6 atoms. One thus expects six spin wave branches, only three of which are at a sufficiently low energy to be accessible to thermal neutron scattering. The data were taken on a single crystal of approximately  $2 \text{ cm}^3$  on triple axis spectrometers at the NBS reactor. The [100] direction is the easy magnetic direction for  $\text{HoFe}_2$ .

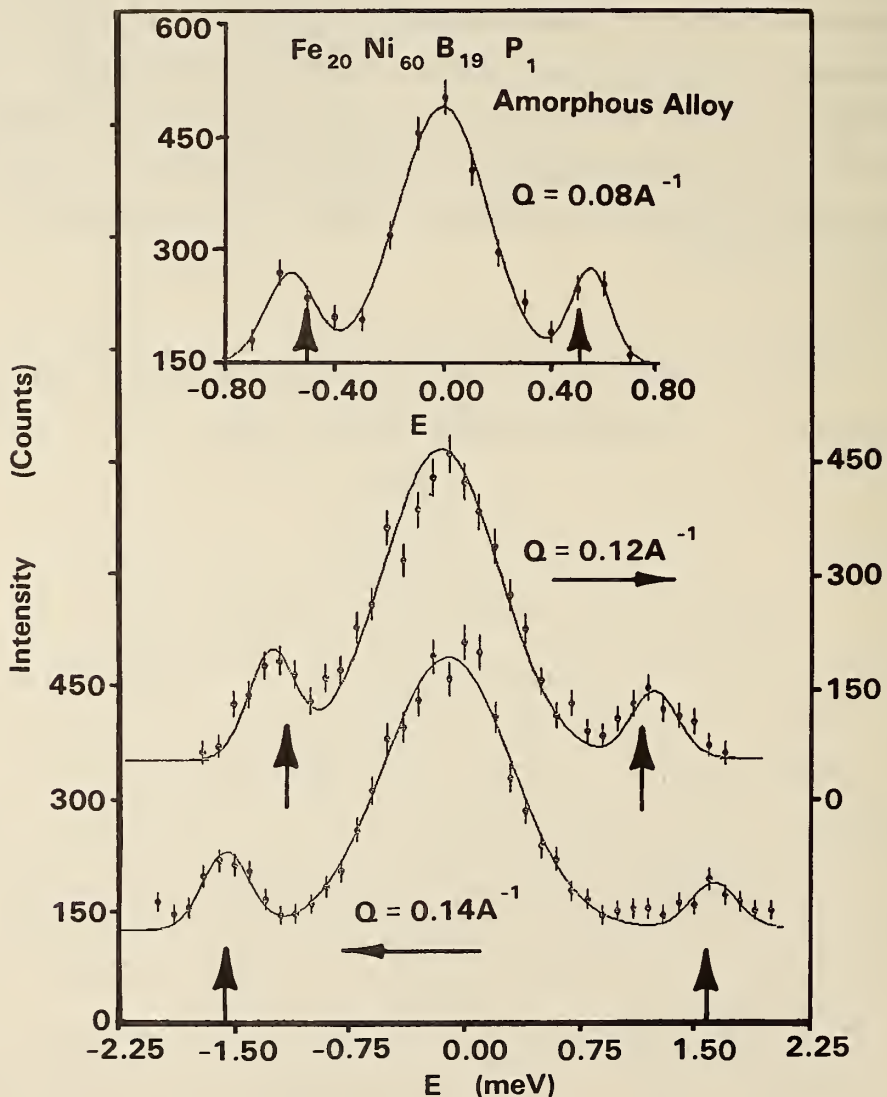


Figure 1. Scattered neutron intensity (arbitrary units) versus neutron energy transfer for  $\text{Fe}_{20}\text{Ni}_{60}\text{B}_{19}\text{P}_1$  amorphous ribbon alloy. Data are shown for wavevector transfer  $q$  of  $0.08$ ,  $0.12$  and  $0.14 \text{ \AA}^{-1}$ , and were taken with an incident energy of  $28 \text{ meV}$ . The solid line is the result of fitting a Gaussian lineshape to the data. The arrows indicate the position of the resolution-corrected spin wave energies.

## RRD COLLABORATIVE PROGRAMS

The lowest three branches for spin waves propagating in the  $[q,q,o]$  direction for  $\text{HoFe}_2$  are shown in figure 1 at room temperature and 10 K (2 branches). Measurement in the  $[q,q,q]$  direction showed no evidence for anisotropy in the spin wave spectra. The spectra are qualitatively similar to those found in previous work on  $\text{ErFe}_2$  [3] and consist of an acoustic mode, a very flat optic mode and a highly dispersive optic branch.

The high energy mode represents an in-phase precession of the iron spins only and has a spin stiffness very close to that of iron metal. In the absence of rare earth ion exchange, which produces the 16.6 meV gap, this mode would become the acoustic mode excitation. At 78 K calculations show that the increased rare earth magnetization raises the  $q = 0$  energy to 34 meV.

The flat branch of the spectrum arises from a molecular field excitation of the rare earth spins by the iron. The absence of measurable dispersion in this mode is a consequence of negligible rare earth-rare earth exchange and places an upper limit of approximate  $\pm 0.01$  meV on the magnitude of this interaction assuming an isotropic model.

The 10 K excitations have been fit to a linear spin wave model with a Hamiltonian containing both exchange and crystal field contributions which yielded the following parameters:  $J_{\text{HoFe}} = -0.43$  meV,  $J_{\text{FeFe}} = 26$  meV,  $J_{\text{HoHo}} = 0$ , and  $\Delta = 0.6$  meV. Agreement between theory and experiment for the acoustic and lower optic mode is within experimental error over the entire Brillouin zone. The model also fits the high energy iron mode at room temperature using a value of  $\langle J_{\text{Ho}}^Z \rangle = 4.7$ , in agreement with elastic neutron scattering data [2].

A careful study was made of the temperature dependence of the energy and intensity of the flat rare earth mode to look for observable crystal field transitions, figure 2 illustrates the observed scattering at the zone boundary for this mode as a function of temperature. At 10 K only a single line of width determined by instrumental resolution was found at an energy of 8.3 meV which represents the ground state to first excited

state energy. As the temperature is raised this mode increases rapidly in intensity and shifts to a slightly higher energy (8.6 meV at 295 K). Concurrently, significant intensity also appears in a very broad maximum about 6.7 meV indicative of a distribution of unresolved energy states in the range approximately 5-8 meV.

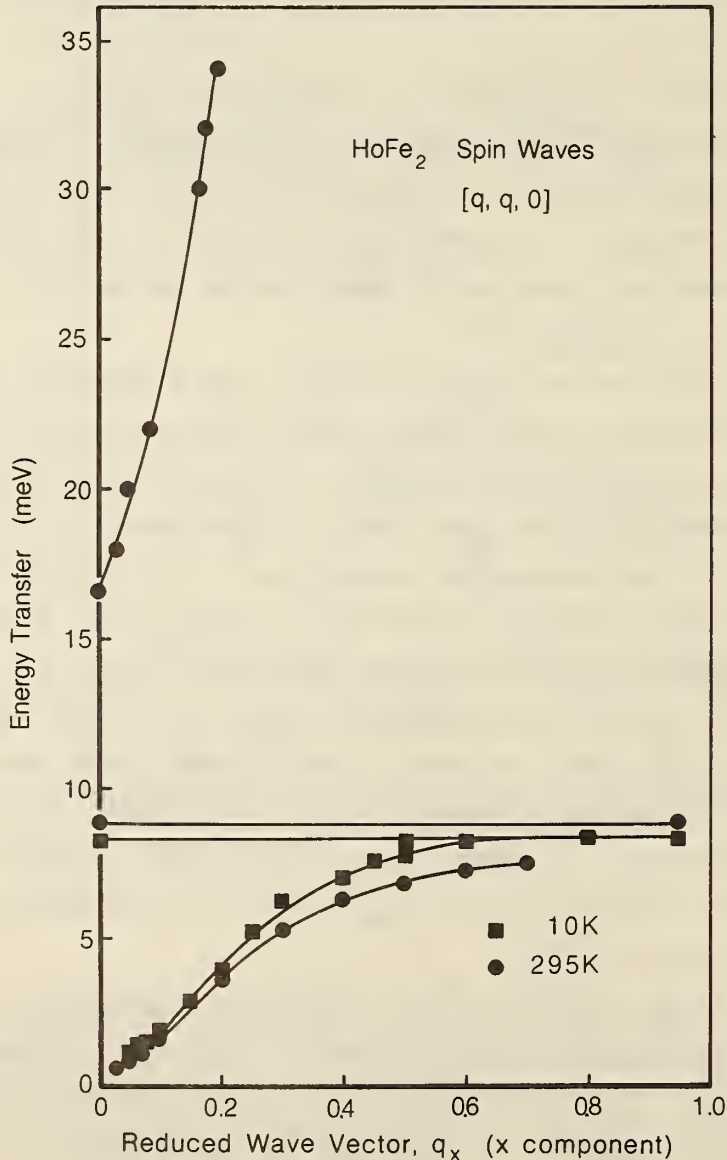


Figure 1. Magnon dispersion in HoFe<sub>2</sub> at room temperature and at 10 K for the [q,q,0] propagation direction.

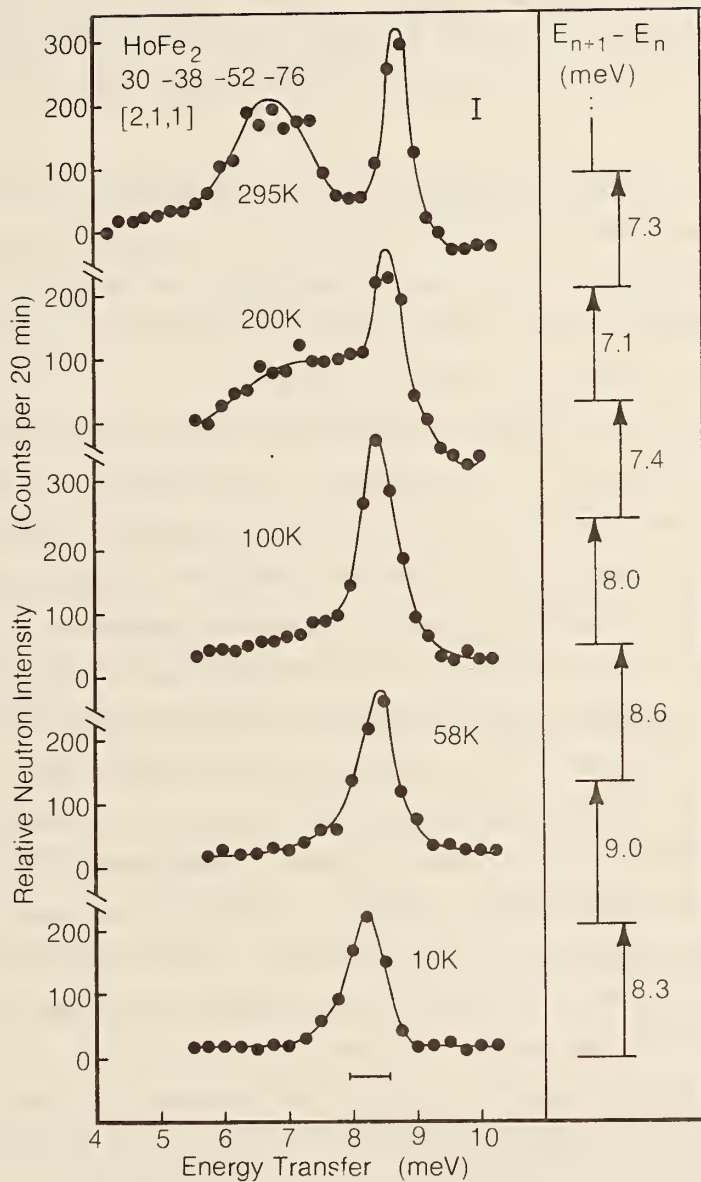


Figure 2. (a) Observed inelastic intensity for the (2,1,1) point in reciprocal space as a function of temperature. Note the increase in scattering near 7 meV as higher states of the calculated crystal field multiplet (b) become populated. The value of exchange ( $g\mu_B H_{\text{exch}}$  in equation 2) used was 7.73 meV and the crystal field parameters were  $B_4 = -8.1 \times 10^{-5}$  meV, and  $B_6^0 = +4.4 \times 10^{-7}$  meV.

## RRD COLLABORATIVE PROGRAMS

It is noted that the "acoustic" mode excitations observed at 295 K and shown in figure 1, broaden severely and become essentially unobservable above about 7 meV as they enter the energy region of the crystal field transitions.

A calculation of the energy levels was made by a direct diagonalization of a Hamiltonian containing both exchange and fourth and sixth order crystal field terms and the results are shown in figure 2b. The eigenstates are almost pure  $J^Z$  states, so that only transitions between adjacent states have finite matrix elements.

The calculation provides a qualitative explanation of the observed scattering intensity. At  $T = 10$  K only the ground state is populated and a single transition at about 9.2 meV is observed. Since the levels immediately above the ground state are separated by more than 8.2 meV, the peak in the scattering intensity initially moves to higher energies as the temperature is raised. At 200 and 295 K, however, crystal field levels with lower energy separations become populated and a broad band of scattering centered at about 6.7 meV is observed.

The model, however, gives a very small matrix element for the ground state to first excited state transition. Comparison of the relative intensities in figure 2a shows that this transition is actually quite weak, considering that at 10 K essentially all of the rare earth spins are in the ground state, but it is not nearly as weak as the model predicts. It should be noted that for  $\text{HoFe}_2$  the [110] and [100] directions are almost equally easy at low temperatures and it is possible that the easy axis of  $\text{HoFe}_2$  is rotated slightly away from [100] at  $T = 10$  K. Further work is in progress on this problem.

- 
1. E. Burzo, Z. Angew. Phys. 32 127(1971).
  2. N. C. Koon and J. J. Rhyne, *Solid State Communications* 26 537 (1978).

RRD COLLABORATIVE PROGRAMS

MAGNETIC NEUTRON SCATTERING FROM AMORPHOUS  $\text{TmFe}_2$

J. Rhyne

and

S. Pickart

(University of Rhode Island, Kingston, RI)

and

H. Alperin

(Naval Surface Weapons Center, White Oak, MD)

and

(National Bureau of Standards, Washington, DC)

The nature of the spin glass "freezing" or "blocking" transition has recently attracted much theoretical and experimental interest<sup>1</sup>. One might expect that a microscopic technique such as neutron scattering should contribute heavily to uncovering such details. Previous neutron measurements indicate anomalies in the small-angle magnetic scattering from a series of crystalline AuFe alloys<sup>2</sup> and amorphous  $\text{YFe}_2$ <sup>3</sup> while changes in the frequency dependence of the scattering were reported for the crystalline CuMn system<sup>4</sup>. We have made total and inelastic scattering measurements also on an amorphous composition,  $\text{TmFe}_2$ , that does not show a conventional ferromagnetic ordered phase at low temperatures. Instead a peak in the susceptibility occurs at about 45 K, suggestive of a spin clustered system with probably antiferromagnetic correlations.

The low angle scattered intensity was measured for scattering vectors  $.02 < q < .12 \text{ \AA}^{-1}$  and found to be of comparable absolute intensity to that in the previous study of  $\text{YFe}_2$ . This is to be contrasted with the scattering observed from  $\text{TbFe}_2$ <sup>3</sup> and  $\text{HoFe}_2$ <sup>5</sup>, which is orders of magnitude larger. These latter alloys have much stronger spin correlations and exhibit conventional bulk ferrimagnetic behavior.

There is one (probably minor) difference between the  $\text{TmFe}_2$  data and the previous  $\text{YFe}_2$  results<sup>3</sup>. First, no peak is observed in the region of the transition temperature suggested by bulk magnetic measurements

( $\sim 45$  K), though there is a definite tendency of the scattering curves to bend over at low temperatures; possibly at lower temperatures or lower  $q$  than attained in the present study a peak might develop. Overall the main feature of the data (which show a large increase in small angle scattering with decreasing temperature) is indicative of the development of regions of short range magnetic order.

In order to detect a possible change in the spin relaxation process on passing through the spin freezing temperature of approximately 45 K (as given by bulk magnetization data) we measured the energy dependence of the scattering at small angles at temperatures of 60 K and 10 K. The results indicate that no great change in the diffusion constant has occurred. The measurement is a difficult one to make with the great precision because of the well-known limitations in energy transfer attainable at small momentum transfers near the forward direction. As a result, the true background of the scans cannot be fixed unambiguously. However, our data appear to rule out more than at most a 30% change in energy width of the scattering from above to below the spin freezing temperature.

The small angle total scattering data described above suggest a similarity in the spin clustering in  $\text{TmFe}_2$  and  $\text{YFe}_2$ , but its exact nature requires much more extensive data to elucidate. The data are not inconsistent with those for the  $\text{AuFe}$  system<sup>2</sup> (taken at much lower  $q$ ), where much sharper peaks were observed.

However, there is a clear difference in the changes in inelasticity of the scattering above and below the transition in the amorphous  $\text{TmFe}_2$  and in  $\text{CuMn}^4$ , in which a striking change in halfwidth occurs (from 0.36 meV above the freezing temperature, to .005 meV below). We must thus conclude that in the concentration range of these alloys there is an intrinsic difference in the spin diffusion processes occurring in the crystalline and amorphous matrices.

RRD COLLABORATIVE PROGRAMS

- 
1. For collected references, see Levy, R. and Hasegawa, R., *Amorphous Magnetism II*, Plenum Press, New York, 1977.
  2. Murani, A., "Nonuniqueness of Freezing Temperature of Spins in Binary Alloys," *Phys. Rev. Lett.* 37, 450-453, 1976.
  3. Pickart, S., Rhyne, J. and Alperin, H., "Anomalous Small-Angle Scattering from Amorphous  $TbFe_2$  and  $YFe_2$ ," *Phys. Rev. Lett.* 33, 424-427, 1974.
  4. Murani, A., Goeltz, G. and Ibel, K., "Evidence for Freezing of Spins in Binary Alloys," *Solid State Comm.* 19, 733-736, 1976.
  5. Pickart, S., Rhyne, J. and Alperin, H., "'Critical' Neutron Scattering in Amorphous  $HoFe_2$  and  $GdFe_2$ ," *AIP Conf. Proc.* 24, 117-118, 1975.

MEASUREMENTS OF THE CRYSTAL-FIELD SPLITTINGS  
 IN SUPERCONDUCTING  $(\text{Ce}_{1-x}\text{Ho}_x)\text{Ru}_2$  ALLOYS

C. J. Glinka & J. W. Lynn  
 (University of Maryland, College Park, MD)

and

(National Bureau of Standards, Washington, DC)

In the superconductor  $\text{CeRu}_2$  rather high concentrations of magnetic heavy rare earth ions may be substituted for the non-magnetic cerium ions before superconductivity is completely quenched. For example,  $\sim 35\%$  of the Ce can be replaced by Ho before  $T_S$  goes to zero and small amounts of Ho actually enhance  $T_S$ . Furthermore, for Ho concentration above  $\sim 25\%$ , bulk magnetic susceptibility data show distinct maxima as a function of temperature which are suggestive of long-range magnetic ordering. Thus the pseudo-binary alloy  $(\text{Ce}_{1-x}\text{Ho}_x)\text{Ru}_2$  is an ideal system for studying the competition between the two cooperative phenomena of superconductivity and magnetism. To this end, neutron scattering is an ideal technique for studying the magnetic properties since the magnetic state may be microscopically probed without being affected by the screening of the superconducting electrons.

In  $(\text{Ce}_{1-x}\text{Ho}_x)\text{Ru}_2$ , a fundamental characterization of the system is a measurement of the splitting of the  $J=8$  manifold of the  $\text{Ho}^{3+}$  ion by the cubic electrostatic field of the crystal. In an initial study<sup>1</sup> of the inelastic scattering from a sample of  $(\text{Ce}_{.73}\text{Ho}_{.27})\text{Ru}_2$ , the observed transitions implied that a triply degenerate  $\Gamma_5$  state lies lowest, so that the ground state is magnetic. Recently we have carried out similar measurements on samples with the compositions  $(\text{Ce}_{.9}\text{Ho}_{.1})\text{Ru}_2$  and  $(\text{Ce}_{.69}\text{Ho}_{.31})\text{Ru}_2$  in order to study the concentration dependence of the crystal-field splitting. The samples were prepared by arc melting measured amounts of the pure elements and then annealing at  $1350^\circ\text{C}$  for 24 hours. Neutron diffraction and metallographic analysis revealed only trace amounts of secondary phases in the resulting materials, whose compositions were determined by emission spectroscopy.

RRD COLLABORATIVE PROGRAMS

Crystal field transitions observed in  $(\text{Ce}_{.90}\text{Ho}_{.10})\text{Ru}_2$  at 10K are shown in figure 1. The transition energies of 3.75 and 15 meV are nearly

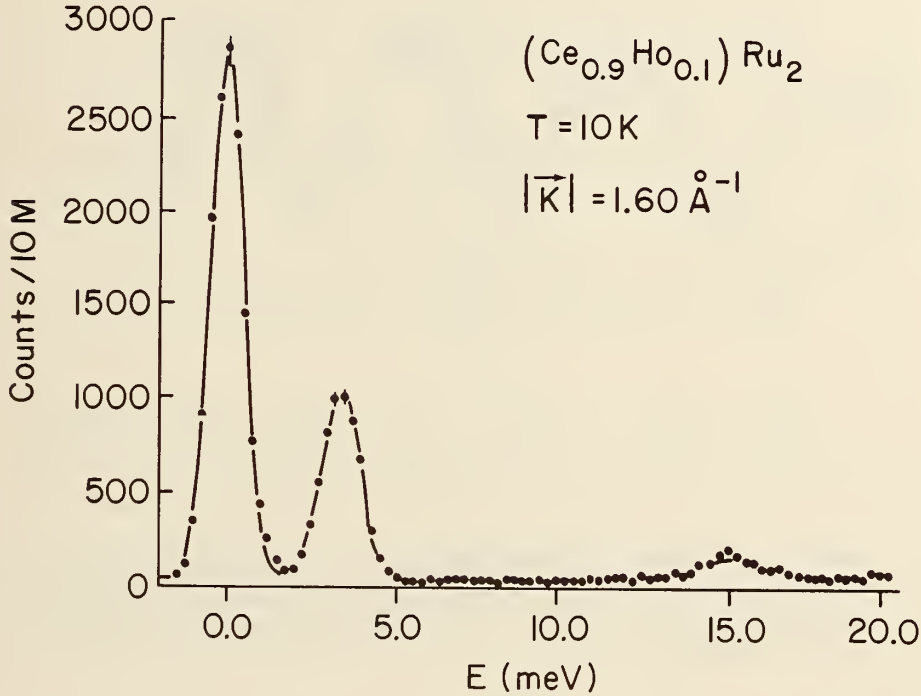


Figure 1. Constant -  $\vec{K}$  scan of the low energy inelastic magnetic scattering from  $(\text{Ce}_{.90}\text{Ho}_{.10})\text{Ru}_2$  at 10K showing two crystal field transitions from the ground state at 3.75 and 15.0 meV.

the same as had been observed in  $(\text{Ce}_{.73}\text{Ho}_{.27})\text{Ru}_2$  and correspond to the two possible transitions out of the  $\Gamma_5^{(1)}$  ground state. With increasing temperature two additional, excited state transitions become observable at 8.5 and 12.0 meV. These may be seen in figure 2 which shows data taken at 50K. The combination of transitions seen in figures 1 and 2 uniquely identifies the crystal field level scheme of the  $\text{Ho}^{3+}$  ion, confirming that the magnetic  $\Gamma_5^{(1)}$  level is the ground state. Similar results were obtained on the high concentration sample,  $(\text{Ce}_{.69}\text{Ho}_{.31})\text{Ru}_2$ . We conclude, therefore, that the  $\text{Ho}^{3+}$  ion has a magnetic ground state over the entire concentration range of interest.

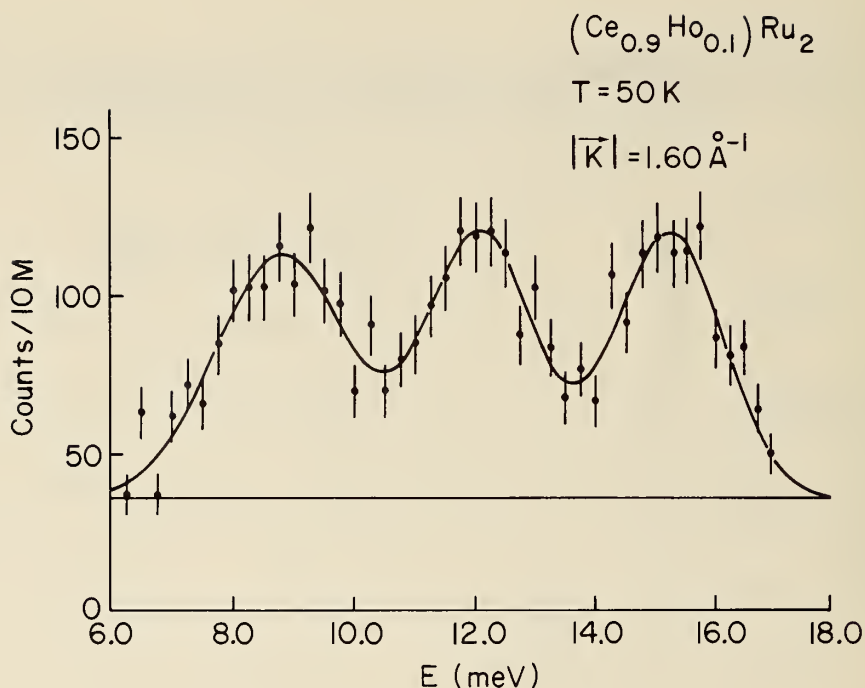


Figure 2. Inelastic magnetic scattering from  $(\text{Ce}_{0.9}\text{Ho}_{0.1})\text{Ru}_2$  at 50K showing, in addition to the ground state crystal field transition at 15 meV, two excited state transitions at 8.5 and 12.0 meV.

Small-angle scattering measurements are now in progress to study the development of magnetic correlations as a function of the holmium concentration in these alloys. In data taken on the 27% Ho sample<sup>1</sup>, these correlations were found to be described by an Ornstein-Zernike correlation function, with the correlation range increasing steadily with decreasing temperature down to 0.5K, but then saturating at a value of  $80\text{ \AA}$ . In contrast to the crystal field measurements, changes in the holmium concentration should have a marked effect on this behavior.

1. J. W. Lynn, D. E. Moncton, W. Thomlinson and L. Passell,  
*Bull Am Phys Soc.* 22, 339 (1976).

RRD COLLABORATIVE PROGRAMS

LOW TEMPERATURE PHASE TRANSITION IN  $\text{Cs}_2\text{NaPrCl}_6$

G. E. Fish

and

J. W. Lynn

(University of Maryland, College Park, MD)

and

(National Bureau of Standards, Washington, DC)

and

H. H. Patterson

(University of Maine, Orono, ME)

and

J. J. Rhyne

The compounds  $\text{Cs}_2\text{NaMCl}_6$  are known to have the face centered cubic structure at room temperature for a wide variety of trivalent ions M, including transition metals, actinides, and rare earths. This class of compounds provides a rather unique model system for study of the rare earths in either concentrated salts or with paramagnetic ions diluted in the diamagnetic La, Lu, or Y hosts, because all the trivalent ion sites are equivalent and have octahedral ( $O_h$ ) symmetry<sup>1</sup>. For the heavy rare earths, the compounds remain cubic down to 1.5 K or have at most a slight non-cubic distortion<sup>2</sup>. However, previous EPR and optical studies have shown that the light rare earth compounds undergo a phase transition below room temperature, but no details of the structure have been reported<sup>3</sup>.

We have studied a single crystal of  $\text{Cs}_2\text{NaPrCl}_6$  with elastic neutron scattering and confirmed a commensurate phase transition at 155 K. No additional Bragg peaks have been seen. Inelastic scattering measurements are being made to determine if this phase change is a second order transition driven by softening of an optical phonon mode, as in the structurally similar compound  $\text{K}_2\text{ReCl}_6$ , where the transverse phonon branch which rotates the  $(\text{ReCl}_6)^{-2}$  octahedra softens first at  $\Gamma$ , then at  $X^4$ . Preliminary data on  $\text{Cs}_2\text{NaPrCl}_6$  reveal a soft  $\Gamma$ -point phonon with energy less than 2 meV at room temperature and with an energy width which

RRD COLLABORATIVE PROGRAMS

is considerably broader than instrumental resolution. Work is in progress to further characterize this mode.

1. L. Morss, M. Siegal, L. Stenger, and N. Edelstein, *Inorg. Chem* 9 1771 (1970)
2. G. E. Fish and H. J. Stapleton, *J. Chem. Phys.* (to be published).
3. C. J. O'Conner, R. L. Carlin, and R. W. Schwartz, *J. Chem. Soc., Faraday Trans. II* 73, 361 (1977).
4. J. W. Lynn, H. H. Patterson, G. Shirane, and R. G. Wheeler, *Solid State Comm.* 27, 859 (1978).

CRYSTAL-FIELD EXCITATIONS IN  $(RE)Mo_6Se_8$

J. W. Lynn

(University of Maryland, College Park, MD)

and

(National Bureau of Standards, Washington, DC)

and

R. N. Shelton

(University of California at San Diego, LaJolla, CA)

Ternary Chevrel-phase superconductors of the general formula  $(RE)Mo_6X_8$  (RE=rare-earth, X=Se, S) exhibit a variety of unique and interesting phenomenon related to the competition between magnetism and superconductivity. The neutron scattering technique is ideal to study the magnetic properties of these systems since the magnetic state can be directly probed on an atomic level without the perturbing influence of the superconducting state such as shielding currents, for example. The first neutron study of the magnetic ordering in these materials was performed<sup>1</sup> on  $ErMo_6Se_8$ . As anticipated on the basis of specific heat studies,<sup>2</sup> strong magnetic Bragg scattering was found to develop at 1K, well below the superconducting transition at  $\sim 5.5K$ , with the samples remaining superconducting. However, the complicated magnetic diffraction

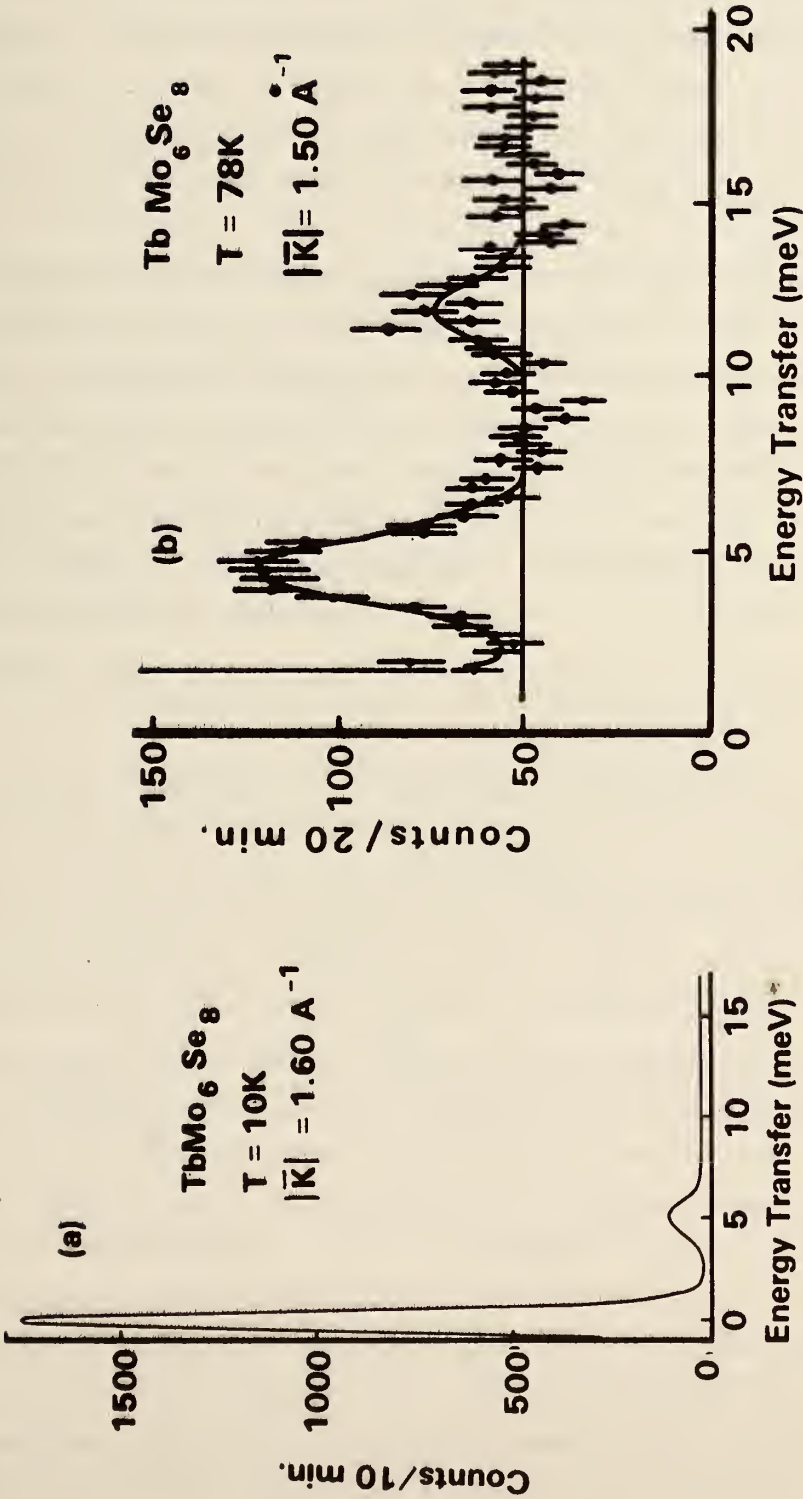


Figure 1. Observed scattering from  $\text{TbMo}_6\text{Se}_8$  at (a) low temperature, where only excitations out of the ground state are observed; (b) at 78K, where an additional transition becomes observable due to the increased thermal population of the crystal field level at 5 meV. The scattering at zero energy transfer in (a) is due to the  $\{111\}$  Bragg peak.

## RRD COLLABORATIVE PROGRAMS

pattern could not be interpreted in a straightforward manner and the possibility that only impurity phases were magnetic could not be ruled out. More recently,  $\text{HoMo}_6\text{S}_8$  was found to become ferromagnetic,<sup>3</sup> at which point the superconductivity established at 1.25 was destroyed.<sup>4</sup> Similar reentrant ferromagnetic behavior has been observed<sup>5</sup> in the related system  $\text{ErRh}_4\text{B}_4$ .

In all of these materials the characteristic magnetic energies are typically 1K or less. We can then anticipate that the crystal field may play a dominant role in determining the magnetic properties of these systems. The crystal structure of the Chevrel phase is rhombohedral ( $R\bar{3}$ ) with one formula unit per unit cell. The rare-earth ions occupy a single primitive lattice which is nearly cubic since the rhombohedral angle is close to  $90^\circ$ . Hence to a first approximation we expect the lifting of the free-ion angular momentum degeneracies can be described by a crystal field with cubic symmetry as calculated by Lea, Leask and Wolf.<sup>6</sup>

The polycrystalline samples used are the same samples studied by specific heat and susceptibility.<sup>2</sup> All the data were taken with the triple-axis technique with a PG(002) analyzer. The monochromator was a "bent" PG(002) crystal for the lower energy transfers, and a "bashed" Cu(220) for the higher ( $>30\text{meV}$ ) energy transfers. Figure 1a shows a typical scan at low temperatures on  $\text{TbMo}_6\text{Se}_8$ . The peak at zero energy transfer is the  $\{111\}$  Bragg reflection. The crystal field transition out of the ground state is clearly seen at  $5.0\text{meV}$ . The transition was unambiguously identified as crystal field in origin due to its temperature and wavevector dependence. At higher temperatures a second excitation appears as shown in Figure 1b. This is consistent with a cubic crystal field, and gives a singlet as the ground state. For  $\text{ErMo}_6\text{Se}_8$ , on the other hand, three transitions out of the ground state were observed. This may indicate that the small rhombohedral distortion has a significant effect on the crystal field in this material, or that there is more than one inequivalent crystallographic site for the Er in these

## RRD COLLABORATIVE PROGRAMS

samples. In the latter case, however, it is not possible to distinguish whether these additional sites are in the Chevrel phase or in an impurity phase.

Extensive measurements have been taken on  $\text{HoMo}_6\text{S}_8$  in an attempt to observe crystal-field excitations in this material, without success. All measurements were taken above the ferromagnetic transition of 0.67K. Scans with an energy resolution of 0.8meV revealed no excitations in the range 0.5→22meV. This indicates that the crystal field excitations lie are severely broadened due to lifetime effects, or the excitations lie outside this energy range. Both possibilities suggest that the sulfides differ sharply from their selenide counterparts. High resolution (92 $\mu\text{eV}$ ) measurements showed no excitations in the region 0.05→1.0 meV and high energy scans revealed no excitations at small wavevectors in the range 30 to 70 meV.

- 
1. J. W. Lynn, D. E. Moncton, G. Shirane, W. Thomlinson, J. Eckert and R. N. Shelton, *J. Appl. Phys.* 49, 1389 (1978).
  2. R. W. McCallum, C. C. Johnston, R. N. Shelton, W. A. Fertig and M. B. Maple, *Sol. St. Comm.* 24, 501(1977). R. W. McCallum (thesis)
  3. J. W. Lynn, D. E. Moncton, W. Thomlinson, G. Shirane and R. N. Shelton, *Sol. St. Comm.* (to be published)
  4. M. Ishikawa and Fischer, *Sol. St. Comm.* 23, 37(1977).
  5. W. A. Fertig, C. C. Johnston, L. E. deLong, R. W. McCallum, M. B. Maple and B. T. Matthias, *Phys. Rev. Lett.* 39, 1164 (1977); D. E. Moncton, D. B. McWhan, J. Eckert, G. Shirane and W. Thomlinson, *Phys. Rev. Lett.* 39, 1164 (1977).
  6. K. R. Lea, M. J. Leask and W. R. Wolf, *J. Phys. Chem. Solids* 23, 1381 (1962).

A TRIPLE AXIS POLARIZED BEAM SPECTROMETER

C. J. Glinka and J. J. Rhyne

and

R. W. Williams

(Naval Surface Weapons Center, White Oak, MD)

A triple axis polarized beam neutron spectrometer is now in operation at the NBSR. The instrument is a fixed incident energy spectrometer which utilizes a pair of Heusler alloy crystals,  $\text{Cu}_2\text{MnAl}$ , as polarizing monochromator and polarization-sensitive analyzer. The crystals, mounted in 3 kgauss permanent H-magnets, are used in transmission geometry and have a measured peak reflectivity of 35% at  $2.4\text{\AA}$  for one spin state and a mosaic spread of 15 minutes. At present, the average polarization of the beam over its  $2.5 \times 3.2 \text{ cm}^2$  area is typically 90%. Over the central region of the beam the polarization is higher, approaching the intrinsic polarizing efficiency of the Heusler crystals which has been measured to be approximately 98%. Efforts are continuing to improve the uniformity of the polarization by eliminating stray fields along the beam path. An rf spin resonance flipper coil, situated in the incident beam, is used to reverse the sense of polarization. A flipping efficiency of 99% over the entire beam area is routinely obtained.

A split-coil superconducting magnet has been received and tested successfully at fields up to 75 kgauss. The magnet has a 3.8 cm bore so that rather large samples may be accommodated and maintained at temperatures from 4 to 300K. Also available for polarized beam work at higher temperatures, up to  $900^\circ\text{C}$ , is a vacuum furnace which mounts between the pole pieces of a conventional vertical field electromagnet.

To illustrate the performance and energy resolution of the spectrometer, a constant-Q scan of the incoherent elastic scattering from nickel is shown in figure 1. The incoherent cross section for Ni is entirely due to isotopic incoherence which has no effect of the spin state of the incident neutrons. The scattered beam thus has the same polarization as the incident beam. The scan in figure 1 illustrates, therefore,

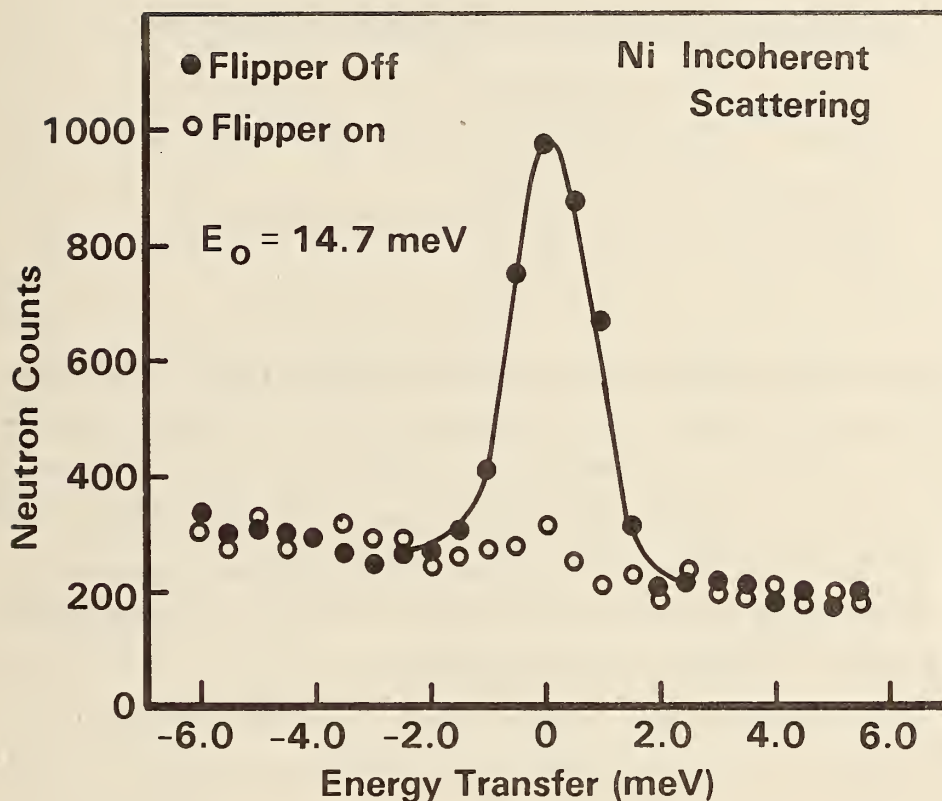


Figure 1. Constant-Q scan of the elastic incoherent scattering from nickel measured with the incident beam polarized "up" (filled circles) and "down" (open circles).

the discrimination which is presently attainable between neutrons scattered with spin "up" (flipper off) and those with spin "down" (flipper on). The small residual peak in the flipper on data is due to the imperfect polarization of the incident beam.

A study of the polarization dependence of the critical scattering from isotropic ferromagnets is currently in progress using the polarized beam spectrometer. Measurements of the magnetic form factors of both the iron and rare earth atoms in Laves phase (RE)Fe<sub>2</sub> compounds are also planned.

RRD COLLABORATIVE PROGRAMS

STUDIES OF THE EFFECTS OF DEUTERIUM IN TITANIUM

H. Alperin

(Naval Surface Weapons Center, White Oak, MD)

and

(National Bureau of Standards, Washington, DC)

and

J. J. Rush

Phonon measurements on a titanium single crystal have been initiated to determine if any lattice decohesion results from the presence of deuterium at interstitial positions in the titanium lattice. Prior to loading with deuterium phonons have been measured in the  $[01\bar{1}0]$  and  $[11\bar{2}0]$  directions at room temperature and at 385C. The crystal has been successfully loaded with ~7% deuterium and measurements at 385°C are in progress.

- 
1. Alperin, H.A, Pickart, S. J., and Rhyne, J. J., "Small Angle Neutron Scattering from Rare-Earth from Alloys", *J. Appl. Cryst* 11, 105 (1978).
  2. Pickart, S. J., Alperin, H. A, and Rhyne, J. J., "Small-Angle Magnetic Scattering from a Dilute Amorphouse Fe (Tb) Alloy", *Phy. Letters*, 64A, 337 (1977).

STRUCTURE AND DYNAMICS OF  $\beta$  V<sub>2</sub>D

H. Jo and S. C. Moss

(University of Houston, Houston, TX)

and

J. M. Rowe and J. J. Rush

The phase diagrams of  $VH_x$  and  $VD_x$  are particularly complex, and show a large difference for the two isotopes. For the composition

## RRD COLLABORATIVE PROGRAMS

$V_2D$  there exists a narrow single phase region only for the deuteride which can be approached directly (with no mixed phase region) from the  $\alpha$  or solute phase. In the  $\beta$  phase, the metal atoms form a body centered tetragonal lattice (to first order) with the deuteriums ordered on alternate [101] planes. The whole structure is monoclinic as determined from neutron powder diffraction measurements. The properties of the system allow one to cool a single crystal from the  $\alpha$  to the  $\beta$  phase without shattering. Although in general,  $\beta$ -phase crystals are multidomain, small samples suitable for diffraction can be obtained. One such sample has been used to collect a full data set which is presently being analysed.

In addition, we have attempted to measure the phonon dispersion relation for a multidomain sample of  $\sim 1/2$ cc. In spite of the fact that the optic modes are known to lie very low in energy from powder measurements, we were unsuccessful in our attempt. Thus, efforts are underway to produce a large single domain crystal using uniaxial stress. This sample will then be used to study the lattice dynamics of this system.

## CHAIN DEFORMATION IN RUBBER

C. Han  
(Polymer Science and Standards Division)

and

B. Mozer

and

J. A. Hinkley and H. Yu  
(University of Wisconsin, Madison, WI)

Small-angle neutron scattering (SANS) has made possible direct determinations of the chain dimensions of polymers in the bulk amorphous state. The technique takes advantage of the isotopic difference in neutron scattering cross sections of deuterium and hydrogen. In this

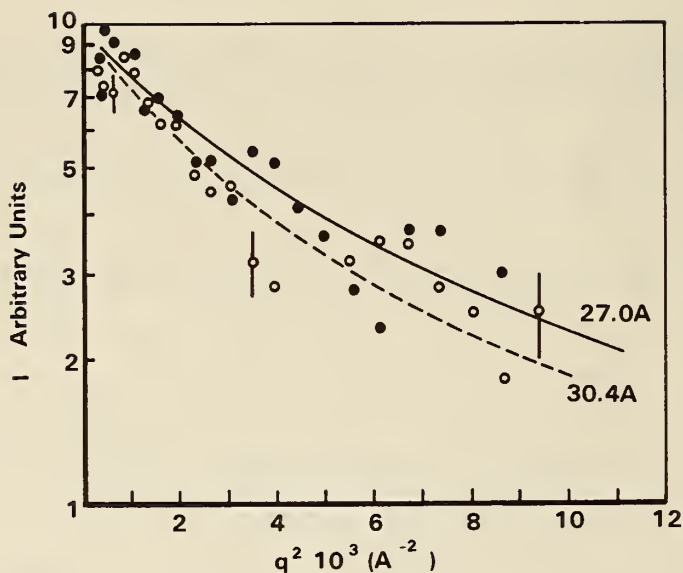


Figure 1. Excess scattered intensity in log scale vs.  $q^2$  (Guinier plot where the ordinate is in arbitrary units) for samples containing 3% deuterated chains (●) for bulk mixture and (○) for network. Error bars, standing for one standard deviation, are given only for a few representative data points. The two curves are drawn according to the Debye form factor which gives the best fit for the mixture (solid curve) and for the network (chained curve).

work, we give a brief account of a study of the chain dimensions in rubber networks by the SANS technique. We ask what happens to the linear dimension of a chain upon cross-linking its ends into a network and how this dimension changes when the network is stretched. In the theory of rubber elasticity, it has generally been hypothesized that the macroscopic extent of stretching of a network is affinely transformed to the extension ratio of each adjoining pair of cross-links. We are now able to test this hypothesis. We could effect the experiment because we were able to prepare uniform networks, whose elastic strands are of monodisperse chain length and cross-links are of uniform functionality. Incorporating a small fraction of perdeuteriopoly (butadiene) (3% or less) in its hydrocarbon matrix, we have performed SANS measurements on the uncross-linked mixtures and on the cross-linked networks with and without an axial strain.

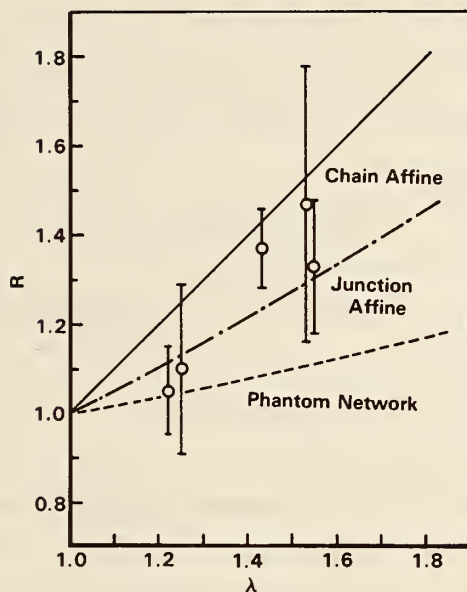


Figure 2. Ratio of the apparent radius of gyration to that in the unstrained state vs. extension ratio.  $R = (S_y^2)^{1/2} / (S_y^2)_{\lambda=1}$ . The error bars are estimated from the sum of relative errors of slope and intercept of the linear extrapolation procedure without taking into account possible correlation between the two. Three curves are drawn respectively for the chain affine model (—) where  $R = \lambda$ , for the junction affine model (-·-·-) where  $R = [(1 + \lambda^2)/2]^{1/2}$ , and for the phantom chain model (-----) where  $R = [(5 + \lambda^2)/6]^{1/2}$  when the cross-link functionality is three.

We first present the results for the determination of chain dimensions in bulk samples. The root mean square radius of gyration  $(S^2)^{1/2}$  (henceforth, just called the radius of gyration) is extracted from the excess scattered intensity,  $I(q)$ , in two ways. The first method is to fit the data at small  $q$  to a least squares straight line. Because the scattering profile is in fact curved for the observed range of  $q_y^2(S_y^2)$ , this method systematically overestimates  $(S_y^2)$ . A simulation study shows that the error is about 20% for the range of  $q$  used. Inasmuch as chain conformations in the bulk amorphous state have been

## RPD COLLABORATIVE PROGRAMS

shown to be well described by the Gaussian coil model, we have also fit the  $I(q)$  data to the Debye form factor for a Gaussian coil. The results of both fitting procedures are collected in table 1. The radius of gyration at infinite dilution derived from the second method is  $36.9 \pm 10.5 \text{ \AA}$ . This agrees with the unperturbed radius of gyration of  $35 \text{ \AA}$  calculated from the literature values taking into account the variation with microstructure.

The study of the chain dimension in a rubbery network is restricted to networks containing 3% (by weight) of deuterated chains, hence we represent the radius of gyration as the apparent one which is not corrected for its possible concentration dependence. On the basis of a plausible assumption that the concentration dependence of  $(S^2)$  for the free chain in the bulk state does not differ from that for the network chain in the unstrained state, we can now compare the chain dimensions in the two states. In figure 1, Guinier plots for the 3% mixture and the 3% network are presented. Within the experimental uncertainty, the apparent radii of gyration are indistinguishable. We therefore conclude that the chain dimension of polybutadiene in the free state is the same as in the unstrained network. An identical experiment on set B samples gave the same result (see table 1).

The results for the study of chain dimensions in a network under uniaxial strain are also collected in table 1. We summarize the data by plotting in figure 2 the ratio of apparent radius of gyration at a given  $\lambda$  to that at the unstrained state ( $\lambda=1$ ) against  $\lambda$ . The experimental data are compared against three different models in figure 2. The first is that of chain affine deformation, whereby every pair of chain segments within an elastic strand moves affinely with the macroscopic strain. The second model is the classical one which we call the junction affine deformation, descriptive of the case when only the cross-link junctions deform affinely with the macroscopic strain. This is the model that is commonly invoked in the statistical mechanical description of elastic free energy of an isolated chain in a network. The third is the model of the phantom network proposed by James and others. Given the experimental uncertainty and the limited range of  $\lambda$  covered,

RRD COLLABORATIVE PROGRAMS

Table 1. The Apparent Root-Mean Square Radius of Gyration, of Poly-(butadiene-d<sub>6</sub>) in Amorphous Bulk Mixtures and in Uniform Networks.

Perdeuteriochain content, %	Method 1 <sup>a</sup>		Method 2 <sup>b</sup>	
	A <sup>c</sup>	B <sup>c</sup>	A	B
	Mixtures			
3	40.6 ± 3.9	35.4 ± 4.4	27.0 ± 4.0	26.3 ± 3.5
2	42.7 ± 4.8		28.8 ± 3.8	
1	40.8 ± 6.3		35.3 ± 8.5	
Infinite dilution			36.9 ± 10.5 <sup>d</sup>	
	Networks (3% perdeuteriochain)			
Extension ratio λ				
1	39.4 ± 4.1	40.6 ± 4.8	30.4 ± 4.8	26.0 ± 6.7
1.22	41.5 ± 5.4			
1.25	43.8 ± 7.6			
1.43	54.8 ± 3.4			
1.53	58.6 ± 12.2			
1.55	53.0 ± 6.2			

<sup>a</sup> From the limiting slope of small  $q$ . <sup>b</sup> Fitting to the Debye form factor. <sup>c</sup> Two sets of samples described in the Experimental Section.

<sup>d</sup> The only value extrapolated to infinite dilution.

we can conclude that our preliminary data are in qualitative accord with the prediction of the model of junction affine deformation.

## C. NON-RFD PROGRAMS

### ACTIVATION ANALYSIS: SUMMARY OF 1978 ACTIVITIES

Thomas E. Gills  
(Inorganic Analytical Research Division)

The Activation Analysis Group of the Inorganic Analytical Research Division is physically located in the NBS Reactor building. It has at present a staff of 8 full-time members and has programs in the areas of reactor neutron activation analysis, photon activation analysis, nuclear track detection and prompt gamma activation analysis. These programs include both basic and applied research projects and analytical programs on a wide variety of sample types. This is a summary of the activation analysis programs and activities during the past fiscal year.

1. Research Programs with Activation Analysis
  - a. The National Environmental Specimen Bank (NESB)  
Thomas Gills, Harry Rook, Robert Greenberg

Development of Sample Storage  
and  
Analysis Techniques for NESB Samples

For the past two years the U.S. National Bureau of Standards has been cooperating with the U.S. Environmental Protection Agency in examining sampling, storage and analytical methods for use in archiving environmental samples for retrospective analysis. During the past year investigations of different parameters, utilizing activation analysis, were made in the sampling and storage areas, particularly for the determination of trace elements. The effects of microbiological action on trace constituents' concentrations and distributions are well documented. However, the mechanism for complete long-term elimination of that microbiological activity has not been well documented. Freezing has long been applied as a technique for storage; however, no study has previously been made to document the reliability of this method of storage for more than a short period of time. Recently, the analysis and sub-

## NON-RRD NBS PROGRAMS

sequent reanalysis of a **selected animal tissue** (bovine liver) that had been stored frozen at  $-80^{\circ}\text{C}$  for a period of one year gave us the first indication that our preliminary protocols for the storage of fresh tissue are valid, i.e., polyethylene sealed samples stored at  $-80^{\circ}\text{C}$ . The original organ had been subset sampled and the remainder homogenized with a commercial food blender and portioned into six polyethylene ice cube trays containing 14 samples each. The trays were individually sealed in 1 mil thick polyethylene film and stored in a chest type  $-80^{\circ}\text{C}$  freezer. Analyses were performed on the subsets of the liver tissue before freezing to provide initial trace elemental concentrations and to verify contamination free homogenization of the sample.

After one year, one tissue cube was removed from each of the six trays and the trays resealed for future studies. The selected tissue cubes were freeze-dried and analyzed using the same analytical procedures utilized in the initial analyses. A comparison of the results of this reanalysis to those originally obtained is given in table 1. No detectable losses occurred as a result of homogenization, freezer storage and freeze-drying of the liver tissue. These findings support recent studies that in freeze-drying, minimal losses and/or contamination of trace elements occur.

The complexity of the chemical composition of many environmental and biological materials and the extreme low levels of toxic elements pose a problem in selecting a method or procedure that would ensure precise and accurate analysis. Methods must be sensitive, specific and capable of measuring an analyte within required uncertainty levels. Recently new or improved analytical methodologies have been developed to analyze typical NESB type samples. The most promising methods include a new multi-element separation procedure coupled with neutron activation which enables the simultaneous determination of Cd, As, Sb, Se, Cu and Cr. As a test of the accuracy of results, previously certified NBS Standard Reference Materials were analyzed. The results are shown in table 2. A second procedure currently under investigation will allow for the

Table 1. Analysis of stored bovine liver storage and analyses protocol

(Concentrations Reported on Weight Basis)  
µg/g

Samples Type	No. of Samples	Fe	Cu	Zn	Mo	Se	Co	As	Analysis Proced. Used
I. Subset Samples(+)	18	76+7	68+10	39+3	.89+ <u>.12</u>	.29+ <u>.05</u>	.007+ <u>0.006</u>	4+ <u>1</u>	RNAA
II. Homogenate(*)	7	79+4	69+5	40+2	.76+ <u>.04</u>	.30+ <u>.05</u>	.077+ <u>0.005</u>	6+ <u>2</u>	RNAA
III. Homogenate(*)	5	74+6	69+3	39+2	.80+ <u>.05</u>	.30+ <u>.03</u>	.073+ <u>0.003</u>	6+ <u>2</u>	RNAA
IV. Subset Set	6	75+4	---	39+1	---	.29+ <u>.02</u>	.075+ <u>0.002</u>	---	INAA
Average	36	76+2	69+1	39+1	.82+ <u>.07</u>	.29+ <u>.01</u>	.075+ <u>0.002</u>	5+ <u>1</u>	
Error: Standard Deviations of Means									
III. Reanalysis after 1 yr (+,*)	6	69+7	70+2	38+1	.82+ <u>.08</u>	.27+ <u>.05</u>	.076+ <u>0.003</u>	4+ <u>1</u>	RNAA

+Fresh or Frozen Tissue  
\*Freeze-dried

NON-RRD NBS PROGRAMS

simultaneous determination of Hg, Pt, Pd, Au and Os. These multi-element techniques will greatly reduce the analytical cost when large numbers of samples are processed during the operation of the specimen bank. The coupling of proper sampling and storage to these improved analytical techniques will allow the accurate determination of trace constituents of importance to human health.

Table 2. Determination of As, Sb, Se, Cr, Cd, and Cu  
in NBS Subbituminous Coal SRM 1635

(concentration in  $\mu\text{g/g}$ )

Element	NBS SRM Subbituminous Coal 1635	
	Certified Values	This Work
As	$0.42 \pm 0.15$	$0.44 \pm 0.05$
Sb	(0.14)	$0.12 \pm 0.01$
Se	$0.9 \pm 0.3$	$0.82 \pm 0.04$
Cr	$2.5 \pm 0.3$	$2.48 \pm 0.08$
Cd	$0.03 \pm 0.01$	$0.029 \pm 0.007$
Cu	$3.6 \pm 0.3$	$3.56 \pm 0.36$

Values in parentheses are NBS information values.

## NON-RRD NBS PROGRAMS

### b. Trace Elements in Solar Cell Silicon

R. M. Lindstrom, R. F. Fleming, H. L. Rook, and P. J. Paulson

The Low-Cost Solar Array project, managed by Jet Propulsion Laboratory for the Department of Energy, has as its goals the production of electricity from sunlight at a cost of \$2.00 per peak watt in 1983, and 50¢ per watt in 1986. This latter goal is a reduction by a factor of 20 from the present cost of photovoltaic power, to a level competitive with more conventional sources of electricity.

One factor of major importance in this cost reduction is the price of silicon from which solar cells are made. For space applications, where cost considerations were secondary and production quantities small, semiconductor-grade silicon was satisfactory and appropriate. It is expected that cheaper silicon, produced in much larger quantity at a lower grade of purity will be optimum for terrestrial applications, and an important determinant of the price of silicon is the degree of purity that will give acceptable solar cell performance. Information to date is still incomplete, but some elements seem to be tolerable in concentrations above 1  $\mu\text{g/g}$  while others must be below 1  $\text{ng/g}$ .

Accurate measurement of concentration at the low nanogram range is difficult, because of the small signal available from the small quantity of analyte, and because of the likelihood of large noise from environmental contamination. A program of measurements by neutron activation analysis (NAA) in collaboration with isotope dilution spark source mass spectrometry (IDSSMS) is underway to address these analytical problems. Interference-free NAA sensitivities in the NBSR have been calculated table 1 and shown to be reasonable representations of reality in favorable cases. The conditions assumed were irradiation to saturation or for 8 hours (whichever is shorter) at  $6 \text{ E}13 \text{ n/cm}^2\text{s}$ , followed by counting for 2 half-lives or 8 hours (whichever is shorter) in contact with a Ge(Li) detector of 15% efficiency (25 cm; relative to 3" x 3" NaI). The determination limit  $L_q$  (Currie, Anal. Chem. 40 586 (1968) is that amount of element which is determinable with 10% relative standard deviation from

NON-RRD NBS PROGRAMS

Table 1. - Interference-Free Determination Limits  
for Neutron Activation

Element	Radio-isotope	$t_{1/2}$	E $\gamma$ (KeV)	Determination Limit		
				Calculated at/cm <sup>3</sup>	Observed ng	
*Sodium	<sup>24</sup> Na	15.0 h	1368	2.5E10	4.2E-4	
*Magnesium	<sup>27</sup> Mg	9.1 m	844	1.2E14	2.0	
*Aluminum	<sup>28</sup> Al	2.2 m	1779	1.0E13	1.9E-1	
Silicon	<sup>31</sup> Si	2.6 h	1266	8.9E15	180	
Chlorine	<sup>38</sup> Cl	37 m	1642	2.3E12	6.7E-2	
Calcium	<sup>47</sup> Ca	4.5 d	1297	2.8E16	8100	
Scandium	<sup>46</sup> Sc	84 d	889	1.6E11	5.3E-3	3E-3
*Titanium	<sup>51</sup> Ti	5.8 m	320	2.1E13	7.2E-1	
*Vanadium	<sup>52</sup> V	3.8 m	1434	2.3E11	8.3E-3	2
*Chromium	<sup>51</sup> Cr	28 d	320	4.2E12	1.5E-1	0.7
*Manganese	<sup>56</sup> Mn	2.6 h	847	1.1E9	4.2E-5	0.1
*Iron	<sup>59</sup> Fe	45 d	1099	6.9E14	28	40
Cobalt	<sup>60</sup> Co	5.3 y	1173	2.1E12	8.9E-2	8E-2
*Nickel	<sup>65</sup> Ni	2.5 h	1482	6.4E12	2.7E-1	200
*Copper	<sup>64</sup> Cu	13 h	511	5.3E9	2.4E-4	
*Zinc	<sup>69m</sup> Zn	14 h	439	2.6E11	1.2E-2	
-	<sup>65</sup> Zn	240 d	1116	6.7E13	3.1	3
Arsenic	<sup>76</sup> As	26 h	559	6.7E9	3.6E-4	
*Zirconium	<sup>95</sup> Zr	66 d	757	1.3E15	86	
-	<sup>97</sup> Zr	17.0 h	658	6.3E12	4.1E-1	
Molybdenum	<sup>99m</sup> Tc	67 h	141	1.2E11	8.1E-3	
Tin	<sup>113</sup> Sn	120 d	392	3.9E12	3.3E-1	
Antimony	<sup>122</sup> Sb	2.7 d	564	1.7E10	1.5E-3	8E-3
Gold	<sup>198</sup> Au	2.7 d	412	3.1E8	4.4E-5	

Determination limit mass of element or atomic concentration in a 1-g sample determinable with 10 percent precision (r.s.d.), based on Poisson counting statistics of the full-energy peak with zero baseline. See Text.

## NON-RRD NBS PROGRAMS

Table 2. Trace Elements in Silicon

<u>Sample No.</u>	<u>Element</u>	<u>Concentration</u>		Estimated Uncertainty % rsd
		ng/g	atoms/cc $\times 10^{-15}$	
W-002-00	Cu	0.24	0.006	30
W-003-00	Mn	4.8	0.12	4
W-005-Mn	Mn	38.	0.96	4
W-007-Cu	Cu	2.6	0.050	18
W-013-Mn	Mn	10.2	0.26	17
W-017-Cu	Cu	502.	11.0	2
W-019-Cu	Cu	12.6	0.28	11
W-020-00	Cu	0.26	0.007	40
W-026-Mn	Mn	0.33	0.008	22
W-027-Mn/Cu	Mn	35.	0.89	20
W-027-Mn/Cu	Cu	56.	1.23	7
W-030-Cr/Cu	Cu	58.	1.29	6
W-031-Cr/Mn	Mn	61.	1.55	4
W-041-Ni/Cr/Cu	Cu	0.22	0.005	40
W-047-Cu/Ni/Zr	Cu	56.	1.24	6
W-051-Cu/Ti	Cu	0.08	0.002	100
W-055-Cu	Cu	1.2	0.027	40
W-056-Cu	Cu	2050.	45.	2
C5ES	Mn	25.	0.64	6
MLBS	Mn	0.093	0.0024	10
B-M3BD	Mn	0.84	0.021	30
B-M11BS	Mn	3.7	0.094	17

Sample W-056-Cu was analyzed by both techniques. Neutron activation found  $235 \pm 5$  ng Cu in the sample, and isotope dilution spark-source mass spectrometry found 234, after a 3 ng blank was subtracted. The concentrations found in many of the above samples differ from predictions or previous analyses, or both.

Poisson counting statistics of the full-energy peak with zero baseline.

A series of silicon samples (supplied by JPL) deliberately doped with trace impurities has been measured. A representative set of data is presented in table 2, from which the quality of the analyses in real samples can be judged.

## NON-RRD NBS PROGRAMS

### c. Gamma Dose Measurements Using A Plastic Detector

B. S. Carpenter and L. J. Picione

The measurement of x-ray and Co-60  $\gamma$ -ray dose and dose distribution by dielectric plastic detectors has been reported in much detail over the last 10 years. The absorbed dose is determined by measuring changes in such quantities as: mass, chemical etch rate, optical absorbance, color, etc., of the plastic detector. The advantages of using plastic detectors are: low cost, handling ease, the dose field is not disturbed, relatively simple readout, long-term document storage, etc.

In the present study Cronar, polyethylene terephlate, detectors were exposed in the following NBS facilities to the indicated doses:

Co-60 (0.2 - 20 MRAD)

10 M-watt Research Reactor (0.1 - 10 MRAD)

Spent Fuel Storage Pool (1 - >20 MRAD)

The reactor exposures were done in RT-4 with a mixed field of neutrons ( $10^{14}$ - $10^{16}$ ) and gamma rays. Included in each plastic sample packet was a radiochromic dye detector for purposes of calibration. The gamma dose was determined by measuring the change in optical density of visible light as a function of chemical etch time (6N-NaOH@40±1°C, 10 min etch intervals).

The results indicate that a maximum optical density at a specific chemical etch time correlates with the gamma dose in the range: 2-20 MRAD. Detectors exposed to an equivalent gamma doses in the reactor and Co-60 facilities show no discernable shift in their gamma response, indicating the neutron exposure does not alter the gamma dose signal. It was also observed that a thin gelatin layer had been placed on one surface of the plastic at the time of manufacture. Chemical removal of this layer prior to irradiation resulted in a complete loss of gamma signal.

Work is continuing in optimizing the dose signal by changing the etchant concentration and temperature.

NON-RRD NBS PROGRAMS

- d. Determination of Thermal Neutron Flux for Fission  
Track Geochronology  
B. Stephen Carpenter

The nuclear track technique (NTT) has found an application in geology since 1962 when Price and Walker (1962) found that natural mica contained a number of fission tracks from the spontaneous fission decay of U-238. With this discovery and the simplified age equation suggested by Price and Walker (1963), the geologist had a new tool for determining ages of various minerals. The age determination from the equation follows:

$$A = \frac{\rho_s}{\rho_i} \cdot \frac{I(\Phi t)\hat{\sigma}}{\lambda_f^{238}}$$

Where,

- A = Age of Sample (yr)  
 $\rho_s$  = Spontaneous fission track density ( $\text{Tcm}^{-2}$ )  
 $\rho_i$  = Induced fission track density ( $\text{Tcm}^{-2}$ )  
 I = Isotopic ratio of  $^{235}\text{U}/^{238}\text{U}$   
 $(\Phi t)$  = Total neutron fluence ( $\text{n}\cdot\text{cm}^{-2}$ )  
 $\hat{\sigma}$  = Effective cross-section for the  $^{235}\text{U}$  (n,f) reaction ( $\text{cm}^2$ )  
 $\lambda_f^{238}$  = Spontaneous fission decay rate of  $^{238}\text{U}$  ( $\text{yr}^{-1}$ ),

was based on the simple theory that the absolute rate at which spontaneous fission events or tracks from U-238 accumulate in minerals is proportional to the uranium content and, therefore, the measurement of both the spontaneous track abundance and the uranium content is necessary. The uranium content is determined simply by inducing fission to a measurable portion of the uranium. This measurement utilizes the fact that thermal neutrons cause fission of U-235. The final procedure of the age measurement is to count the spontaneous tracks, then the sample is exposed to a known thermal neutron fluence in a nuclear reactor and

## NON-RRD NBS PROGRAMS

the newly induced tracks are counted. From the ratio of these two track densities, together with the thermal neutron fluence, the age is then calculated.

The simplicity of both the technique and theory have caused many users difficulties and problems in the determination of ages. One of the problems arose in selecting the best decay constant since several values exist. To a large extent this problem has been resolved by users reporting the value used in the determination. However, the neutron fluence value cannot be as easily resolved, since each nuclear reactor is unique and their neutron spectra will vary.

The neutron flux,  $\Phi(\text{ncm}^{-2}\text{s}^{-1})$ , is comprised of two components and is defined as:

$$\Phi = \phi_{\text{th}} + \int_{0.5\text{ev}}^{\infty} \phi_{\text{epi}}(E)dE$$

where  $\phi_{\text{th}}$  is the thermal neutron flux,  $\phi_{\text{epi}}$  is the epithermal neutron flux per unit of energy and  $dE$  is the energy interval. The contribution from each of these components to the total neutron flux is a function of sample position relative to the core during irradiation and type of moderation used. As the neutron flux changes with energy so does the effective cross-section,  $\hat{\sigma}$  for the  $^{235}\text{U}(\text{n},\text{f})$  reaction which is defined as

$$\hat{\sigma} = \sigma_0 \left( 1 + \frac{\phi_{\text{epi}} \cdot I_0}{\phi_{\text{th}} \cdot \sigma_0} \right)$$

where  $\sigma_0$  is the  $2200 \text{ m}\cdot\text{s}^{-1}$  value of the cross-section for U-235,  $582 \times 10^{-24} \text{ cm}^2$ , and  $I_0$  is the resonance integral for the  $^{235}\text{U}(\text{n},\text{f})$  reaction at infinite dilution.

NON-RRD NBS PROGRAMS

$$I_o = \int_{0.5\text{ev}}^{\infty} \frac{\sigma(E)}{E} dE = 280 \times 10^{-24} \text{cm}^2.$$

So if the flux is not highly thermalized, a large fraction of fissions will be induced from U-235, as well as U-238 and Th-232, by epithermal neutrons.

There are several ways by which either the total neutron flux or the thermal neutron flux can be determined. One method of determining the neutron flux as suggested by Fleisher et al. (1975), Carpenter and Reimer (1974), and Kleeman and Lovering (1970) is to use glasses with known uranium content which are then irradiated with metal foils. The radioactivity produced from the metals during the irradiation is used to determine the neutron flux. Then the neutron flux observed by the metal foil is related to the track density produced in the glass.

In order to determine the thermal activity,  $A_{th}$ , induced from the total activity,  $A_{tot}$ , in the foil monitor, it is necessary to know the cadmium ratio  $R_{Cd}$  of the metal foil for the irradiation position used. If the absorption of part of the epithermal neutrons in the cadmium shield is neglected, then  $A_{th} = A_{tot}(1-1/R_{Cd})$ . Finally, the thermal neutron flux is calculated from the activation equation.

$$\phi_{th} = \frac{A_{th}}{N\sigma_m} (1 - e^{-\lambda_m t})^{-1}$$

where  $N$  is the number of target atoms present in the metal foil;  $\sigma_m$  is the thermal cross section of the atoms in the metal foil,  $\text{cm}^2$ ;  $\lambda_m$  is the decay constant of the product nuclide; and  $t$  is the irradiation time.

## NON-RRD NBS PROGRAMS

- e. Simultaneous Determination of Arsenic, Antimony Cadmium, Chromium, Copper, and Selenium in Environmental Material, by Radiochemical Neutron Activation Analysis

M. Gallorini, R. R. Greenberg, and T. E. Gills

In studies of environmental pollution, elements such as arsenic, antimony, chromium, cadmium, copper, and selenium are among the most interesting due to their toxic nature. These elements are usually found at very low concentration in most samples of interest. The accurate analysis of these elements can be accomplished only by techniques that are very sensitive and selective. Neutron activation analysis usually meets these requirements; however, in many cases the elements to be determined must be separated selectively from neutron activated matrices. Utilizing Radiochemical Neutron Activation Analysis (RNAA), one can obtain maximum sensitivity, accuracy, and selectivity.

Usually, the choice of the radiochemical procedure to be followed is dependent upon the elements to be determined, the nature of the materials to be analyzed, and the simplicity of the chemistry. Several radiochemical procedures such as solvent extraction, distillation, ion exchange chromatography, precipitation and electrodeposition can be used to obtain satisfactory results.

However, when used alone most of these procedures are not suitable for simultaneous multielement analysis. Furthermore, when several chemical steps are necessary, quantitative separation becomes extremely difficult; often, the determination of chemical yields, which can contribute to the analytical error is required.

In this work a multielement radiochemical separation procedure has been tested and optimized to determine six elements simultaneously in different NBS environmental Standard Reference Materials (SRM's). Hydrated Manganese Dioxide (HMD), an inorganic ion exchanger was used for the retention and subsequent determination of As, Cr, Sb, and Se, while a solvent extraction system using diethyldithiocarbamate compounds was used to determine Cd and Cu.

NON-RRD NBS PROGRAMS

Table 1. Determination of As, Sb, Se, Cr, Cd, and Cu in NBS orchard leaves and bovine liver. concentration in  $\mu\text{g/g}$

Element	NBS SRM Orchard Leaves 1571		NBS SRM Bovine Liver 1577	
	Certified Values	Found Values	Certified Values	Found Values
As	$10 \pm 2$	$9.7 \pm 0.4$	(0.055)	$0.054 \pm 0.004$
Sb	$2.9 \pm 0.3$	$2.8 \pm 0.1$	(-----)	$0.012 \pm 0.002$
Se	$0.08 \pm 0.01$	$0.09 \pm 0.01$	$1.1 \pm 0.1$	$1.06 \pm 0.06$
Cr	$2.60 \pm 0.3$	$2.67 \pm 0.15$	$0.090 \pm 0.015$	$0.085 \pm 0.009$
Cd	$0.11 \pm 0.01$	$0.116 \pm 0.008$	$0.27 \pm 0.04$	$0.30 \pm 0.02$
Cu	$12 \pm 1$	$11.6 \pm 0.4$	$193 \pm 10$	$185 \pm 7$

The reported value for each element consisted of ten determinations. Values in parenthesis are NBS information values.

NON-RRD NBS PROGRAMS

Table 2. Determination of As, Sb, Se, Cr, Cd, and Cu in NBS SRM western coals  
concentration in  $\mu\text{g/g}$

Element	NBS SRM Western Coals	
	Certified Values	Found Values
As	$0.42 \pm 0.15$	$0.44 \pm 0.05$
Sb	$(0.15) \pm$	$0.12 \pm 0.01$
Se	$0.9 \pm 0.3$	$0.82 \pm 0.04$
Cr	$2.5 \pm 0.3$	$2.48 \pm 0.08$
Cd	$0.03 \pm 0.01$	$0.029 \pm 0.007$
Cu	$3.6 \pm 0.3$	$3.56 \pm 0.36$

---

The reported value for each element consisted of ten determinations. Values in parentheses are NBS information values.

In an attempt to demonstrate applicability to matrices having different chemical compositions, the following NBS materials were analyzed: Orchard Leaves (SRM 1571), Bovine Liver (SRM 1577), and Sub-bituminous Coal (SRM 1635).

The results are shown in tables 1 and 2. The results indicate very good agreement between certified and found values, demonstrating that the procedure is accurate.

The retention of arsenic, selenium, chromium, and antimony on HMD in  $1\text{M HNO}_3$  is highly selective and quantitative, while the elution of Cd and Cu is complete.

The decontamination of the elements of interest from Sodium-24 and other radioactive matrix interferences can be estimated to be a factor of  $10^8$ .

## NON-RRD NBS PROGRAMS

The simplicity of the method permits a rapid isolation of the radioisotopes of interest without many chemical steps. The quantitative recovery avoids the calculation of the chemical yield. The sensitivity and accuracy obtained in this work demonstrates the validity and the precision of this radiochemical procedure.

### f. Development of a RNAA Procedure for the Determination of Hg and Noble Metals in Rocks

M. Gallorini and T. E. Gills

The analysis of rocks for the determination of Hg, Os, Ru, Pt, Au and Ir are always difficult due to the very low concentration of these elements. Activation Analysis has the sensitivity for these ultra-low determinations when coupled to radiochemical separations.

Radiochemical separations procedures found in the literature for many of these elements are often involved due mainly to the nature of the chemistry of noble metals. This work presents a radiochemical separation procedure which allows the determination of seven elements simultaneously. The general scheme adopted is shown in figure 1.

The samples and carriers were dissolved by fusion in a nickel crucible using a mixture of  $\text{Na}_2\text{O}_2$  and NaOH (10:2). The fusion was carried out in a Vycor tube under an air stream at  $850^\circ\text{--}900^\circ$  as to quantitatively retained the mercury in a joined tube cooled at liquid nitrogen temperatures.

Osmium and Ruthenium were then separated using a fractional distillation of their tetroxides which were distilled from sulfuric acid solution by adding sodium bromate. The two tetroxides were then absorbed and collected in cold sodium hydroxide. Gold, Platinum, Iridium and Palladium, remaining in "pot" solutions, were absorbed on ion-exchange resin (IONAC SR-3) from a solution 6M in HCL. This ion-exchange resin showed high retention and selectivity for these metals.

## NON-RRD NBS PROGRAMS

Table 1. The analysis of U.S.G.S. rock (PCC-1) using radiochemical activation analysis

<u>Element</u>	<u>μg/g Found</u>	<u>Mean</u>	<u>σ</u>	<u>Literature μg/g</u>
Hg	11.2, 9.13, 10.1, 9.9, 8.8, 9.3, 9.1, 8.9	9.60	± 0.8	7.7, 10, 4
Os	13, 9.99, 8.93, 12.5	11.1	± 1.7	6.7, 6.4, 11, 12.3
Ru	13, 11.3, 10, 13.7, 12	12.0	± 1.4	6.5, 8.4, 9.5, 9.8, 10.3, 11.3
Au	0.7, 0.78, 0.7, 0.71, 0.8, 0.73	0.74	± 0.04	0.6, 0.7, 0.73, 0.8, 0.8, 1.4, 1.6, 3.2
Pt	14, 13, 12, 11, 8.7	11.6	± 2.3	5.1, 3.5, 8, 15
Pd	5.6, 5.5, 6.8, 8, 7	6.6	± 1	3.0, 5.9, 6.0, 7, 13, 29
Ir	3.9, 3.4, 4.6, 5.1	4.1	± 0.6	3.5, 2.6, 5, 5.1, 5.2, 5.6, 5.7, 6.6, 7.1, 8

The results obtained in the analysis of U.S.G. (PCC-1) rock are shown in table 1. The concentrations found are compared with those reported in the literature. The quite wide spread for some elements reported in literature reflects the difficulty of determining low concentrations of noble metals. The results obtained with this method, are in good agreement with and inside the range of the reported values.

The multielement capability of this radiochemical procedure with its degree of sensitivity places radiochemical activation analysis among the best analytical techniques for the determination of these elements at ppb levels. The method is relatively simple, quantitative, and accurate.

## NON-RRD NBS PROGRAMS

### g. The Use of Radiochemical Activation Analysis For The Determination of Hg and Cd

R. R. Greenberg

A radiochemical separation procedure has been developed to separate Hg and Cd from other neutron-activated products. The procedure is based on solvent extraction and involves the use of Nickel Diethyldithiocarbamate [Ni (DDC)<sub>2</sub>] to remove Hg and Zinc Diethyldithiocarbamate [Zn (DDC)<sub>2</sub>] to remove Cd.

The basic procedure followed involved dissolving the samples with HNO<sub>3</sub> and H<sub>2</sub>SO<sub>4</sub> in a Telfon-lined bomb to prevent loss of Hg during dissolution. After dissolution H<sub>2</sub>O<sub>2</sub> was added to the solution to destroy the various NO<sub>x</sub> compounds formed.

The pH of each solution was adjusted to 1.5 with NH<sub>3</sub> and the solution was transferred to separatory funnels containing 20 ml of 0.005 M Ni(DDC)<sub>2</sub> in chloroform. After shaking for 2 minutes, the organic phase containing Hg was drained from each funnel and 20 ml of 0.005 M Zn(DDC)<sub>2</sub> in chloroform was added. Each funnel was shaken for two minutes and the organic phase containing Cd and most of the Cu was drained into a second separatory funnel. Cd was then back extracted by shaking for 15 seconds with 20 ml of 2M HCl.

This procedure was tested on SRM 1577 (Bovine Liver) and good agreement with the certified values of Hg and Cd was observed.

### h. Prompt Gamma Activation Analysis

G. E. Gordon, W. H. Zoller, W. B. Walters, D. L. Anderson,  
M. P. Failey

(University of Maryland, College Park, MD),

R. M. Lindstrom

A collimator and shutter have been installed in the V5 reflector position at the NBS reactor by the University of Maryland group in cooperation with the NBS staff, in order to initiate studies of a new

## NON-RRD NBS PROGRAMS

analytical technique: neutron-capture prompt  $\gamma$ -ray activation analysis (PGAA). A detection system based on a large, high resolution Ge(Li) detector surrounded by a NaI crystal has been developed for measurement of prompt  $\gamma$ -rays of energies ranging from 80 keV to 11 MeV. With a temporary external beam tube in place, neutron and  $\gamma$ -ray backgrounds were investigated prior to design and construction of a well-shielded beam tube and massive shielding for the detection system. With the backgrounds made suitably low, it has been possible to investigate  $\gamma$ -ray spectra of a wide range of samples. These spectra are being analyzed to identify species contributing the observed lines. Whenever an element's presence is suspected, standards of the pure element or simple compounds must be irradiated to determine its complete spectrum. This is necessary in order to determine which lines are useful for analytical purposes and which have interferences from other elements. From the results to date, it appears that PGAA will be able to measure the following elements in many types of samples: H, B, C, N, Na, Al, Si, S, Cl, K, Ca, Ti, V, Mn, Fe, Sm and Gd. Many other elements will be measurable in certain classes of samples. Furthermore, the list of elements is incomplete, as not all lines have yet been identified in the spectra. The quantitative application of the method is being tested using a wide range of NBS Standard Reference Materials whose elemental compositions are well characterized. Measurements have been made for about twelve elements in several standards. In general, the agreement with previous measurements is quite good.

## NON-RRD NBS PROGRAMS

### i. Analysis of Archaeological Artifacts by Instrumental Neutron Activation Analysis

M. J. Blackman

Trace and minor elemental concentrations were used to construct characteristic elemental profiles for a number of different types of archaeological artifacts and geological source samples. Artifacts were matched with source samples to determine the geological origin of the raw material and/or the place of manufacture of the artifact. The objective was to attempt to answer questions concerning the development and evolution of exchange systems and cultural contacts between peoples.

Continuing research on three different types of material is being conducted. Seventy-five obsidian artifacts from two archaeological sites in southern Iran, dating from the 4th through the 2nd millennia B.C. and source samples from several obsidian flows in central Turkey, western Turkey and the Armenian S.S.R. have been sampled and analyzed. Seven distinct elemental groups have been recognized in the artifacts and three of these groups have been assigned to known obsidian occurrences, two in western Turkey and one in the Armenian S.S.R.

Over one-hundred clay objects, including tablet blanks, beads, figurines, and spindle whorls from four archaeological sites in Iran and one site in Iraq have been sampled and analyzed. The objective was to use classes of clay objects which have a low probability of being trade items to delineate the trace and minor element variability in the local clays from each of the five sites. Excavated clay sealings used to seal objects which may have been traded between the various sites were then compared to the profiles generated for the clay objects to attempt to establish exchange networks. This research is on-going and no definite conclusions can as yet be reported.

The third type of material being investigated is ceramics from the late 4th and early 3rd millennia levels at Tal-e Malyan, Iran, the site

## NON-RRD NBS PROGRAMS

of the ancient city of Anshan and from several small villages in the same general area. The objective is to attempt to establish, through trace and minor element profiling of the ceramics, the local and regional influence of the developing center at Anshan. This research is also ongoing with an insufficient number of samples so far analyzed to draw any conclusions.

### j. Absolute Determination of Phosphorus in Neutron Transmutation Doped Silicon

R. F. Fleming

Very uniform and precise phosphorus doping of silicon ingots is achieved by irradiation in a thermal neutron flux via the reaction  $^{30}\text{Si} (n, \gamma \ ^{31}\text{Si}, \beta^-) \ ^{31}\text{P}$  [IEEE Transactions on Electron Devices, Vol. ED-23, #8, p. 800 (August, 1976)]. Such high quality doped silicon, used for solar cell and power thyristor production, is being processed in ton/year quantities at various nuclear reactors around the world. Determination of the phosphorus concentration in the range of  $10^{13}$ - $10^{17}$  atoms/cm<sup>3</sup> is a very difficult analytical problem if carried out after the fact.

It has been recognized [Bickford, N. A. and Fleming, R. F., "Silicon Irradiation Facilities at the NBS Reactor", to be published in the Proceedings of the Neutron Transmutation Doping Conference, Columbia, Missouri (1978)] that a direct, absolute measurement of the phosphorus in the ingot can be obtained by gamma counting the 2.62 hour Si-31 activity with a calibrated detector:

$$M_p = \frac{A_0 \tau}{\epsilon \Gamma \gamma}$$

Where  $M_p$  = total P-31 in the silicon ingot

$A_0$  = decay corrected count rate

$\tau$  = irradiation time

$\epsilon$  = detector efficiency for  $E = 1266$  KeV

$\Gamma_\gamma$  = number of 1266 KeV gammas/decay of Si-31

## NON-RRD NBS PROGRAMS

The absolute accuracy of this technique clearly depends on how well the branching ratio,  $\Gamma_\gamma$ , is known. Unfortunately only a single, 25 year old measurement exists [Lyon, W. S. and Manning, J. J., "Radioactive Si-31", Phys. Rev., 93, 501 (1954)], and it appears to be in error by as much as 50 percent. Therefore, a careful measurement of the gamma-ray branching ratio has been undertaken jointly with Dr. Francis Schima of the Center for Radiation Research. Preliminary results indicate that a determination at the +3 percent level will be obtained.

### k. Determination of Helium-3 Depth Profiles in Metal Tritides

R. F. Fleming

A joint effort has been undertaken with Sandia Laboratories, Albuquerque, to investigate the use of thermal neutron beams to determine the amount and depth profile of helium-3 in metal tritides by means of the  $^3\text{He}(n,p)^3\text{H}$  reaction. The metal tritides,  $\text{MT}_2$  are stoichiometrically loaded with tritium which, as it undergoes its natural 12-year beta decay, produces the helium-3. These tritides are fabricated as targets for high yield 14-MeV neutron generators which are used for defense, medical therapy, and analytical purposes. The buildup of the helium-3 and its migration in the tritide may have a significant effect on the long term integrity of the neutron targets.

Initial measurements with implantation-loaded He-3 targets have given proton spectra which are very encouraging. It appears that sensitivities of less than  $10^{15}$  He-3 atoms/cm<sup>3</sup> are possible and that, by unfolding the proton spectrum measured with a surface barrier detector and using the appropriate stopping power, depth resolutions of less than 100Å can be obtained.

Work is now underway to modify the NBS Reactor horizontal beam BT-3 to allow the study of actual metal tritide samples.

## NON-RRD NBS PROGRAMS

### 1. Field Test of Reactor Track-Etch Neutron Flux Monitor

B. S. Carpenter

As a part of the international reactor safeguards program, track-etch monitors are currently being evaluated as a reliable method for providing an independent record of reactor power history. Lack of reliable and complete supporting data in past tests of the monitors has made interpretation of past test results almost impossible. The need therefore is to evaluate the track-etch monitors carefully and accurately by testing them under well defined experimental conditions.

The track-etch monitor is an externally-powered device designed to record the neutron flux from operating reactors and other sources for extended periods of time. A strip of 35 mm wide polymer tape is driven past a group of six fissionable nuclides which are exposed to the local neutron flux. A given fraction of the fission fragments generated penetrate the tape producing radiation damage tracks that are subsequently etched and counted to permit a reconstruction of the temporal flux history to which the monitor was exposed. The monitor is equipped with 15.2 meters of tape which is adequate for over one year's operation at the nominal speed of 2.9 cm per day. Under these conditions the monitor is designed to operate at a neutron flux of  $10^6 \text{ n}\cdot\text{cm}^{-2}\text{S}^{-1}$ . This reactor operating history should show the periods of operation, shutdown periods and/or other significant changes in reactor operating conditions. Any data concerning the neutron flux level, flux spectrum and gamma flux at the monitor's test location will be noted and recorded. Similar types of monitors have been installed in other reactors under the supervision of the Arms Control and Disarmament Agency and the International Atomic Energy Agency.

A similar monitor was also installed in the Nuclear Channel #2 Detector Well of the NBS Research Reactor for 56 days from 25 July to 19 September 1978. This monitor was exposed to a thermal neutron flux

## NON-RRD NBS PROGRAMS

of  $1 \times 10^6 \text{ n} \cdot \text{cm}^{-2} \text{ s}^{-1}$  and a gamma dose rate of 140 R/h. The radiation activity from the monitor after removal from the detector well was  $< 0.1 \text{ mR/hr}$ . The NBS Research Reactor is the best characterized reactor in the world and should provide reliable tests and data of the track-etch monitor.

In collaboration with NBS, IAEA plans to install and evaluate the track-etch monitor at several typical U.S. power reactors for a period of three to six months under well-documented conditions of environmental and reactor operations.

### m. NDA-Gamma-Ray Spectrometry

B. S. Carpenter

In order to compile an archival gamma-ray spectrum library of known  $^{235}\text{U}$  enrichment levels, counting standards were prepared from the NBS SRM Uranium Isotopic Standards. These standards were prepared with the help of L. A. Machlan and J. S. Maples, of the Inorganic Analytical Chemistry Division, from the  $\text{U}_3\text{O}_8$  stock material fired at  $800^\circ\text{C}$  for one hour, then a nominal 300 mg of material was transferred into thin-window lucite holders and sealed.

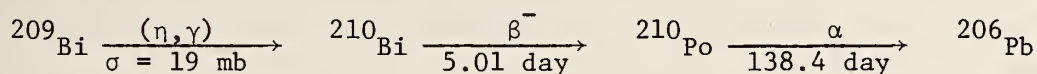
Data reduction techniques and methods for determining the atom percent of U-235 on low-enriched materials ( $\leq 10$  percent) have been applied to the archival gamma-ray spectrum library of known U-235 enrichment levels. The result of this work has been to establish calibration curves for the determination of the U-235 atom percent.

## NON-RRD NBS PROGRAMS

### n. Determination of Trace Concentrations of Bismuth by Activation Analysis

R. F. Fleming

When bismuth is irradiated with thermal neutrons and the resulting five day Bi-210 is allowed to decay, one obtains a source of Po-210 which decays by alpha particle emission:



This Po-210 alpha activity may therefore be counted to provide an analysis for bismuth. Among the stable elements bismuth is unique in producing a long-lived alpha activity.

Since alpha counting is characterized by high efficiencies and low backgrounds, the method should be accurate, sensitive and reliable. Alpha detection will be done using both electronic counters for high accuracy and rapid determination, and the plastic track detectors - developed by Drs. Carpenter and Pilione - for highest sensitivity when precision better than  $\pm 5$  percent is not required. The only possible interference with the 5.3 MeV Po-210 alpha is that from the natural decay chains of uranium and thorium. These can be exactly accounted for by running a parallel unirradiated sample as a blank.

Two approaches to the alpha counting will be developed: nondestructive direct counting of the sample, and counting the extracted Po-210 following post-irradiation dissolution of the sample.

#### 1. Non-destructive Counting

This technique can determine bismuth at the sub- $\mu\text{g}$  level, but requires an accurate value of the alpha particle range in the matrix (or a bismuth standard with the same matrix) to obtain values for the concentration. The nuclear track technique, which is at least 100 times more sensitive than electronic detection, will also provide a mapping of the bismuth surface distribution.

## NON-RRD NBS PROGRAMS

### 2. Post-irradiation Dissolution

If after irradiation all of the Bi-210 is allowed to decay and the sample dissolved, the resulting Po-210 can be spontaneously plated out on a silver foil (yield  $>99.7$  percent) for counting. By counting against an SRM alpha standard the bismuth concentration is obtained directly. Using this technique, bismuth can be determined at the sub-ng level, interferences from thorium are eliminated, and those from uranium are reduced by at least a factor of ten.

A second nuclear method using photon activation analysis and Ge(Li) counting with the reaction  $^{209}\text{Bi}(\gamma, 3n)^{206}\text{Bi}$  has been developed by Dr. George Lutz. Accurate results have been obtained at the 10 ppm level and the method is completely independent of the neutron induced alpha activity method.

#### o. Cadmium Analysis by Radiochemical Neutron Activation Analysis

R. Greenberg

Cadmium has been suspected of causing detrimental health effects in humans even at very low levels. Since Cd is commonly found at the trace or ultra-trace level, many analytical techniques do not have the sensitivity to accurately determine the concentration of this element in many environmentally important materials. In a recent interlaboratory comparison of oyster material carried out by the International Atomic Energy Agency, the reported values of the Cd concentration ranged from 0.4 to 4.4  $\mu\text{g/g}$  [Intercalibration of Analytical Methods on Marine Environmental Samples - Progress Report No. 13]. This illustrates the problems involved in determining the "true" Cd concentration in biological materials even when this concentration is relatively high. These problems become more serious as the Cd content decreases. In addition, there are some instances in which the total amount of material available for analysis

## NON-RRD NBS PROGRAMS

is very small, such as for hair samples or certain types of atmospheric particulate samples. Analytical techniques capable of measuring very small amounts of Cd are therefore required.

Radiochemical Neutron Activation Analysis (RNAA) has been routinely used at the NBS to analyze Cd in a variety of environmentally important matrices. The method used to separate Cd from other neutron-activated products is solvent extraction. Zinc diethyldithiocarbamate [ $\text{Zn}(\text{DDC})_2$ ] in chloroform will quantitatively extract Cd from an aqueous solution over a pH range from 1 to 12. In addition to the extraction of Cd,  $\text{Zn}(\text{DDC})_2$  will also extract Cu, which can interfere with the Cd analysis by producing a high background level of radiation. This can be avoided by first extracting with  $\text{Bi}(\text{DDC})_3$  in chloroform which removes Cu, but not Cd. Copper concentrations can, therefore, be determined in addition to Cd.

This two-extraction radiochemical separation procedure is very versatile and is often used as part of a larger multielement analysis scheme. As demonstrated in section e and g of this report. Hydrated manganese dioxide (HMD) was used to retain As, Sb, Se, and Cr prior to extraction and the eluted fraction is then extracted with  $\text{Bi}(\text{DDC})_3$  to remove Cu, and then with  $\text{Zn}(\text{DDC})_2$  to remove Cd.

A number of NBS Standard Reference Materials were analyzed by the previously mentioned procedure, and the Cd and Cu results obtained are compared with the certified values in the following tables. Very good agreement is observed, demonstrating the accuracy of this technique.

NON-RRD NBS PROGRAMS

Table 1. Cadmium in various SRMs

	<u>Concentration-<math>\mu\text{g/g}</math></u>	
	<u>This Work</u>	<u>Certified</u>
Orchard Leaves (SRM 1571)	0.116 $\pm$ 0.008	0.11 $\pm$ 0.01
Pine Needles (SRM 1575)	0.194 $\pm$ 0.009	< 0.5
Bovine Liver (SRM 1577)	0.295 $\pm$ 0.015	0.27 $\pm$ 0.04
Rice Flour (SRM 1568)	0.029 $\pm$ 0.005	0.029 $\pm$ 0.004
Wheat Flour (SRM 1567)	0.030 $\pm$ 0.005	0.032 $\pm$ 0.007
Sub Bituminous Coal (SRM 1635)	0.030 $\pm$ 0.002	0.03 $\pm$ 0.01
River Sediment (SRM 1645)	10.2 $\pm$ 0.4	10.2 $\pm$ 1.5
Urban Particulate (SRM 1648)	71.2 $\pm$ 3.7	75 $\pm$ 7

Table 2. Copper in various SRMs

	<u>Concentration-<math>\mu\text{g/g}</math></u>	
	<u>This Work</u>	<u>Certified</u>
Orchard Leaves (SRM 1571)	11.6 $\pm$ 0.4	12 $\pm$ 1
Pine Needles (SRM 1575)	3.04 $\pm$ 0.16	3.0 $\pm$ 0.3
Bovine Liver (SRM 1577)	185 $\pm$ 7	193 $\pm$ 10
Rice Flour (SRM 1568)	2.12 $\pm$ 0.09	2.2 $\pm$ 0.3
Wheat Flour (SRM 1567)	2.21 $\pm$ 0.10	2.0 $\pm$ 0.3
Sub Bituminous	3.56 $\pm$ 0.18	3.6 $\pm$ 0.3

## NON-RRD NBS PROGRAMS

### p. Organic Mercury in Tissues

R. Zeisler, T. E. Gills

Increased interest of ecologists and analysts has been focused on the ratio of organic mercury to total mercury content of biological and environmental samples. The determination of the total mercury content of these matrixes using NAA procedures has been extensively investigated in the past years, and some RNAA methods are considered fully reliable for this purpose. So far, the determination of organic mercury has been carried out by use of other methods, e.g., gas-chromatography. Thus, two samples have to be analyzed by different methods to yield the desired information on the ratio of organic mercury to total mercury content.

Well developed extraction and volatilization techniques are currently being investigated for the isolation of methylmercury from biological tissues. Since the possible radiolytic damage to organic mercury compounds during irradiation cannot be fully assessed, we are developing and applying a modified extraction technique to be used in a pre-irradiation and "normal" RNAA scheme. This will yield information about the changes of the chemical form of organic mercury during irradiation.

The separation of organo- or methylmercury is based on the volatilization of methylmercury cyanide formed in the reaction of methylmercury in a sample with hydrocyanic acid released by the interaction of a cyanoferrate with sulfuric acid at elevated temperatures. The methylmercury cyanide released is captured on cysteine paper in a microdiffusion cell. The paper is then placed in a flux of neutrons and the mercury quantitatively determined by neutron activation analysis.

The feasibility of this method is currently being tested. Szilard-Chalmers reactions that can change the chemical status of the mercury and possible losses of mercury from the sample have to be assessed. Test analyses have proven that irradiation has to be performed in sealed quartz containers. Samples can then be counted either "instrumentally" in the irradiation container or after using the combustion methods. Both

## NON-RRD NBS PROGRAMS

require comparable samples and standard configurations. The use of mercury deposits on filter paper (comparable to the proposed cysteine paper) is being evaluated.

In addition, the volatilization method for mercury determination after the reduction of the inorganic mercury by  $\text{SnCl}_2$  will give the possibility of cross-checking of the mercury contents. The reduction method is claimed to be selective for the inorganic mercury (only 0.5% of the organomercury is released). This is, however, critically dependent on the chemical treatment of the samples. This has to be carefully investigated.

The procedure utilizes the volatility of mercury and its compounds; more importantly the inherent sensitivity of neutron activation analysis along with minimum use of reagents and solvents should provide increased accuracy over currently used methods.

### q. Determination of Iodine in Foods by Radiochemical Activation Analysis

H. L. Rook, R. M. Lindstrom

Iodine is an essential element in the human diet. The recommended daily allowance is only 150 micrograms per day, so that in order to measure the intake of iodine accurately, analyses of foods at a level of 1 ppm or less is required. In addition, there is little information on the reproducibility of available analytical methods. We recently measured iodine in six freeze-dried food materials, as a contribution to an interlaboratory comparison coordinated by M. Heckman of Ralston Purina Company. Orchard Leaves (SRM 1571) and Oyster Tissue (SRM 1566) were analyzed in parallel. Duplicate samples of all materials were irradiated for periods up to five minutes in the RT3 pneumatic facility of the NBS Reactor and combusted in a flowing oxygen atmosphere. Chlorine and

## NON-RRD NBS PROGRAMS

Table 1. Iodine content of foods and SRMs

Sample	Iodine found ( $\mu\text{g/g}$ , by wt)	Mean I concentration ( $\mu\text{g/g}$ )
SRM 1571	0.177	0.183
Orchard Leaves	0.185 0.188	
SRM 1566	2.87	2.79
Oyster Tissue	2.71	
Stew	0.057 0.046	0.051
Corn	0.0094 0.0084	0.0089
Milk	6.24 6.42	6.33
Vegetables	0.064	0.066
Protein	0.068	
Wheat	0.0099	0.0095
Cereal	0.0090	
Tuna	0.59 0.63	0.61

bromine were separated by passing through hydrated manganese dioxide and the iodine trapped on silvered quartz wool. The procedure has been published [H. L. Rook, J. Radioanal. Chem. 39, 351 (1977)].

Our results are given in the attached table 1. Comparison among eight laboratories shows poor agreement. Other investigators using chemical methods for analyses appear to be limited by blanks. Agreement with the other activation analysis laboratory reporting, however, was better; but, there was a calibration discrepancy even there. Clearly the state of iodine analysis in foods requires further work.

## NON-RRD NBS PROGRAMS

### r. Silicon Irradiation Facilities at the NBS Reactor

N. A. Bickford and R. F. Fleming

A program of silicon irradiation is being carried out at the National Bureau of Standards 10MW, heavy water moderated reactor using the reaction  $^{30}\text{Si}(n,\gamma)^{31}\text{Si}(\beta^-)^{31}\text{P}$  to achieve phosphorus doping of high uniformity at precisely known levels.<sup>1</sup>

#### Characterization of Irradiation Facilities

When comparing irradiation facilities for transmutation doping of silicon, two quantities, in addition to the spatial uniformity of the neutron flux, are important: 1) the P-31 production rate and 2) the rate of radiation damage. The P-31 production rate is determined by the magnitude of the thermal neutron flux while the radiation damage rate has three components:

- 1) The unavoidable damage resulting from the  $^{30}\text{Si}(n,\gamma)^{31}\text{Si}$  reaction itself, which is essentially proportional to the P-31 production.
- 2) The damage resulting from high energy neutrons whose energies are well above any appreciable cross section for the  $^{30}\text{Si}(n,\gamma)^{31}\text{Si}$  reaction.
- 3) The damage resulting from the intense gamma ray field.

In order to establish some measured quantities which can be used to characterize irradiation facilities we should consider the several radioactivities that are produced when pure silicon is irradiated in a reactor flux. When the 2.62 hour half life Si-31 decays there is a 1266.1 KeV gamma ray emitted with an intensity of about 0.07%.<sup>2</sup> The specific activity of this gamma line is of course directly proportional to the P-31 doping rate. The high energy neutrons always present in any reactor spectrum produce three other activities in silicon via the reactions  $^{28}\text{Si}(n,p)^{28}\text{Al}$ ,  $^{29}\text{Si}(n,p)^{29}\text{Al}$  and  $^{30}\text{Si}(n,\alpha)^{27}\text{Mg}$ . Both the Al-28 and the Mg-27 activities are also produced by thermal neutron reactions on any aluminum or magnesium impurity that may exist in the silicon. The 6.52 minute Al-29 activity is unique and results in a gamma ray at

NON-RRD NBS PROGRAMS

1273.3 KeV. This suggests that a simple characterization of a silicon irradiation facility can be accomplished by irradiating high purity silicon and then gamma counting the Si-31 and the Al-29 activities produced.

The corrected count rate,  $A_0$ , for any particular activity is defined as

$$A_0 = \frac{\lambda N e^{\lambda t_1}}{(1-e^{-\lambda \tau})(1-e^{-\lambda \Delta})} \left[ \frac{e^{\lambda \delta} - 1}{\lambda \delta} \right]$$

where

$$\lambda = \frac{\ln 2}{\text{half life}} = \text{decay constant}$$

$N$  = net counts in the photo peak

$t_1$  = decay time from end-of-irradiation to start-of-count

$\tau$  = irradiation time

$\Delta$  = counting live time

$\delta$  = counting dead time

We propose the ratio  $A_0(^{31}\text{Si})/A_0(^{29}\text{Al})$  as a measure of the ratio of phosphorous production to neutron damage in an irradiation facility. Although the silicon damage function has a significantly different energy dependence than the  $^{29}\text{Si}(n,p)^{29}\text{Al}$  cross section, both are sensitive to the flux of high energy neutrons. The fact that the gamma ray energies of the two activities are only 7 keV apart means that the difference in the Ge(Li) detector efficiencies can be ignored and no detector calibration is necessary. The measurement consists of counting the 1273.3 keV line of Al-29 and then, after it and the 1267.9 keV single escape line from Al-28 have decayed away, counting the 1266.1 keV Si-31 line.

The measurement of  $A_0(^{31}\text{Si})$  and of the ratio  $A_0(^{31}\text{Si})/A_0(^{29}\text{Al})$  were carried out on the vertical tubes G2 and G4 and on the pneumatic tube

NON-RRD NBS PROGRAMS

Table 1. Doping parameters in NBS reactor

IRRADIATION FACILITY	$A_0(^{31}\text{Si})^{**}$	$\frac{A_0(^{31}\text{Si})}{A_0(^{29}\text{Al})}$
G2*	1.0	0.74
G2 (2" Above)*	0.99	-
G2 (6" Above)*	0.89	0.40
G4*	1.28	0.83
RT4	0.086	9.51

\*Core Gap Center-Line

\*\*Normalized to G-2 Center-Line Value

RT4. The results are shown in the table 1. We see that G4 not only has a higher P-31 production rate than G2, but that the production-to-damage ratio is somewhat improved. Notice also that at 6 inches above core midplane in G2, which is in the fueled region, the production-to-damage ratio has dropped significantly. The results in RT4 show that if high P-31 production rates are not necessary it is possible to obtain doping with greatly reduced fast neutron damage. The predicted phosphorous doping rate of  $7.5 \times 10^{13}$  atoms  $\text{cm}^{-3} \text{hr}^{-1}$  is in good agreement with measured values.

1. Bickford, N. A. and Fleming, R. F., "Silicon Irradiation Facilities at the NBS Reactor", *Proc. Second International Conference on Neutron Transmutation Doping of Semi-conductors* (1978)

## NON-RRD NBS PROGRAMS

### 2. SRM Certification Program

T. E. Gills

An essential function of the National Bureau of Standards (NBS) is the production and certification of materials that have accurately established characteristics which can be used to determine that a measurement system provides meaningful information. These materials, identified as standard reference materials (SRM's), are certified for particular chemical or physical properties. During the last fiscal year activations analysis both instrumental and radiochemical, was used in the certification and homogeneity testing of 17 different SRM's. Such an effort was made possible through the group's capability in multielemental analysis made possible by an effective automation and data reduction system.

The following is a list of various matrices analyzed by Activation Analysis.

<u>SRMs</u>	<u>Other Materials</u>
a. Rice Flour	a. Polymers
b. Wheat Flour	b. Silicon
c. Copper Benchmarks	c. Graphite
d. Eastern Coals	d. Plastic Ware
e. Western Coals	e. Flu Vaccine
f. Air Particulate Dust	f. Freeze-Dried Foods
g. Bovine Serum	g. Raney Nickel
h. River Sediment	h. IAEA Oyster
i. Fly Ash	i. Shark Tissue
j. Bauxite	j. Recycled Fuel Oil
k. Orchard Leaves	
l. Trace Metals in Water	
m. Spinach	
n. Pine Needles	
o. Bovine Liver	
p. Tomato Leaves	
q. NBS Oyster	

Though most of the group analyses were done on NBS SRMs, many materials analyzed came from within NBS or the private sector.

## NON-RRD NBS PROGRAMS

### a. Analysis of New Fly Ash SRM

R. R. Greenberg

Standard Reference Material 1633 (Fly Ash) was widely used in the analytical community and after this material was sold out a new Fly Ash SRM (1633a) was prepared. The homogeneity of this material was checked using Instrumental Neutron Analysis (INAA). During homogeneity testing the concentrations of eight elements were determined and submitted for OSRM certification.

Two different sample sizes were used for homogeneity testing -- 50 mg and 250 mg. Two 50 mg samples and one 250 mg sample were taken from each of 12 bottles of the new SRM. The samples were irradiated with primary standards and samples of the old Fly Ash SRM in three different rabbits. Midway through irradiation, each rabbit was removed from the reactor, flipped end over end, and reinserted into the reactor to ensure a uniform neutron flux within the rabbit. The primary standards consisted of multielement solutions pipetted onto Whatman 41 filters and were described in last year's progress report. After irradiation, the samples and standards were allowed to decay for one month and were counted 15 cm from the detector. Data reduction was accomplished using the NBS computer code QLN-1 supplemented by hand integration of poorly defined peaks.

The concentrations of eight elements determined in the 50 mg samples are listed in table 1. The concentrations of these elements in the 250 mg samples, and the overall average concentrations in the Fly Ash are listed in table 2. The observed standard deviations are consistent with the counting statistics demonstrating the homogeneity of this material for sample sizes of 50 mg or more.

The results of the analyses of the old Fly Ash SRM are compared in table 3 with the certified and literature (1) values. Very good agreement was observed.

---

1. J. M. Ondov et al., *Anal. Chem.* 47, 1102 (1975).

NON-RRD NBS PROGRAMS

Table 1. Fly ash SRM 1633

Fly ash SRM 1633a - concentration -  $\mu\text{g/g}$  unless % indicated

50 mg Samples

Sample	<u>Cs</u>	<u>Sc</u>	<u>Cr</u>	<u>Fe(%)</u>	<u>Co</u>	<u>Sb</u>	<u>Eu</u>	<u>Th</u>
<u>Rabbit 1</u>								
1B-1	10.2	38.3	198	9.31	46.1	7.13	3.95	25.1
2B-1	11.4	38.6	201	9.22	45.9	6.85	3.87	25.4
6B-1	11.4	39.1	201	9.44	46.7	6.90	4.07	25.9
10B-1	10.9	39.3	204	9.21	45.8	6.71	3.97	25.6
13B-1	10.7	39.1	203	9.34	46.8	7.00	3.93	25.6
1T-1	11.1	38.3	198	9.24	46.2	6.74	3.92	25.3
2T-1	10.7	38.3	202	9.28	46.0	6.76	3.88	25.4
5T-1	10.5	39.6	206	9.28	45.9	6.47	3.96	25.8
9T-1	10.7	38.5	196	9.37	45.5	7.05	3.88	25.0
12T-1	10.4	38.9	201	9.24	45.7	6.56	3.93	25.2
13T-1	9.6	39.6	200	9.38	45.5	6.94	4.01	25.5
$\bar{X}$	10.7	38.9	201	9.31	46.0	6.80	3.94	25.4
$2\sigma$	1.0	0.9	6	0.14	0.8	0.42	0.11	0.5
<u>Rabbit 2</u>								
1B-2	11.2	38.7	200	9.50	46.1	6.94	3.91	25.7
2B-2	10.8	38.7	196	9.41	45.7	6.85	3.80	25.6
6B-2	12.0	39.2	200	9.49	46.2	6.42	3.99	25.9
10B-2	10.5	39.4	203	9.48	46.4	6.68	3.85	26.2
12B-2	11.0	39.2	201	9.46	46.1	7.04	3.97	26.3
13B-2	10.7	39.0	196	9.52	46.2	7.20	3.88	25.9

NON-RRD NBS PROGRAMS

Rabbit 2 cont.

1T-2	10.9	38.6	199	9.40	45.6	6.96	3.85	25.1
2T-2	11.0	38.8	202	9.61	46.5	6.69	4.00	25.6
5T-2	11.7	39.1	199	9.42	46.2	6.67	3.92	25.9
9T-2	10.2	39.0	197	9.57	45.8	6.73	3.95	25.6
12T-2	11.2	38.4	199	9.50	45.5	6.63	3.81	25.0
13T-2	11.1	38.9	198	9.69	47.0	6.80	3.87	25.3
$\bar{X}$	11.0	38.9	199	9.50	46.1	6.80	3.90	25.7
$2\sigma$	1.0	0.6	4	0.17	0.8	0.42	0.14	0.8

## NON-RRD NBS PROGRAMS

Table 2  
Fly Ash SRM 1633a - Concentration -  $\mu\text{g/g}$  unless % indicated

Rabbit	250 mg Samples									
	<u>3</u>	<u>Cs</u>	<u>Sc</u>	<u>Cr</u>	<u>Fe(%)</u>	<u>Co</u>	<u>Sb</u>	<u>Eu</u>	<u>Th</u>	
1B-3		11.1	38.9	200	9.40	46.3	6.66	3.87	25.2	
2B-3		11.2	39.1	201	9.33	46.5	6.81	3.82	25.3	
6B-3		11.0	38.6	201	9.22	45.2	6.58	3.81	24.9	
10B-3		10.8	38.8	200	9.36	45.5	6.98	3.92	25.6	
12B-3		11.2	38.7	202	9.35	46.2	6.46	3.93	25.2	
13B-3		10.5	39.2	205	9.32	46.5	6.79	3.80	25.3	
1T-3		10.6	38.9	198	9.40	46.3	6.72	3.86	25.4	
2T-3		11.0	39.5	200	9.43	46.2	6.95	3.82	25.1	
5T-3		9.9	39.0	198	9.26	46.1	6.50	3.92	26.1	
9T-3		10.8	38.4	198	9.27	45.3	6.65	3.86	25.2	
12T-3		10.8	38.7	200	9.29	46.1	6.89	3.95	25.8	
13T-3		10.6	38.8	198	9.41	46.3	6.71	3.86	25.1	
$\bar{X}$		10.8	38.9	200	9.34	46.0	6.73	3.87	25.4	
$2\sigma$		0.7	0.6	4	0.13	0.9	0.33	0.10	0.7	
					<u>Overall</u>					
$\bar{X}$		10.8	38.9	200	9.38	46.1	6.78	3.90	25.5	
$2\sigma$		0.9	0.7	5	0.23	0.8	0.39	0.13	0.7	

Table 3

## Fly Ash SRM 1633

Concentration -  $\mu\text{g/g}$  unless % indicated

	<u>Cs</u>	<u>Sc</u>	<u>Cr</u>	<u>Fe(%)</u>	<u>Co</u>	<u>Sb</u>	<u>Eu</u>	<u>Th</u>
1633-1*	8.76	27.2	133	6.20	42.4	7.22	2.90	24.9
1633-2*	9.42	27.4	133	6.24	42.2	6.61	2.92	25.5
1633-3*	9.11	27.1	131	6.27	42.5	6.33	2.93	25.0
1633-4*	8.66	27.3	134	6.37	42.2	7.31	2.87	25.2
1633-5**	9.13	27.0	133	6.24	42.2	6.93	2.95	24.8
1633-6**	9.24	27.2	133	6.35	42.5	6.41	2.84	24.5
$\bar{X}$	9.05	27.2	133	6.28	42.3	6.80	2.90	25.0
$2\sigma$	0.58	0.3	2	0.13	0.3	0.8	0.08	0.7
Certified			131+2		(38)			(24)
Literature	8.6+1.1	27+1	127+6	6.2+0.3	41.5+1.2	6.9+0.6	2.5+0.4	24.8+2.2

\*Sample size = 50 mg

\*\*Sample size = 250 mg

## NON-RRD NBS PROGRAMS

### 3. Facilities

R. M. Lindstrom and R. F. Fleming

A major addition to the data acquisition and processing facilities of the group was the purchase of a Nuclear Data 6620 Nuclide Identification System. This system allows simultaneous operations from two display terminals in adjacent counting rooms. Each terminal contains two independent ADCs (expandable in the future), so the result is as if four multichannel analyzers had been acquired. The system also contains 96 K words of 16-bit memory, two disks with a total of 10 M bytes storage capacity, a real-time clock, a magnetic tape deck, fast printer, and Teletype. Software is available for data acquisition and display, peak search and nuclide identification, a comprehensive set of file manipulations, and program development in FORTRAN, BASIC, and MACRO assembler. All system resources are available to a user at any of the three terminals.

This system offers the opportunity to make a number of improvements in our operations. With data processing now available in the counting room, experiments can be monitored and modified as the measurements are in progress without waiting overnight for a computer run. Qualitative analysis in particular is much easier, with the gamma-ray tables now stored in the computer. Interactive spectral data analysis is now practical, with the user able to modify the method of data reduction to fit the situation at hand. As we gain experience with the file structure, real-time statistical control over the performance of the counting systems will be implemented, with a major improvement on the quality as well as the quantity of data.

## NON-RRD NBS PROGRAMS

### FISSIONABLE DEPOSIT MASS ASSAY

D. M. Gilliam, W. E. Slater, J. A. Grundl  
(Nuclear Radiation Division)

The Neutron Field Standards section has continued to improve and expand its mass assay program for the NBS collection of Reference and Working Fissionable Deposits. A new alpha particle counting system has been set up and put into routine operation. In addition to many routine comparisons this system was used to compare the NBS U-235 Reference Deposit (23S-2-2) with a very carefully assayed deposit (LASL Spare No. 1) from the Los Alamos Scientific Laboratory. A second comparison with the LASL deposit was made by fission counting at the NBSR thermal column.

#### 1. Alpha Particle Counting System

A low-geometry alpha particle counting system has been built to allow routine mass assay intercomparisons and long-term integrity checks for our fissionable deposit collection.

Figure 1 shows a schematic diagram of the arrangement of the system. Flat and parallel surfaces and careful assembly technique make possible highly reproducible vertical spacing--an imprecision of less than  $\pm 0.006$  mm. The effect of this error in spacing reproducibility on the counting efficiency is less than 0.03% and is usually hidden by statistical error. Larger geometric errors occur due to the deviation of the deposit backings from perfect flatness. A measuring microscope is used to determine the average deposit height (without touching the deposit), so that departures from flatness up to  $\pm 0.1$ mm can be tolerated without incurring errors in excess of  $\pm 0.2\%$ .

The fixed low-geometry configurations themselves are regarded as artifact standards, comparable in long-term integrity to the most durable standard alpha-emitting deposits.

Table 1 gives the results of the comparison of LASL Spare No. 1 and the UNB U-235 Reference Deposit.

#### 2. Fission Counting Comparison

NON-RRD NBS PROGRAMS

Using a large fission chamber on loan from the Lawrence Livermore Laboratory, the comparison of the LASL standard and the NBS Reference Deposit was repeated by counting the fission rate of each deposit simultaneously in a well collimated beam extracted from the NBSR thermal column.

These results are also given in table 1. The mass used for LASL spare No. 1 was 1550.4 $\mu$ g.

Table 1. U-235 Isotopic Mass of NBS Reference Deposit 25S-2-2

Published Value	248.3 <u>+1.2%</u> $\mu$ g
New Value from LASL Spare No. 1 via $\alpha$ counting	247.0 <u>+0.5%</u> $\mu$ g
New Value from LASL	247.5 <u>+0.7%</u> $\mu$ g

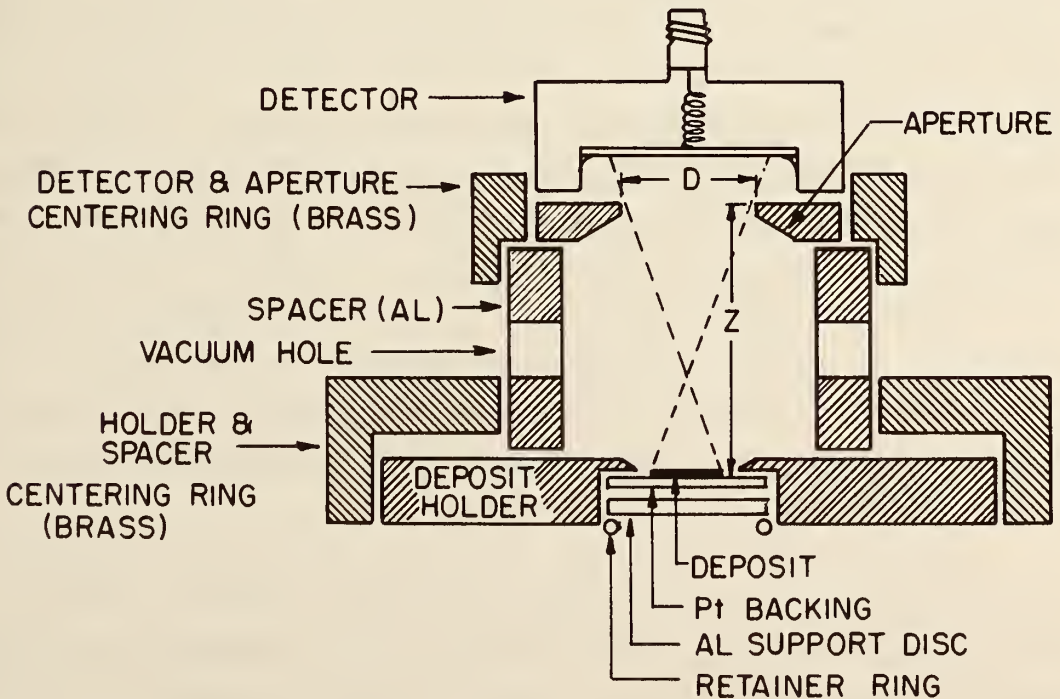


Figure 1. Schematic View of Alpha Counting Geometry. Five spacer cylinders of various heights permit values of Z from 15mm to 114mm. Three sizes of aperture diameters from 6.3mm to 29.4mm are available.

## NON-RRD NBS PROGRAMS

### PRECISION GAMMA-RAY WAVELENGTHS

E. G. Kessler, Jr., R. D. Deslattes, W. C. Sauder and A. Henins  
(Center for Absolute Physical Quantities)

The unique high resolution crystal spectrometer, figure 1, we have operating at NBS has produced a significant body of new results.<sup>1</sup> Initial operation has been in the range  $0.05 < E < 1.0$  MeV. First definitive results were published in early 1978.<sup>2</sup> These gave values for Au-198 411 and 675 keV together with Ir-192 206, 296, 308, 316, 468, 588, 604 and 612 keV. These results have a typical  $1\sigma$  estimate below 0.5 ppm. This represents a more than forty-fold improvement over previous work.

A special feature of this work is that through absolute measurements using crystals calibrated by x-ray/optical interferometry, results are obtained directly connected to the Rydberg constant  $R_\infty$ . This facilitated revised evaluations of  $\mu$ -mesic and  $\pi$ -mesic x-ray lines and revised comparison with quantum electrodynamic calculations for the  $\mu$ -mesic case. The revised reference wavelengths, together with improved comparisons and analysis lead to the pattern of substantial agreement between theory and experiment shown in figure 2. This resolves a long-standing difficulty historically linked to the vacuum polarization correction to muonic x-ray spectra.<sup>3</sup> In the case of pionic spectra the main objects of interest are the strong interaction shifts and the  $\pi$ -mass. Our new reference wavelength values have led to removal of previously apparent inconsistencies between  $\mu$ -mass values derived from different calibration algorithms.<sup>4</sup>

Subsequent work, carried out in collaboration with two visiting scientists<sup>5</sup> has produced new values for prominent reference lines in Yb-169 and for Tm 84 keV. In the case of Yb-169, new values have been obtained for the lines at 63, 93, 110, 119, 130, 177, 198, 261, and 307

## NON-RRD NBS PROGRAMS

keV. In those cases of groups of three levels connected by cascade-crossover relations, closure tests failures were about 0.1 ppm. In addition to the  $\gamma$ -ray studies, a separate measurement of W  $K\alpha_1$  from an electron bombarded anode of a natural tungsten was carried out.<sup>6</sup> This result was such as to resolve historical conflicts between different routes to estimating the location of Au-198 411 keV.

In a joint effort with the visitors<sup>5</sup> mentioned above, we have undertaken design and assembly of a new two-crystal diffraction instrument. The new design incorporates many features not found in the initial attempt. These include: a greater angular range -  $30^\circ$  instead of  $5^\circ$ ; a more fully compensated optical path for the angle interferometers; full computer control including atmospheric compensation; and, provisions for use of a stationary radiation source such as an in-pile n- $\gamma$  source or the primary proton target in a meson factory or an elemental anode in an electron accelerator. Construction is complete as of mid-August. Calibration and computer programming are underway. Initial measurements of high Z x-ray spectra are expected in September at the NBS 4 MeV electron Van de Graaff.

Finally, after many years since the initial proposal,<sup>7</sup> we are, in August, to make a first attempt to measure a particularly narrowed annihilation radiation component. The narrowing process used involves singlet-triplet mixing and thermalization by elastic collisions in a rare gas (He) moderator at cryogenic temperatures. A massive transfer cask with internal manipulators has been fabricated and tested. It will receive from the NBS reactor a Cu-64 source of about 10 kilocuries. This will be transported to the  $\gamma$ -ray measurement facility and inserted by remote manipulation into the low temperature Dewar. After cool-down, a superconducting solenoid provides the 2 kilogauss field needed to optimally mix triplet and singlet wavefunctions. It is hoped that August will see the first trial run of this system. If it performs as predicted, a new and more accurate value for the electron's Compton wavelength,  $\lambda_c$ , will be obtained. When this is combined with the Rydberg constant,  $R_\infty$ , one obtains a value for the Sommerfeld fine-structure

## NON-RRD NBS PROGRAMS

constant,  $\alpha$ . In favorable circumstances, this value will compare well in accuracy with that available from other sources.

Following its initial application to high Z x-ray spectra, it is of interest to consider application of our new fixed-source instrumentation to in-pile capture- $\gamma$  sources. This will permit extension of the range of our optically based measurements through the range  $2.0 < E < 10$  meV. In addition to providing new and more accurate reference values in this region, we envision two rather definite scientific opportunities. In the first place, we can measure the cascade associated with  $n + {}^{14}\text{N} \rightarrow {}^{15}\text{N}_c$  and  $n + {}^1\text{H} \rightarrow {}^2\text{D}$ . A mass spectrometer measurement of the difference between the  ${}^{15}\text{N}{}^1\text{H}$  and  ${}^{14}\text{N}{}^2\text{H}$  molecules (or ions) is equivalent to this energy via the Einstein relation. It is easy to show that these measurements imply a value for the electrochemical Faraday.<sup>8</sup> Leaving questions of accuracy aside, one also can think of applying the high resolution and linearity of our instrumentation to the problem of unscrambling complex nuclear spectra in the region of 2-4 MeV. This is of particular interest in view of the recent success of the coupled Boson model of nuclear excitation at just slightly lower energies, it is reasonable to expect to see breakdown of the nucleon pairing associated with the coupled Boson picture as one moves toward higher energies where ultimately a statistical picture must prevail. For several reasons, such studies as those just mentioned are not easily imagined to take place on the NBS reactor. There are three reasons for this: first, the NBS reactor is a very busy place with many NBS workers and visitors active at any given time; second, the tangent ports which might be used for n- $\gamma$  work have been preempted except for possible short term access; third, there is a relatively low flux available,  $\sim 10^{13} \text{ s}^{-1} \cdot \text{cm}^{-2}$ . It therefore seems desirable to propose such activity for the higher flux facility ( $8 \times 10^{14} \text{ cm}^{-2} \cdot \text{s}^{-1}$ ) at Grenoble which is also a place where  $\gamma$ -ray work is accorded a higher priority. A proposal to this effect is in preparation.

NON-RRD NBS PROGRAMS

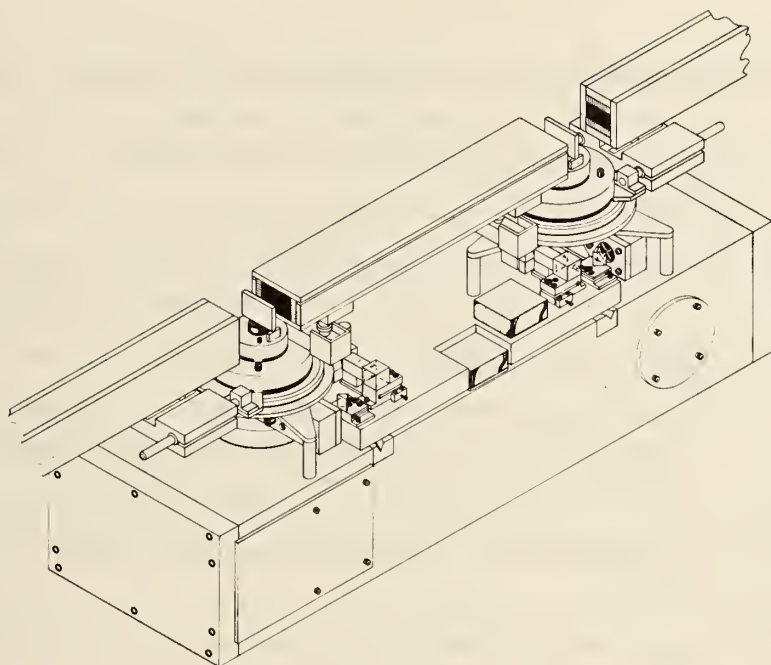


Figure 1. The two axis transmission spectrometer.

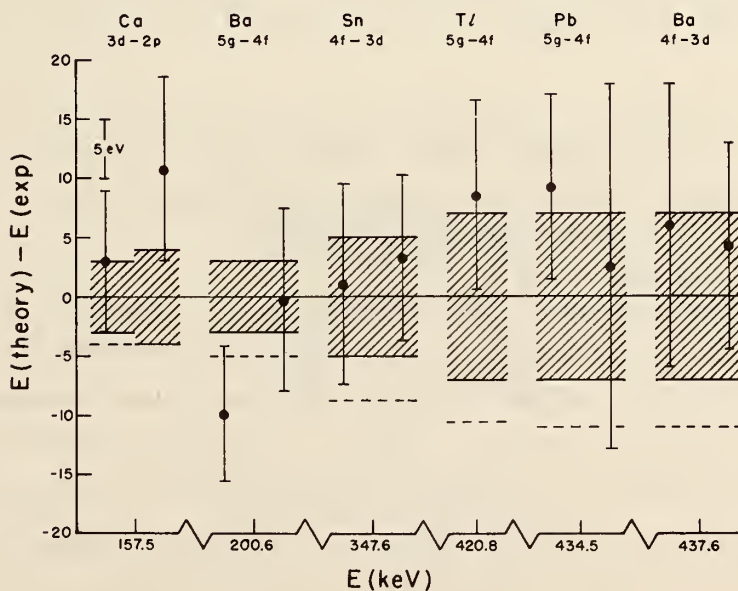


Figure 2. Comparison of recent muonic x-ray data with theory. The hatched bands represent theoretical uncertainties. In the absence of the revised  $\gamma$ -scale, the theory bands would be centered on the dashed lines and the agreement between theory and experiment would be degraded.

## NON-RRD NBS PROGRAMS

1. A detailed description of instrumentation and procedures is in preparation.
2. E. G. Kessler, Jr., R. D. Deslattes, A. Henins and W. C. Sauder, *Phys. Rev. Lett.* 40, 171 (1978).
3. C. K. Hargrove, E. P. Hincks, R. J. McKee, H. Mes, A. L. Carter, M. S. Dixit, D. Kessler, J. S. Wadden, H. L. Anderson and A. Zehnder, *Phys. Rev. Lett.* 39, 307 (1977); T. Dubler, K. Kaeser, B. Robert-Tissot, L. A. Schaller, L. Schellenberg and H. Schneuwly *Nuclear Phys.* A294, 397 (1978).
4. A. L. Carter, M. S. Dixit, M. K. Sundaresan, J. S. Wadden, P. J. S. Watson, C. K. Hargrove, E. P. Hincks, R. J. McKee, H. Mes, H. L. Anderson and A. Zehnder, *Phys. Rev. Lett.* 37, 1380 (1976).
5. These visitors are: Dr. Ludo Jacobs, Leuven University and Mol Laboratories, Belgium and Dr. Wolfgang Schwitz, Fribourg University and SIN, Switzerland.
6. E. G. Kessler, Jr., R. D. Deslattes and A. Henins, Wavelength of the  $W K\alpha^1$  x-ray Line, submitted to *Physical Review A*.
7. W. C. Sauder and R. D. Deslattes, *Jour. Res. NBS* 71A, 347 (1967).
8. This point was originally brought to our attention by B. N. Taylor about two years ago.

## CAVITY FISSION NEUTRON SOURCE IRRADIATION FACILITY

V. Spiegel, E. D. McGarry, and R. A. Dallatore  
(Nuclear Radiation Division)

The NBS cavity fission source operates at the center of a 30 cm diameter spherical cavity located at the center of the NBS Research Reactor graphite thermal column. Figure 1 shows the source-detector capsule in detail and its location within the thermal column cavity. Two disks of U-235 metal (16 mm dia x 0.13 mm thick) are placed above and below a cylindrical cadmium box, which encloses the passive detectors for exposure.

Fission neutron fluxes of  $\sim 2 \times 10^{10}$  n/cm<sup>2</sup> sec are obtained between the source disks at a separation distance of 1 cm. For thin detectors, which are disk shaped and up to 12 mm in diameter, flux gradients are

## NON-RRD NBS PROGRAMS

mild. In the axial direction the flux at  $\pm 1$  mm from the midplane is less than 5% greater than at the midplane; center-to-edge ratios are about 1.3 for a 12 mm dia. disk detector. This small radial flux gradient does not require that detector disks be extremely uniform. A radial nonuniformity of 20% in a detector for example changes the activation rate by less than 0.5%.

Fission neutron return for spherical cavities in graphite has been studied extensively by means of neutron transport calculations in connection with the general development of standard neutron fields in spherical geometry. For the 30 cm cavity at NBS, the response of fission threshold detectors to fission neutrons returning to the cavity center is less than 0.5% of the uncollided fission neutron flux; for higher threshold detectors with 95% of its response above about 2 MeV the response to the cavity return flux is less than 0.1%.

The NBS cavity fission source is not used generally for low-energy integral detectors when high accuracy is required. The cavity return correction for the U-235(n,f) reaction, for example, is nearly 10%. Self

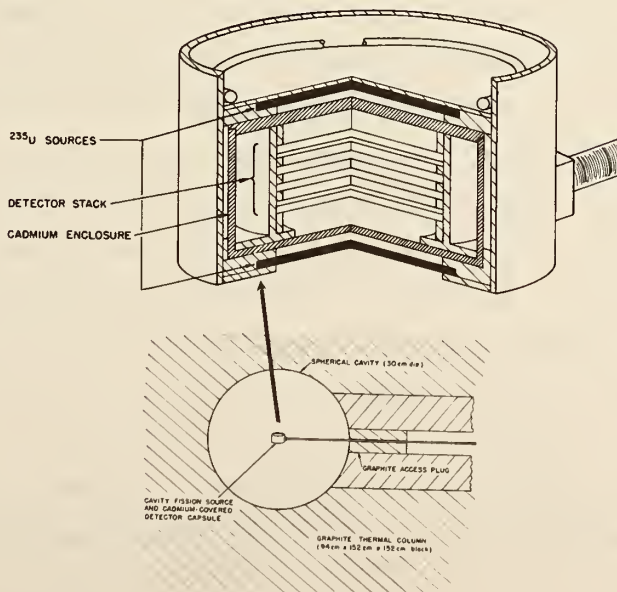


Figure 1. NBS Cavity Fission Source.

NON-RRD NBS PROGRAMS

shielding of this near-1/E cavity return flux for conventional activation foil thicknesses makes this correction uncertain to about twenty percent.

Disk detector irradiations are monitored by means of the  $\text{In}(n,n')$  reaction in monitor foils placed adjacent to the exposed detectors. The absolute neutron flux is obtained with the same  $\text{In}(n,n')$  reaction using the procedure of flux transfer from the Cf-252 fission neutron irradiation facility. In this procedure an  $\text{In}(n,n')$  foil activation is first obtained in a known Cf-252 fission neutron flux. Based on this calibration the  $\text{In}(n,n')$  activation during a cavity fission source exposure is translated to an average U-235 fission neutron flux at the In foil monitor position.

The expression governing the flux transfer in terms of truncated cross section is

$$[(nv)_o]_{\text{cvy}} = \frac{G_{\text{cf}}}{G_{\text{cvy}}} \cdot \frac{\sigma_{\text{cf}}(>E_p)}{\sigma_{\text{cvy}}(>E_p)} \cdot \frac{\Psi_{\text{cf}}(>E_p)}{\Psi_{\text{cvy}}(>E_p)} \cdot \frac{D_{\text{cvy}}}{D_{\text{cf}}} \cdot [(nv)_o]_{\text{cf}},$$

where  $(nv)_o$  = fission neutron flux and "cvy" denotes the U-235 cavity fission neutron flux at the In monitor position/ and "cf" the Cf-252 fission neutron flux for the In calibration exposure.

The ratios on the right side of the equation are, in order, the decay correction factors (G),  $\text{In}(n,n')$  truncated reaction cross sections ( $\sigma$ ), spectrum fractions ( $\Psi$ ), and In detector responses in the cavity and at the Cf irradiation facility. The truncated cross section ratio is  $1.028 \pm 0.010$  and the spectrum fraction ratio  $1.021 \pm 0.014$ . Combined with a typical error of + 1.0% for decay correction factors and detector response ratios, and  $\pm 1.4\%$  for the Cf-252 fission neutron flux,  $[(nv)]_{\text{cf}}$ , the flux transfer procedure yields a free-field U-235 cavity fission neutron flux to an accuracy of approximately  $\pm 2.5\%$  ( $1\sigma$ ).

Fission neutron fluences of up to  $\sim 1 \times 10^{15}$  n/cm<sup>2</sup> may be obtained at the NBS facility in day-long irradiations. The small irradiation volume restricts multiple foil packages to thicknesses of a few millimeters.

## D. SUMMARY OF REACTOR OPERATIONS

All aspects of reactor operations continued to be excellent. Once again, outstanding on-line performance, reactor utilization and fuel efficiency were achieved. A summary of the overall operating statistics for this and previous years is presented in the following table.

NBSR Operating Summary

	<u>1976</u>	<u>1977</u>	<u>1978</u>
Reactor Operations to date, MWH	396,000	459,000	525,000
Reactor Operations for year, MWH	68,000	63,000	66,000
Hours Reactor Critical	6,900	6,400	6,800
Number of Days at 10 MW	283	262	277
On-line Time at 10 MW	78%	72%	76%
Average U-235 Burnup	55%	56%	52%
Number of Unscheduled Shutdowns	2	3	9
Number of Irradiations	2,360	2,255	2,140
Irradiations, Total Hours	7,250	7,400	5,900
Hours per irradiation	3	3.3	2.8
Number of Visitors	7,000	3,000	3,000

## E. SERVICE PROGRAMS

### ACTIVATION ANALYSIS PROGRAM OF THE FOOD AND DRUG ADMINISTRATION AT THE NBSR

J. T. Tanner  
(Food & Drug Administration, Washington, DC)

#### 1. Analysis of Cement Kiln Dust

It has recently been discovered<sup>1</sup> that the addition of cement kiln dust to cattle feed decreased the amount of feed required by the animals and improves the quality of their meat.

The effect of the dust was first observed by Georgia cattle ranchers. They were liming their pastures with dust from a cement kiln and dumped some into their cattle feed. The cattle ate the feed and gained more weight than expected. Wheeler and Oltjen<sup>2</sup> of the U.S.D.A. verified the finding.

The dust is a complex, calcium-rich mixture of minerals that is entrained when hot air is pulled out of the cement kiln. It does not contain the alkalis and hardners necessary for cement to set. About 30 percent of its effect<sup>2</sup> results from a simple buffering action in the gastrointestinal track. The other 70 percent might arise because: (a) the dust contains some element that has not yet been recognized as an essential nutrient for cattle; (b) the intense heat of the kiln causes the minerals in the dust to behave in some manner that is beneficial to cattle; or (c) that the small size of the particles allow them to be absorbed from the gastrointestinal track more easily than conventional mineral supplements.

The Food and Drug Administration has no laws restricting the cement kiln dust use in cattle feed, however, legal action may be taken if any dust residue appears in the meat.

The cement kiln dust was analyzed by Neutron Activation Analysis. Table 1 summarizes the results. These results along with analyses by other FDA scientists will be studied to determine any potential hazard to the consumer which may arise from this practice.

SERVICE PROGRAMS

Table 2. Trace element content of Sea-Derived food ingredients

Substance	Al	As	Ca	Cl	Co	Cr	Cu	Fe	La	Ni	Na	Pb	Sb	Sc	Se	V	Zn
<u>Agar</u>																	
76-26-640	44	-	2800	1550	0.038	0.21	<20	21	0.6	1050	10,200	0.8	0.14	<0.001	0.07	0.96	8.3
76-28-120	43	-	1900	1600	0.04	0.18	<18	20	0.9	970	10,800	0.7	0.18	<0.001	<0.09	0.82	18
76-35-592	168	-	2300	6500	0.07	3.1	<24	140	0.6	1000	10,300	<1	0.03	0.019	0.09	0.6	7.2
76-35-593	175	-	2900	5300	-	<20	-	-	-	1400	8,400	-	-	-	-	0.64	-
76-57-407	464	-	6300	300	0.20	0.7	<50	269	<2	2500	1,800	<4	0.12	0.053	0.3	2.1	192
<u>Alginate Acid</u>																	
76-76-307	102	-	7500	3400	0.10	2.0	<25	55	1.0	<900	7500	<1	<0.03	0.008	<0.1	0.34	3.7
76-76-308	91	-	7200	3400	0.1	1.8	<25	60	0.9	900	8300	1.0	0.07	0.007	<0.1	0.27	3.6
<u>Ammonium Alginate</u>																	
76-76-302	101	-	10,000	3050	0.06	1.2	15	80	1.1	<500	3200	<1	0.03	0.006	<0.08	0.25	2.2
<u>Calcium Alginate</u>																	
76-76-304	112	-	27400	2000	0.06	1.0	<48	51	0.8	<2000	66000	1.0	0.05	0.01	<0.1	0.4	1.8
<u>Potassium Alginate</u>																	
76-76-303	157	-	2100	3300	0.07	1.5	25	39	0.8	1000	2350	6	0.06	0.008	<0.08	0.29	2.2
<u>Sodium Alginate</u>																	
76-35-595	61	-	11000	700	0.06	1.4	50	122	0.8	<1500	77000	<1	0.03	0.089	<0.1	0.3	3
76-35-596	21	-	8800	1750	0.04	1.1	<32	81	0.6	1500	73500	<1	0.03	0.024	0.06	0.22	2.8
76-76-305	113	-	1200	3400	0.08	1.6	<50	52	0.8	<1700	90700	<1	0.07	0.013	<0.06	<0.2	<1
<u>Propylene Glycol Alginate</u>																	
76-35-217	123	-	11000	1100	0.09	1.1	25	57	<1	<1000	15000	<1	0.04	0.006	<0.1	0.35	1.9
76-57-409	64	-	2600	550	0.04	0.6	<25	30	1.2	860	11300	<1	0.24	0.003	<0.2	0.34	<2
76-76-306	99	-	9200	1900	0.11	3.5	<25	68	1.4	<900	16500	<1	0.06	0.002	<0.09	0.31	1.5
<u>Algae Brown (ie:lp.)</u>																	
76-28-395	72	95	12,000	99,000	0.14	0.6	<300	150	0.4	<9000	28000	35	0.04	0.035	0.17	2	13
76-28-396	68	80	12,000	98,000	0.20	0.5	-	244	0.6	9000	29000	34	0.04	0.031	0.18	<2	10
76-35-594	61	71	12,000	10,900	-	-	-	-	-	8400	28000	-	-	-	-	3	-
76-57-408	167	85	11,600	111000	0.42	0.2	-	468	0.6	<9000	28000	40	0.03	0.061	<0.2	<2	29
76-57-413	112	87	17,000	113000	0.85	1.5	-	720	0.8	<8000	32000	46	0.05	0.059	<0.1	<2	101
76-37-420	-	-	-	-	-	-	-	-	-	-	-	-	-	-	-	-	-
<u>Carrageenan</u>																	
76-06-727	50	-	48500	16,300	0.16	0.36	<40	32	<0.4	<1200	25000	10	0.04	0.004	<0.09	0.4	2.9
76-06-768	425	-	13700	7,900	0.20	1.3	<50	188	0.8	<2000	38000	21	0.17	0.045	0.62	3.2	10
76-28-397	131	-	3200	460	0.15	0.41	57	72	<0.4	7500	42000	9	0.04	0.018	<0.09	0.36	1.4
76-28-398	71	-	2100	1050	0.17	0.19	<25	64	0.4	3400	50,000	5	0.04	0.009	<0.07	0.56	2.5
76-35-590	96	-	35000	24700	0.06	1.0	<48	53	1.0	<2000	20,000	22	0.06	0.005	<0.1	1.3	2.3
76-35-591	77	-	32000	20600	0.07	0.8	<35	63	0.8	<1300	18,400	23	0.03	0.003	<0.1	1.5	1.8
76-57-412	303	-	9500	<200	0.12	1.5	<36	190	<1	3300	22700	<3	0.11	0.040	<0.3	0.8	190

## SERVICE PROGRAMS

### 2. Analysis of Sea-Derived Food Ingredients

To support the Generally Recognized As Safe (GRAS) Review committee, the FDA collected and analyzed a series of samples to determine whether there might be an unusual accumulation of toxic elements in these sea-derived ingredients. In the interest of obtaining broadest range of elements per analysis the samples were analyzed by Neutron Activation Analysis (NAA) and Induction Coupled Plasma-Emission Spectroscopy.

Table 2 summarizes the NAA results. There were no unexpected results. Kelp (whole seaweed) had high levels of arsenic which placed it in the category of high arsenic contaminating foods.

This survey was intended as a broad screen to detect any unusual accumulation of heavy metals in these substances. It appears that during the processing of certain seaweeds to obtain agar, algimates, and carrageenan, there is no accumulation on mineral substances. The highest levels are observed in the unprocessed, dried seaweeds such as kelp.

- 
1. T. H. Maugh II, *Science* 199, 413 (1978).
  2. W. E. Wheeler & R. R. Oltjen, U.S.D.A. Report No. ARS-NE-88, December, 1977.

### ATF'S FORENSIC ACTIVATION ANALYSIS PROGRAM

William D. Kinard

(U. S. Treasury Department, Rockville, Maryland)

Neutron Activation Analysis (NAA) still plays a valuable role in the analysis of evidentiary materials submitted to our laboratory. The ability to analyze materials for their trace constituents, nondestructively, is a distinct asset in those cases where the physical integrity of the submitted evidence must be preserved for courtroom presentation.

## SERVICE PROGRAMS

During the past year, our laboratory used NAA in the examination of 55 actual criminal cases, as well as in several on-going research projects. The material examined by this technique consisted of hair, paint, glass, soil, explosive residues, and bullet lead, amounting to some 151 hours of reactor time.

The value of NAA for the examination of paint and human hair is being critically assessed, thus prompting a concentrated effort, by our laboratory, to see whether a trace elemental profile of these materials is of any value.

Promising analytical data has been gathered and will be the subject of a report during the coming fiscal year.

# F. STAFF ROSTER

## REACTOR RADIATION DIVISION

566

R. S. Carter, Chief  
 T. M. Raby, Deputy Chief  
 E. C. Maxwell, Admin. Officer\*  
 E. Simms, Receptionist  
 L. Sprecher, Secretary\*  
 C. Freedman, Secretary\*

Division Staff  
 R. Casella  
 B. Mozer  
 F. Shorten

Neutron S-S Physics  
 J. J. Rush  
 Carol O'Connor, Secy.

Neutron Radiography  
 Donald A. Garrett

Engineering Services  
 J. H. Nicklas

Reactor Operations  
 T. M. Raby  
 J. F. Torrence  
 P. Lewis, Secy.

Magnetic and  
 Amorphous Materials  
 J. Rhyne  
 H. Alperin (GW)  
 N. Koon (GW)  
 R. Williams (GW)  
 J. Lynn (GW)

Crystallography  
 E. Prince  
 A. Santoro  
 C. Choi (GW)  
 A. Tudgay (1/2)  
 D. Fravel (1/2)

Metal Hydrides and  
 Molecular Materials  
 J. Rowe  
 A. Cinquepalma  
 D. Fravel (1/2)  
 W. Rymes (1/2)  
 G. Fish (PD)  
 C. Glinka

Mechanical Design  
 E. Guglielmo  
 J. Sturrock

Reactor Operators  
 R. Beasley  
 M. Bell  
 N. Bickford  
 H. Brake  
 J. Browning  
 D. Cea  
 A. Chapman  
 H. Dilks  
 W. Mueller  
 D. Nelson  
 J. Ring  
 R. Stiber  
 D. Wilkinson  
 B. Young

Biological Materials  
 A. Wlodawer  
 A. Tudgay (1/2)

\* Part-time  
 PD - Postdoctoral  
 GW - Guest Worker

STAFF ROSTER

NON-RRD NBS STAFF LOCATED AT REACTOR

Division 354

P. Cassidy  
K. Eggert  
T. Hobbs  
F. Moore  
J. Shubiak

Division 532

M. Baier  
R. A. Dallatore  
C. Eisenhauer  
D. Gilliam  
J. A. Grundl  
E. McGarry  
I. G. Schroder  
R. Schwartz  
W. Slater  
V. Spiegel

Division 551

D. Anderson  
J. Bailey  
J. Blackman  
B. Carpenter  
R. Fliming  
M. Gallorini  
T. Gills  
C. Grabnegger  
S. Harrison  
J. Koslozis  
R. Lindstrom  
G. Lutz  
J. Maples  
J. Mitchell  
L. Pilione  
H. Rook  
N. Sato  
R. Zeisler

GUEST WORKERS AND COLLABORATORS

Division 520

R. Deslattes  
A. Henins  
L. Jacobs  
E. Kessler  
W. Sauder  
W. Schwitz  
J. Snyder

Division 522

R. Dove  
H. Marshall

Division 532

C. Bowman  
K. Duvall

Division 541

J. Kelly  
T. Madey

Division 544

S. Greer

Division 550

D. Sweger

Division 553

R. Bowen  
C. Han  
M. Mathew

Division 562

B. Christ

Division 564

C. Bechtold

Division 565

A. Mighell  
D. Minor  
R. Roth  
W. Thurber

STAFF ROSTER

Division 741

P. Brown

Office 501

H. Berger

Office 506

D. Becker

Argonne National Laboratory

R. Armani  
T. Brun  
H. Flotow  
O. Hinks  
S. Susman

Battelle, N. W.

W. Nicholson

Bell Laboratory

Brookhaven National Laboratory

Federal Bureau of Investigation

R. Asbery  
D. B. Davies  
J. Haverkost  
J. W. Kilty  
E. Mitchell  
C. Peters  
J. P. Riley

Food and Drug Administration

M. Fiedman  
L. Schroeder  
W. Stroube, Jr.  
J. Tanner

Harry Diamond Laboratory

C. Heimbach

NASA-Langley Research Center

R. Buckingham

National Gallery of Art

B. Miller  
C. Parkhurst  
C. Olin

National Institutes of Health

D. Davies  
R. Frank  
W. Hagins  
W. Robinson

Naval Air Defense Command

M. Stellabotte  
W. Williams

Naval Air Rework Facility

R. Chavez

Naval Research Laboratory

C. Bond  
P. D'Antonio  
A. Ehrlich  
M. Fatemi  
J. Karle  
N. Koon  
V. Rath

Naval Surface Weapons Center  
(White Oak Laboratory)

H. Alperin  
M. Lia  
D. Polansky  
R. Williams

Oak Ridge National Laboratory

J. Cleland  
R. Westbrook  
R. Young

Picatinny Arsenal

C. S. Choi  
H. J. Prask  
S. Trevino

STAFF ROSTER

Smithsonian Institution

M. Blackman  
T. Chase  
J. Mishara  
S. O'Dell  
J. Olin  
L. Zacherman

U. S. Geological Survey

P. Baedeker  
J. Morgan  
J. J. Rowe

U. S. Treasury Department

J. M. Hoffman  
W. Kinard

American University

R. Abbundi  
R. A. Segnan

Colorado State University

C. E. Patton

Georgetown University

K. Barkigia

Harvard University

G. A. Ferguson  
M. Lewis

Reed College

W. Parker

Royal Canadian Military Academy

L. Bennett

University of Arkansas

D. Wolfman  
T. Rolnick

University of California  
(Lawrence Livermore Laboratories)

J. Browne  
S. Hankins

(San Diego Campus)

R. Shelton

University of Connecticut

J. Budnick

University of Chicago

E. Anders  
M. Janssens

University of Houston

H. Jo  
S. Moss

University of Illinois

C. Satternthwaite  
R. Standley

University of Maine

H. Patterson

University of Maryland

D. Anderson  
C. Choquette  
W. Cunningham  
M. Failey  
P. Gallagher  
M. Germani  
I. Gokmen  
C. Gulovali  
G. Kowalczyk  
E. Lepel  
J. Lynn  
J. Muhlbaier  
I. Olmez  
D. Reamer  
E. Schneider  
A. Sigled  
A. Small  
K. Steffansoon

STAFF ROSTER

W. Walters  
J. Weber  
M Yiu  
W. Zoller

University of Paris

B. Le Meindre

University of Pittsburgh

S. Sankar  
W. Wallace

University of Rhode Island

S. Pickart

University of Salford (U.K.)

D. Martin

University of Wisconsin

J. Hinkley  
H. Yu

Allied Chemical Corporation

G. Leibowitz  
A. Maeland

B-K Dynamics

N. Chesser

Caterpillar Tractor Company

W. Evans

Fedders Air Conditioning Company

W. Simpkins

General Electric Company

F. Luborsky  
J. Walter

IBM Corporation

D. Bouloin

Monsanto Research Corporation

W. Brotherton

OLDELFT Corporation

D. Bracher

## G. PUBLICATIONS

### COLLABORATIVE PROGRAMS

- ABBUNDI, R., RHYNE, J. J., SWEGER, D. M., and SEGNAN, R., "Magnetic Relaxation Phenomena in Dy-Sc Alloys." (to be published).
- ALPERIN, H. A., PICKART, S. J., and RHYNE, J. J., "Small Angle Neutron Scattering From Rare-Earth-Iron Alloys." (to be published).
- CASELLA, RUSSEL C., "Neutrino Scattering in a Modified GIM Model." *IL NUOVO CIMENTO*, 42A, 377-369(1977).
- CASELLA, RUSSEL C., "Isotopic Shifts in Complex Crystals." *Phys. Rev. B*, 17(8), 3381-86(1978).
- CHOI, C. S. and PRINCE, E., "Triaminoguanidinium Nitrate by Neutron Diffraction." (to be published).
- CHOI, C. S., and PRINCE, E., "Refinement of  $\alpha$ -Lead Azide by Neutron Diffraction." *Acta Cryst.*, B33, 3536-37 (1977).
- GARRETT, DONALD A., "ASTM Recommended Practice for Thermal Neutron Radiography of Materials and Components." (to be published).
- GARRETT, DONALD A., "The Observation of Electrolyte Phenomena in Lithium Iodide Pacemaker Batteries with Neutron Radiographic Interrogation." Proceedings for Reliability Technology for Cardiac Pacemaker - Symposium Three. (to be published).
- GARRETT, DONALD A., "Neutron Radiography Using Electronic Imaging Technology." *Society of Photo-Optical Instrumentation Engineer* (1978).
- GLINKA, C. J., ROWE, J. M., LIBOWITZ, G. G., and MAELAND, A. "Neutron Crystal-Field Spectroscopy of  $CeD_{2.12}$ ." (to be published).
- GLINKA, C. J., ROWE, J. M., RUSH, J. J., RAHMAN, A., SHINHA, S. K., and FLOTOW, H., "Inelastic Neutron Scattering Lineshapes in  $PdD_{0.63}$ ." *Physical Review B*, 17(2), 488-93(1978).
- HINKLEY, J. A., HAN, C. C., MOZER, B. and YU, H., "Chain Deformations in Rubber." *Macromolecules*, V11(4), 836-38(1978).

## PUBLICATIONS

- FORESTER, D. W., KOON, N. C., SCHELLENG, J. H., and RHYNE, J. J., "Spin Glass and Magnetic Blocking Transitions in Amorphous YFe<sub>2</sub>." (to be published).
- KOON, N. C. and RHYNE, J. J., "Crystal Field Effects on the Spin Wave Dispersion Relations of Cubic Rare Earth-Iron Laves Phase Compounds." *Rare Earths and Actinides*, 37, 112(1978).
- KOON, N. C. and RHYNE, J. J., "Excited State Spin Waves in ErFe<sub>2</sub>." *Solid State Comm.*, 26, 537(1978).
- MARTIN, D. J. and RHYNE, J. J., "Re-Analysis of Dysprosium Magnetostriction," *J. Phys. Chem.*, 4123-26(1977).
- PICKART, S. J., ALPERIN, H. A., and RHYNE, J. J., "Small Angle Magnetic Scattering from a Dilute Amorphous Fe(Tb) Alloy." *Physics Letters*, 64A(3), 337-39(1977).
- PRINCE, E., and CHOI, C. S., "Ammonium Azide." *Acta Crysta.*, B34, 2606-08(1978).
- PRINCE, E., WLODAWER, A., and SANTORO, A., "Flat-Cone Diffractometer Utilizing a Linear Position-Sensitive Detector." *J. Appl. Cryst.*, 11, 173-78(1978).
- RHYNE, J. J., KOON, N. C., MILSTEIN, J. B., and ALPERIN, H. A., "Spin Waves in ErFe<sub>2</sub>", *Physica B*, 86-88, 149(1977).
- RHYNE, J. J., SANKAR, S. G., and WALLACE, W. E., "Sublattice Magnetization of ErFe<sub>2</sub>-H." *The Rare Earths in Modern Science and Technology*.
- RHYNE, J. J., FISH, G. E., SANKAR, S. G., and WALLACE, W. E., "Magnetic Properties of Laves Phase Rare Earth Hydrides", (to be published).
- RHYNE, J., PICKART, S., and ALPERIN, H., "Magnetic Neutron Scattering from Amorphous TmFe<sub>2</sub>." *J. Appl. Phys.* 49(3), 1691-92(1978).
- RHYNE, J. J. and KOON, N. C., "Magnetic Excitations in HoFe<sub>2</sub>." *J. Appl. Phys.*, 49(3), 1691-92(1978).
- ROWE, J. M. and RUSH, J. J., "The Dynamics of Hydrogen in Metals." *Proc. of International Symposium on Neutron Inelastic Scattering.* (to be published).
- ROWE, J. M., RUSH, J. J., and PRINCE, E., "Neutron Diffraction Study of the Structure and Phase Transitions of Alkali Cyanide Crystals." (to be published).

PUBLICATIONS

- ROWE, J. M., RUSH, J. J., CHESSER, N. J., HINKS, D. L., and SUSMAN, S., "Neutron Scattering Study of Rotation-Translation Interactions in  $(\text{KCN})_{0.25}(\text{KBr})_{0.75}$ ." *J. Chem. Phys.*, 68(9), 4320-21(1978).
- ROWE, J. M., RUSH, J. J., CHESSER, N. J., and MICHEL, K. H., "Nature of the Phase Transition in KCN at 168 K.", *Phys. Rev. Letters*, 40(7), 455-58(1978).
- ROWE, J. M., "Low-temperature Lattice Properties of PdD alloys." *Metal Phys.*, 8(1), L7(1978).
- ROWE, J. M., RUSH, J. J., PRINCE, E., and CHESSER, N. J., "Neutron Scattering Studies of Crystal Dynamics and Order-Disorder Phase Transitions in Alkali Cyanides.", *Ferroelectrics*, 16, 107-09(1977).
- RUSH, J. J. and ROWE, J. M., "Neutron Quasielastic Scattering Study of  $\text{ND}_4^+$  Orientational Fluctuation in  $\beta$ -Phase  $\text{ND}_4\text{Br}$ ." (to be published).
- RUSH, J. J. and ROWE, J. M., "Comments on 'High Temperature Thermodynamics of Palladium-Hydrogen II. Temperature Dependence of Partialmolar Properties of Dilute Solution in Hydrogen in the range 500-700 K.'" *J. Chem. Phys.*, 68(8), 3954(1978).
- SANTORO, A., RUSH, J. J., and MAELAND A., "Neutron Powder Diffraction Study of Titanium-Copper Deuteride." (to be published).
- SANTORO, A., ROTH, R. S., and MINOR, D., "Neutron Powder Diffraction Study of  $\text{M-LiTa}_3\text{O}_8$ ." *Acta. Cryst.*, B33, 3945-47(1977).
- SHORTEN, F. J., "NBS Reactor: A Summary of Activities, July 1976 to June 1977," *NBS Technical Note 969*, (1978).
- STEENBERGER, C. and RUSH, J. J., "Neutron Scattering Study of Rotational Dynamics in Dimethyltin Difluoride." (to be published).
- TAYLOR, A., CARPENTER, F. C., and Wlodawer, A., "Leucine Aminopeptidase (Bovine Lens): An Electron Microscopic Study." (to be published).
- WLODAWER, A., ROBERTS, J., and HOLCENBERG, J. S., "Characterization of Crystals of L-Glutaminase-Asparaginase from Acinetobacter Glutaminasificans and Pseudomonas 7A." *J. Mol. Biol.*, 112, 515-19(1977).

## PUBLICATIONS

### INDEPENDENT PROGRAMS

- BOYER, W., TANNER, T., and GAJAN, J., "Multiement Analytical Techniques at the Food and Drug Administration," *American Laboratory*, 10, 51-65 (1978).
- BOWEN, R. L., McCLENDON, L. T., and GILLS, T. E., "Adhesive Bonding of Various Materials to Hard Tooth Tissues XV: Sorption of Moldant Ions Evaluated by Neutron Activation Analysis," *Journal of Dental Research*, (1977).
- CAPAR, G., TANNER, T., FRIEDMAN, H., and BOYER, W., "Multiement Analysis of Animal Feed, Animal Wastes, and Sewage Sludge," *Environmental Science and Technology*, (to be published).
- CARPENTER, B. S., SAMUEL, D., WASSERMAN, I., AND YUWILER, A., The  $^{17}\text{O}$  ( $n, \alpha$ )  $^{14}\text{C}$  Reaction as a Tool for Determining the Location and Rate of Turnover of Monoamines in the Brain", (to be published).
- CARPENTER, B. S., D'AGOSTINO, M.D. and YULE, H. P., Editors, "Computers in Activation Analytical Analysis and Gamma-Ray Spectroscopy", (to be published).
- CARPENTER, B. S., "Determination of Thermal Neutron Flux for Fission Track Geochronology", *Geological Survey Open-File Report 78-701*, p. 60, (1978).
- CARPENTER, B. S. and REIMER, G. M., "Uranium Analysis of Natural Waters by Fission Tracks", *ANS Transactions*, 26, p. 172, (1977).
- CARPENTER, B. S., "Mapping and Detecting Selective Elements by Nuclear Track Techniques", *Proc. of the Nuclear Methods in Environmental and Energy Conference*, (1977).
- CARPENTER, B. S., SAMUEL, D., WASSERMAN, I. and YUWILER, A., "A Study of Lithium Uptake and Location in the Brain Using the Nuclear Track Technique", *J. Radioanal. Chem.*, Vol. 37, p. 523 (1977).
- High Energy Heavy Ion Induced X-Ray Emission Analysis.  
J.B. Cross, R. Zeisler, E.A. Schweikert, *Nucl. Instrum. Meth.* 142, 111 (1977).
- FRIEDMAN, M. H., and TANNER, T., "A Computer Language for Reducing Activation Analysis Data," *Journal of Radioanalytical Chemistry*, (1978).

## PUBLICATIONS

- FILBY, R. H. and CARPENTER, B. S., "Application of Nuclear Techniques to the Characterization of Trace Elements in Petroleum and Coal Conversion Products", *ANS Transactions*, 26, p. 163, (1977).
- GALLORINI, M., GREENBERG, R. R., and GILLS, T. E., "Simultaneous Determination of Arsenic, Antimony, Cadmium, Chromium, Copper and Selenium in Environmental Material by Radiochemical Neutron Activation Analysis", *Anal. Chem.*, Vol. 50, No. 11, p. 1479, 1978.
- GILLS, T. E., GALLORINI, M. and GREENBERG, R. R., "The Measurement of Selected Toxic Elements in Biological Matrices Using Radiochemical Activation Analysis", *Proc. of the Third International Conference on Nuclear Methods in Environmental and Energy Research*, (1977).
- GILLS, T. E., GALLORINI, M., and GREENBERG, R. R., "The Measurement of Selected Toxic Elements in Biological Matrices Using Radiochemical Activation Analysis", *Proc., 3rd International Conferernce on Nuclear Methods in Environmental and Energy Research*, (to be published).
- GILLS, T. E., GALLORINI, M., "The Determination of Trace Elements in New Food Grain SRM's Using Neutron Activation Analysis, (to be published).
- GREENBERG, R. R., GALLORINI, M., and GILLS, T. E., "Cadmium Analysis by Radiochemical Neutron Activation Analysis", (to be published).
- NEUENDORF, D. W., and YOST, K. J., "Composition of Particles Emitted from the Nicosia Municipal Incinerator", (to be published).
- GREENBERG, R. R., ZOLLER, W. H., and GORDON, G. E., "Composition and Size Distribution of Particles Released in Refuse Inceneration", *Environmental Science & Technology*, 12, p. 566, (1978).
- GREENBERG, R. R., GALLORINI, M. and GILLS, T. E., "Cadmium Analysis by Radiochemical Neutron Activation Analysis", *Proc. of Environmental Health Perspectives* (1978).
- GALLORINI, M., GREENBERG, R. R., and GILLS, T. E., "Simultaneous Determination of Arsenic, Antimony, Cadmium, Chromium, Copper, and Selenium in Environmental Material by Radiochemical Neutron Activation Analysis", *Anal. Chem.*, 50, 11, pp. 1479-1481, (1978).
- GREENBERG, R. R., ZOLLER, W. H., and GORDON, G. E., "The Contribution of Refuse Incineration to Urban Aerosols", *Proc., 4th Joint Conference on Sensing of Environmental Pollutants*, (1977).

## PUBLICATIONS

- KAMPS, L., TROTTER, J., YOUNG, S., CARSON, J., ROACH, A. G., SPHON, A., TANNER, T., McMAHON, B., "Polychlorinated Quadraphenyls Identified in Rice Oil Associated with Japanese Yusho Poisoning," *Bulletin of Environmental Contamination and Toxicology*, (to be published).
- KESSLER, E. G., Jr., DESLATTES, R. D., and HENINS, A., "Wavelength of the  $WK\alpha_1$  X-Ray Line", (to be published).
- KESSLER, E. G., Jr., DESLATTES, R. D., HENIS, A., and SAUDER, W. C., "Redetermination of  $^{198}\text{Au}$  and  $^{132}\text{In}$   $\gamma$ -Ray Standards Between 0.1 and 1.0 MeV", *Phys. Rev. Lett.* 40, 171 (1978).
- LINDSTROM, R. M., HARRISON, S. H., and HARRIS, J., "Accurate Calibration of Gold Film Standards by Neutron Activation and Gravimetry, (to be published).
- LINDSTROM, R. M., and FLEMING, R. F., "Optimized Measurement of Aluminum in High-Purity Silicon," *Proc. 3rd Int. Conf. Nucl. Methods in Env. and Energy Res.*, (to be published).
- LINDSTROM, R. M., "Radial Efficiency Gradients in Ge(Li) Gamma Detectors," *Radioanal. Chem.* 39, 153-161 (1977).
- LUTZ, G. J., STEMPLE, J. S., and ROOK, H. L., "Evaluation by Activation Analysis of Elemental Retention in Biological Samples After Low Temperature Ashing," *J. of Radioanal. Chem.*, 39, 1-2, p 277-283 (1977).
- TANNER, T., and FRIEDMAN, H., "Neutron Activation Analysis for Trace Elements in Foods," *Journal of Radioanalytical Chemistry*, 37, 529-538 (1977).
- MCGINLEY, J. R., STOCK, G. J., SCHWEIKERT, E. A., CROSS, J. B., ZEISLER, R., and ZIKOVSKY, L., "Nuclear and Atomic Activation with Heavy Ion Beams." *J. Radional. Chem.*, 43, 559 (1978).
- MOODY, J. R., and LINDSTROM, R. M., "Selection and Cleaning of Containers for Storage of Trace Element Samples, *Anal. Chem.*, 49, 2264-2267 (1977).
- THURBER, W. R., and CARPENTER, B. S., "Determination of Boron in Silicon by the Nuclear Track Technique and Correlations with Resistivity and Capacitance-Voltage Measurements," *J. of the Electrochemical Society*, 125, 654 (1978).
- WAGNER, G. A. and CARPENTER, B. S., "Liquid Nitrogen Enhancement of Partially Annealed Fission Tracks in Glass", *Nature*, 267, p. 182, (1977).

## PUBLICATIONS

WAINERDI, R. E., ZEISLER, R., SCHWEIKERT, E. A., "Activation Analysis Opportunities Using a  $5 \cdot 10^{12}$  to  $5 \cdot 10^{13}$  n/sec 14 MeV Generator." *J. Radioanal. Chem.*, 37, 307 (1977).

ZEISLER, R., LUX, F., SEIDENBERGER, H., SCHONENBERGER, H., BECK, W., "Studies on the Distribution of Platinum in Tumor-Bearing Rats After the Application of Platinum Coordination Complexes Used in Cancer Chemotherapy", *Proc. Internation Symposium on Nuclear Activation Techniques in the Life Sciences*, (to be published).

U.S. DEPT. OF COMM. BIBLIOGRAPHIC DATA SHEET	1. PUBLICATION OR REPORT NO. NBS TN 995	2. Gov't Accession No.	3. Recipient's Accession No.
4. TITLE AND SUBTITLE  NBS REACTOR: Summary of Activities July 1977 to June 1978		5. Publication Date May 1979	6. Performing Organization Code
		7. AUTHOR(S) Frederick J. Shorten	
9. PERFORMING ORGANIZATION NAME AND ADDRESS  NATIONAL BUREAU OF STANDARDS DEPARTMENT OF COMMERCE WASHINGTON, D.C. 20234		10. Project/Task/Work Unit No.	11. Contract/Grant No.
		12. Sponsoring Organization Name and Complete Address (Street, City, State, ZIP)  Same as item 9.	
15. SUPPLEMENTARY NOTES			
16. ABSTRACT (A 200-word or less factual summary of most significant information. If document includes a significant bibliography or literature survey, mention it here.)  This report summarizes all those programs which depend on the NBS reactor. It covers the period from July 1977 through June 1978. The programs range from the use of neutron beams to study the structure and dynamics of materials through nuclear physics and neutron standards to sample irradiations for activation analysis, isotope production, radiation effects studies, neutron radiography and nondestructive evaluations.			
17. KEY WORDS (six to twelve entries; alphabetical order; capitalize only the first letter of the first key word unless a proper name; separated by semicolons)  Activation analysis; crystal structure; diffraction; isotopes; molecular dynamics; neutron; neutron radiography; nondestructive evaluation; nuclear reactor; radiation.			
18. AVAILABILITY <input checked="" type="checkbox"/> Unlimited  <input type="checkbox"/> For Official Distribution. Do Not Release to NTIS  <input checked="" type="checkbox"/> Order From Sup. of Doc., U.S. Government Printing Office, Washington, DC 20402, SD Stock No. SN003-003- 02070-2  <input type="checkbox"/> Order From National Technical Information Service (NTIS), Springfield, VA, 22161		19. SECURITY CLASS (THIS REPORT)  UNCLASSIFIED	21. NO. OF PRINTED PAGES  147
		20. SECURITY CLASS (THIS PAGE)  UNCLASSIFIED	22. Price  \$4.50

# NBS TECHNICAL PUBLICATIONS

## PERIODICALS

**JOURNAL OF RESEARCH**—The Journal of Research of the National Bureau of Standards reports NBS research and development in those disciplines of the physical and engineering sciences in which the Bureau is active. These include physics, chemistry, engineering, mathematics, and computer sciences. Papers cover a broad range of subjects, with major emphasis on measurement methodology, and the basic technology underlying standardization. Also included from time to time are survey articles on topics closely related to the Bureau's technical and scientific programs. As a special service to subscribers each issue contains complete citations to all recent NBS publications in NBS and non-NBS media. Issued six times a year. Annual subscription: domestic \$17.00; foreign \$21.25. Single copy, \$3.00 domestic; \$3.75 foreign.

Note: The Journal was formerly published in two sections: Section A "Physics and Chemistry" and Section B "Mathematical Sciences."

### DIMENSIONS/NBS

This monthly magazine is published to inform scientists, engineers, businessmen, industry, teachers, students, and consumers of the latest advances in science and technology, with primary emphasis on the work at NBS. The magazine highlights and reviews such issues as energy research, fire protection, building technology, metric conversion, pollution abatement, health and safety, and consumer product performance. In addition, it reports the results of Bureau programs in measurement standards and techniques, properties of matter and materials, engineering standards and services, instrumentation, and automatic data processing.

Annual subscription: Domestic, \$11.00; Foreign \$13.75

## NONPERIODICALS

**Monographs**—Major contributions to the technical literature on various subjects related to the Bureau's scientific and technical activities.

**Handbooks**—Recommended codes of engineering and industrial practice (including safety codes) developed in cooperation with interested industries, professional organizations, and regulatory bodies.

**Special Publications**—Include proceedings of conferences sponsored by NBS, NBS annual reports, and other special publications appropriate to this grouping such as wall charts, pocket cards, and bibliographies.

**Applied Mathematics Series**—Mathematical tables, manuals, and studies of special interest to physicists, engineers, chemists, biologists, mathematicians, computer programmers, and others engaged in scientific and technical work.

**National Standard Reference Data Series**—Provides quantitative data on the physical and chemical properties of materials, compiled from the world's literature and critically evaluated. Developed under a world-wide program coordinated by NBS. Program under authority of National Standard Data Act (Public Law 90-396).

NOTE: At present the principal publication outlet for these data is the Journal of Physical and Chemical Reference Data (JPCRD) published quarterly for NBS by the American Chemical Society (ACS) and the American Institute of Physics (AIP). Subscriptions, reprints, and supplements available from ACS, 1155 Sixteenth St. N.W., Wash., D.C. 20056.

**Building Science Series**—Disseminates technical information developed at the Bureau on building materials, components, systems, and whole structures. The series presents research results, test methods, and performance criteria related to the structural and environmental functions and the durability and safety characteristics of building elements and systems.

**Technical Notes**—Studies or reports which are complete in themselves but restrictive in their treatment of a subject. Analogous to monographs but not so comprehensive in scope or definitive in treatment of the subject area. Often serve as a vehicle for final reports of work performed at NBS under the sponsorship of other government agencies.

**Voluntary Product Standards**—Developed under procedures published by the Department of Commerce in Part 10, Title 15, of the Code of Federal Regulations. The purpose of the standards is to establish nationally recognized requirements for products, and to provide all concerned interests with a basis for common understanding of the characteristics of the products. NBS administers this program as a supplement to the activities of the private sector standardizing organizations.

**Consumer Information Series**—Practical information, based on NBS research and experience, covering areas of interest to the consumer. Easily understandable language and illustrations provide useful background knowledge for shopping in today's technological marketplace.

Order above NBS publications from: Superintendent of Documents, Government Printing Office, Washington, D.C. 20402.

Order following NBS publications—NBSIR's and FIPS from the National Technical Information Services, Springfield, Va. 22161.

**Federal Information Processing Standards Publications (FIPS PUB)**—Publications in this series collectively constitute the Federal Information Processing Standards Register. Register serves as the official source of information in the Federal Government regarding standards issued by NBS pursuant to the Federal Property and Administrative Services Act of 1949 as amended, Public Law 89-306 (79 Stat. 1127), and as implemented by Executive Order 11717 (38 FR 12315, dated May 11, 1973) and Part 6 of Title 15 CFR (Code of Federal Regulations).

**NBS Interagency Reports (NBSIR)**—A special series of interim or final reports on work performed by NBS for outside sponsors (both government and non-government). In general, initial distribution is handled by the sponsor; public distribution is by the National Technical Information Services (Springfield, Va. 22161) in paper copy or microfiche form.

## BIBLIOGRAPHIC SUBSCRIPTION SERVICES

The following current-awareness and literature-survey bibliographies are issued periodically by the Bureau:

**Cryogenic Data Center Current Awareness Service.** A literature survey issued biweekly. Annual subscription: Domestic, \$25.00; Foreign, \$30.00.

**Liquified Natural Gas.** A literature survey issued quarterly. Annual subscription: \$20.00.

**Superconducting Devices and Materials.** A literature survey issued quarterly. Annual subscription: \$30.00. Send subscription orders and remittances for the preceding bibliographic services to National Bureau of Standards, Cryogenic Data Center (275.02) Boulder, Colorado 80302.

**U.S. DEPARTMENT OF COMMERCE**  
**National Bureau of Standards**  
Washington, D.C. 20234

OFFICIAL BUSINESS

Penalty for Private Use, \$300

POSTAGE AND FEES PAID  
U.S. DEPARTMENT OF COMMERCE  
COM-215



SPECIAL FOURTH-CLASS RATE  
BOOK

---